

POLITECNICO DI TORINO

Master Degree in Biomedical Engineering

Master Thesis

Cerium Oxide Nanoparticles as antioxidant agents: Study of interaction with muscle cells under simulated microgravity



**Politecnico
di Torino**



Supervisor

Prof. Danilo DEMARCHI

External supervisors

Prof. Gianni CIOFANI

PhD Giada GENCHI

Candidate

Sara GORRIERI

257925

Academic Year 2020-2021

Abstract

Oxidative stress is a well-known condition underlying several pathological conditions, such as heart failure and neurodegenerative diseases, but also skeletal muscle atrophy that occurs after prolonged periods of muscle disuse, such as bed immobilization and space travel. The commonly used strategy for oxidative stress treatment/prevention is the administration of antioxidant agents. Among the latter, cerium oxide nanoparticles, also called nanoceria, show self-regenerative antioxidant action mimicking that one of the main human antioxidant enzymes (i.e., superoxide dismutase and catalase), and are excellent candidates for a persistent alleviation of oxidative stress. Nanoceria would ensure overcoming of limitations related to the usage of low molecular weight antioxidant agents, normally requiring repeated administrations.

Purpose of this Master's Degree Thesis in Biomedical Engineering is to investigate the interaction between nanoceria and skeletal muscle cells in mechanical unloading conditions, i.e. under simulated microgravity ($s - \mu g$), for a possible application of this kind of nanomaterials against muscle waste induced by spaceflight.

The experimental work of this Thesis started with nanomaterial synthesis by wet chemistry approach. In-depth characterization of the nanoparticles was then performed to assess their chemical composition, size, stability, and antioxidant capabilities. To the purpose, transmission electron microscopy, X-ray photoelectron spectroscopy, dynamic light scattering, and photometry were used. Biocompatibility investigations were conducted with two different cell models for skeletal muscle tissue, namely C2C12 mouse myoblasts and primary human skeletal myoblasts. Afterwards, identification of the rotational conditions for microgravity simulation and for induction of mild oxidative stress in the skeletal muscle cultures was pursued with a random positioning machine. Interaction of nanomaterials and cell cultures was studied under different regimes of rotation (constant and random speed modes): it was documented by phase contrast optical microscopy and by confocal microscopy upon application of cytochemistry techniques. Quantitative analyses concerning cell-nanomaterial interaction under simulated microgravity were conducted by flow cytometry and inductively-coupled plasma-optical emission spectroscopy.

Cell viability was assessed upon administration of increasing concentrations of antioxidant nanoparticles in both static and dynamic conditions, denoting high biocompatibility of the chosen nanoparticles. Simulated microgravity was moreover found to be a pro-proliferative stimulus for mouse muscle cells, with potential applications in tissue engineering and regenerative medicine. On the other hand, simulated microgravity induced a mild oxidative stress on differentiating human cell cultures that deserves further investigations.

The study of the interaction of nanoceria and muscle cells under microgravity conditions showed that, under the conditions tested only a small fraction of nanoceria is internalized, suggesting a low antioxidant effect of nanoceria under these conditions. The poor interaction could be due to the continuous mixing of fluids induced by the movement of the random positioning machine.

Based on these results, this Thesis work leaves open several issues such as the promotion of the nanomaterial-cell interaction in simulated microgravity, the evaluation of the antioxidant effect of nanoceria and the validation of the results achieved during myoblast proliferation and differentiation for the stimuli that the random positioning machine appears likely to impose.

Acknowledgements

I would like to express my sincere thanks to all of the following people.

My supervisors Prof. Danilo Demarchi and Prof. Gianni Ciofani for their guidance, support and especially for giving me the opportunity to do my thesis at the Italian Institute of Technology.

To my co-supervisor Giada who assisted me during my time in IIT. A special thanks for the help, advice, precious teachings and motivation I received.

To the European Space Agency for funding the InterGravity project under grant I-2019-01703.

To all the people I was blessed to collaborate with during this experience. In particular Matteo for his support in the acquisition of the confocal images, and to the collaboration of people from the IIT in Genoa who allowed the enrichment and completion of the results found.

Even if a simple thank you is not enough, to my mom and dad who never let me lack love, support, advice and encouragement.

To the whole group in Turin, to Antonio's roommates for all the moments spent together, the support and so much more.

To Pippo, my number two critic, who with love, patience and attention has always inspired me to be more confident, to believe in myself, helping me to overcome all my crises, even the most useless ones.

Table of Contents

List of Tables	XI
List of Figures	XII
1 Introduction	1
1.1 Skeletal Muscle Tissue	2
1.1.1 Skeletal muscle physiology	2
1.1.2 Myogenesis	4
1.1.3 Muscle alterations	6
1.2 Free Radicals and Oxidative stress	8
1.2.1 Free radicals	8
1.2.2 Free radicals sources in Skeletal Muscle	11
1.2.3 Oxidative damage in muscle tissue	12
1.2.4 Antioxidant defense system	15
1.3 Microgravity as mechanical stimulation to induce oxidative stress .	19
1.3.1 Devices to simulate microgravity conditions	19
1.3.2 Effects of microgravity on muscle cells	23
1.4 Cerium oxide nanoparticles: a nanotechnological approach for the treatment of oxidative stress	25
1.4.1 Antioxidant nanotechnologies: state of the art	25
1.4.2 Cerium oxide nanoparticles	26
1.4.3 Cerium oxide nanoparticles applications in nanomedicine . .	30
2 Aim of the project	32
3 Materials and Methods	34
3.1 Materials	34
3.1.1 Chemicals	34
3.1.2 Cell lines	35
3.1.3 Instruments	35
3.1.4 Materials	35

3.2	Synthesis of cerium oxide nanoparticles	36
3.3	Nanoparticle characterization	37
3.3.1	Transmission electron microscopy (TEM)	38
3.3.2	X-Ray Diffraction (XRD), X-Ray Photoelectron Spectroscopy (XPS) and Thermogravimetric Analysis (TGA)	38
3.3.3	Size and Zeta Potential measurements	39
3.4	Total antioxidant capacity	39
3.5	Microgravity simulation: experimental set-up	40
3.6	Cell culture	42
3.6.1	Cell sub-culture and freezing	43
3.7	Cytotoxicity tests on C2C12 cell line	44
3.7.1	Pico-Green assay	44
3.8	Evaluation of oxidative stress extent in cells	45
3.8.1	Flow Cytometry	45
3.8.2	Assessment of cells oxidative stress level: C2C12 cell line	47
3.8.3	Assessment of cells oxidative stress level: HSkM cell line	47
3.9	Study of interaction between muscle cells and Nanoceria in simulated microgravity	48
3.9.1	Inductively coupled plasma-optical emission spectrometry (ICP-OES)	48
3.9.2	Flow Cytometry to evaluate NPs internalization	49
3.9.3	Cytochemistry	49
4	Results and Discussions	51
4.1	Nanoceria characterization	51
4.1.1	TEM imaging	51
4.1.2	X-Ray Photoelectron Spectroscopy (XPS)	52
4.1.3	Size and Zeta Potential measurements	56
4.1.4	X-Ray Diffraction (XRD) analysis	59
4.1.5	Thermogravimetric analysis (TGA)	60
4.2	Photometry for quantification of nanoparticle antioxidant capacity	62
4.3	Cytotoxicity tests	64
4.4	Study of NC internalization under simulated microgravity	69
4.5	Evaluation of oxidative stress induced by microgravity simulation	73
4.5.1	Evaluation of oxidative stress induced by microgravity simulation: HSkM cell line	76
5	Conclusions	80

A	Nanoparticles characterization techniques	82
A.1	X-Ray photoelectron spectroscopy (XPS)	83
A.2	Dynamic light scattering (DLS)	84
A.3	X-Ray diffraction (XRD)	85
A.4	Thermogravimetric Analysis (TGA)	86

List of Tables

4.1	Atomic percentages and peaks' positions detected via XPS	53
4.2	Hydrodynamic radius (Size d.nm) and polydispersion index (PdI) obtained in different experimental conditions. The results are reported as the mean and standard deviation of four measurements made on the samples.	57
4.3	Z Potential values obtained in different experimental conditions. The results are reported as the mean and standard deviation of three measurements made on the samples.	58
4.4	Long-term stability monitored at normal gravity and under simulated microgravity: size measurements.	58
4.5	Long-term stability monitored at normal gravity and under simulated microgravity: Z Potential.	59
4.6	Crystal size and strain values obtained from XRD analysis.	60
4.7	Critical temperatures and weight loss percentages of uncoated and coated NPs derived using the TGA curves.	61
4.8	Antioxidant property of nanoparticles and soluble compounds (in Trolox equivalents).	63
4.9	Preliminary investigation on myoblast response to increasing concentrations of CellROX Green dye for quantification of <i>ROS</i> ⁺ -cells by flow cytometry.	73

List of Figures

1.1	Schematic representation of the muscle fiber. Reproduced from Bonetto et. al. [10]	4
1.2	Schematic representation of the differentiation process from myoblasts to myotubes at top, representative images of in vitro cultures at bottom. Reproduced from Abmayr et al. [11]	5
1.3	Schematic representation of the electron transport process during oxidative phosphorylation. Reproduced from Peterson et al. [20]	12
1.4	Random positioning machine components. Reproduced from S.J. Pardo et al. [27]	20
1.5	Schematic representation of the random positioning machine with samples placed on the central plate. Reproduced from A.G. Borst et al. [29]	22
1.6	Schematic representation of the mechanism of action against free radicals of the nanoceria: ROS scavenging and surface regeneration properties. Reproduced from S.Das et al. [31]	28
3.1	Schematic representation of the synthesis and coating process of cerium oxide nanoparticles by direct precipitation using ethylene glycol as reaction cofactor.	37
3.2	Random positioning machine - RPM (Airbus RPM2.0).	41
3.3	Schematic representation of the design of the mold for silicone cell culture vessels for simulated microgravity studies.	41
4.1	Images from Transmission electron microscopy at two different magnifications. Uncoated NPs are reported in the three images on the top, and coated NPs on the bottom.	52
4.2	Wide scans obtained by XPS technique.	53
4.3	High resolution scan of the Ce 3d region of the NC IIT sample.	54
4.4	High resolution scan of the Ce 3d region of the NCsigma sample.	54

4.5	High resolution spectra of the oxygen peaks. On the top, the peak of oxygen detected in the NC IIT sample and below the peak detected in the NCsigma sample.	55
4.6	High resolution scan of the N 1s region of the NC IIT sample. . . .	56
4.7	Size distribution data of FBS-coated NC IIT	57
4.8	Z-Potential distribution data of the long-term stability monitoring.	59
4.9	Spectrum obtained by XRD analysis: NC IIT at the top, NC sigma in the center.	60
4.10	Comparison of TGA curves of coated (green line) and uncoated (red line) NPs.	61
4.11	Calibration curve for Trolox standard in antioxidant capacity quantification assay.	62
4.12	Biocompatibility test of increasing concentrations of NC (a) and PDNPs (b) with proliferating C2C12 myoblasts. Fluorescence is associated to ds-DNA content of the cultures.	64
4.13	Biocompatibility test of increasing concentrations of NC (a) and PDNPs (b) with proliferating HSkM. Fluorescence is associated to ds-DNA content of the cultures.	65
4.14	Representative phase contrast microscopy images of C2C12 cell cultures after 24 h of exposure to increasing concentrations of NC and to simulated microgravity (20 deg/s).	66
4.15	Biocompatibility test of increasing concentrations of NC and simulated microgravity with proliferating C2C12 myoblasts. Fluorescence is associated to ds-DNA content of the cultures.	66
4.16	Representative phase contrast microscopy images of C2C12 cell cultures after 24 h of exposure to increasing concentrations of PDNPs and to simulated microgravity (20 deg/s).	67
4.17	Biocompatibility test of increasing concentrations of PDNPs and simulated microgravity with proliferating C2C12 myoblasts. Fluorescence is associated to ds-DNA content of the cultures.	67
4.18	Study of the internalization of cerium oxide nanoparticles carried out with three different concentrations. Results from flow cytometric analysis, referred at three different observation times and cells maintained at normal gravity.	70
4.19	Microscope images of C2C12 cells acquired after 48h of microgravity exposure. Control condition at normal gravity (1g) top, cells exposed to microgravity shown instead in bottom images. The images in the left column refer to the condition without Nanoceria (-NC) and those on the right to the condition with Nanoceria (+NC).	71

4.20	Histogram relative to the percentage of internalized Nanoceria obtained by flow cytometry: comparison between the conditions of normal gravity and microgravity.	72
4.21	Images obtained by confocal microscopy. The top images refer to normal gravity condition, while the bottom images refer to microgravity condition.	72
4.22	Histogram for the percentage of internalized nanoceria obtained by ICP-OES:comparison between the conditions of normal gravity and microgravity.	73
4.23	Preliminary testing of C2C12 cell response to a pro-oxidant insult provided through tBH administration.	74
4.24	Effects of NC administration on C2C12 myoblasts exposed to a pro-oxidant agent at different time point from tBH administration.	75
4.25	RPM-induced oxidative stress on C2C12 cell line after 24 and 72 h of exposure. 3D clinorotation at 25 deg/s.	76
4.26	Investigations of the effects of different 3D clinorotation speeds on C2C12 cell cultures in terms of oxidative stress.	77
4.27	Representative images of phase contrast optical microscopy of early differentiating HSkM (a), and investigation of the effects of constant speed 3D clinorotation at 20 deg/s on HSkM cultures in terms of oxidative stress (b).	78
4.28	Investigation of the effects of random speed 3D rotation at 8-20 deg/s on HSkM cultures in terms of oxidative stress.	79

Chapter 1

Introduction

Movement and maintenance of posture are the two key distinguishing characteristics of all vertebrates, and skeletal muscles, along with bones, are responsible for this. Skeletal muscle is an excitable tissue that responds through a contraction to voluntary stimuli sent by the central nervous system. It is a highly mechanosensitive tissue, and for this reason, the quantity and intensity of the stimuli received play an essential role in determining the mass and performances of muscles. [1].

Gravity is the constant mechanical stimulus to which all living things on Earth are subjected. Considering that the muscular structure has developed by adapting to the constant load imposed by the force of gravity, it is clear that any small variation in this force will cause alterations within the tissue [1] [2].

Situations in which muscles suffer from the lack of gravity load are, for example, bed rest, leg immobilization, denervation but also space travel [1]. Muscle disuse is the common feature of all these cases and is also the cause of the decrease in motor neuron activity, the reduction in the rate of protein synthesis and the increase in catabolic processes. These processes result in a condition called muscle atrophy characterized by loss of muscle mass and strength [3].

Recent studies [3] [4] [5] have correlated muscle atrophy, which occurs following muscle discharge, with the condition of oxidative stress (OS).

The oxidative stress condition occurs when the production of reactive oxygen species (ROS) exceeds the body's antioxidant defense capabilities. When the antioxidant defenses are no longer able to keep the concentration of ROS below, there is a need to intervene with external antioxidant therapies [6].

This Master's Thesis project will analyze the reactions of skeletal muscle tissue after exposure to weightlessness, henceforth called microgravity or simulated microgravity when reproduced with a special instrument. The focus of this thesis project will be mainly to evaluate the interaction between nanomaterials with antioxidant properties and muscle cells exposed to simulated microgravity.

This first introductory chapter is composed of four main sections aimed at introducing the problem underlying this thesis project.

The first section provides a brief overview of muscle tissue focusing on the physiology of the skeletal muscle cells, the stages of the differentiation process leading to the formation of the mature muscle cell and the analysis of pathologies affecting skeletal muscle tissue.

Particular attention will be given in the second section to the conditions in which the presence of free radicals plays a key role in the evolution of the disease. The second section deals with the condition of oxidative stress that occurs in skeletal muscles, highlighting its sources, possible causes and consequences.

The common strategy to overcome the problems due to oxidative stress is the administration of antioxidant agents. However, traditional antioxidants show several problems. The analysis of these problems, leading to the consideration of a nanotechnology approach as an alternative solution to combat oxidative stress, is discussed in the concluding part of the chapter.

Focusing on the tissue of interest, this second section concludes by describing and listing the processes that, compromised by the condition of oxidative stress, contribute to the generation and worsening of the atrophic condition.

In the third section the problem of the absence of gravity is examined. Are then described the main tools used in the laboratory to simulate the condition of weightlessness and then the changes observed at the cellular level after exposure to microgravity.

In the last section of this introductory chapter are described the characteristics and applications in the field of nanomedicine of cerium oxide nanoparticles, chosen as a nanotechnological approach to counteract and prevent the condition of oxidative stress given the problems of traditional antioxidant agents.

1.1 Skeletal muscle Tissue

1.1.1 Skeletal muscle physiology

This first section aims to describe the physiology of muscle cells by examining the elements that make up the muscle fiber. Muscles of the human body can be classified into two morphologically distinct groups: smooth muscles, which are not under conscious control (involuntary muscles), and striated muscles.

Striated muscles are in turn divisible into two groups, cardiac and skeletal muscles. These last are also called voluntary muscles because, through a contraction, they respond to voluntary stimuli received from a nerve impulse [7].

The structure of skeletal muscle consists of numerous muscle fibers grouped into fascicles. This particular bundling of fibers gives the muscle its classic striated appearance [7].

The muscle fibers are covered by a cell membrane, called the sarcolemma, which encloses the inner cellular components and the cytoplasm, also called the sarcoplasm. The sarcolemma also enters the myofiber, generating a system of transverse tubes (T-tube system) that represent the main point for ion exchange.

Within the sarcoplasm, there is a second network of longitudinally developed tubules whose role is to regulate the concentration of calcium ions within the myofiber. This second tubular network is called the sarcoplasmic reticulum (SR) [8]. Each myofiber is surrounded by a basal lamina called the endomysium. Perimysium, on the other hand, is the name of the membrane that surrounds the bundles of muscle fibers. These two membranes are crossed by blood vessels that feed the fiber and by nerves directed towards the inside of the fiber [9] [8].

Each muscle fiber is composed of many contractile and supporting proteins called myofibrils. These are actin, myosin, tropomyosin, and troponin and are responsible for muscle contraction. In particular, the binding between actin and myosin is the key event in muscle contraction.

The physical organization of actin and myosin within the fiber defines the structure of the sarcomere which is the functional unit of the muscle fiber.

Sarcomeres are arranged longitudinally along the muscle fiber, and the boundary between two consecutive sarcomeres is defined by two lines composed of Z proteins, called Z-lines, which maintain the architecture of the sarcomeres [7].

Traversing the sarcomere from these two extremes, several thin myofilaments composed of two actin filaments arranged to form a spiral structure are encountered. Towards the more central portion of the sarcomere, these thin filaments are paired with thicker filaments, myosin. The myosin tails bind directly to the most central portion of the sarcomere, called the H-line and formed by structural proteins. The central end of the actin filaments also binds to this central structure, but in an indirect manner through linking proteins, the nebulins.[7].

Actin is a thin protein filament made of G-actin monomers, which are arranged to form a double helix structure. Along the double helix of the actin filament runs another helical protein which is tropomyosin on which the troponin proteins are located [8]. Troponin is the protein that regulates muscle contraction and is composed of three polypeptide subunits: troponin I, C, and T that bind to F-actin, calcium ions, and tropomyosin filaments, respectively.

Tropomyosin is a helical protein involved, along with troponin, in the control of muscle contraction by preventing actin-myosin binding.

Finally, the myosin filament is composed of two regions: the first is the portion where the myosin is anchored to the M-line of the sarcomere; instead, the second region contains an active site for binding ATP and is the point where the binding between the actin filament and the myosin head occurs [8].

Muscle fibers can be classified into three types depending on the speed, length of contraction, and how ATP is produced. Type 1 fibers are also called slow oxidative

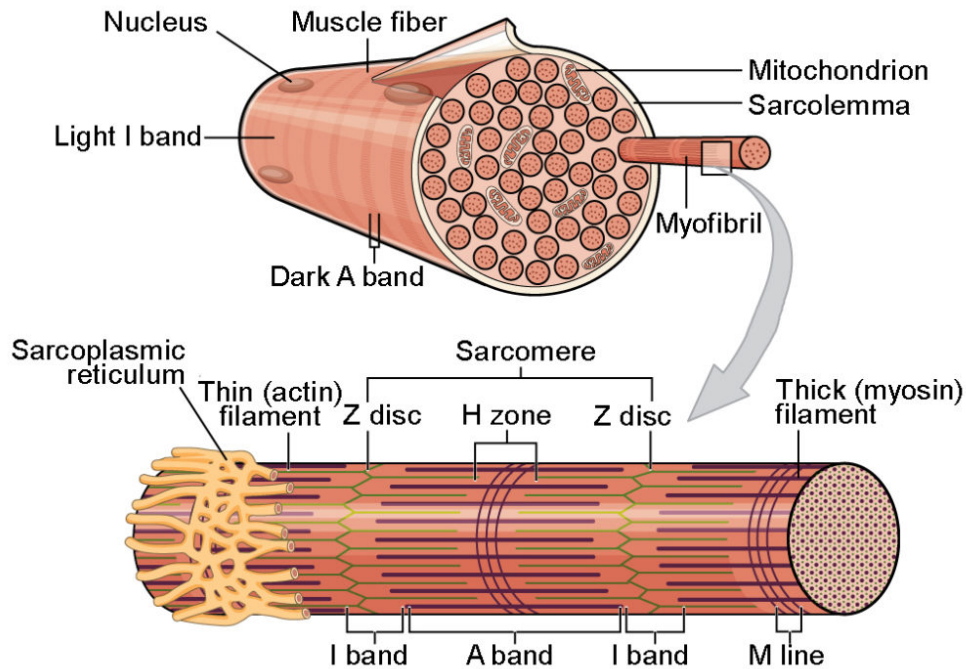


Figure 1.1: Schematic representation of the muscle fiber. Reproduced from Bonetto et. al. [10]

fibers because most ATP is produced at the mitochondrial level using oxygen reserves. This process of ATP synthesis is called oxidative phosphorylation and will be described in more detail in the following sections. Muscles composed primarily of this type of fiber are better suited for endurance exercises.

The intermediate fibers, IIa fibers, are rich in mitochondria like slow fibers but also have sufficient glycolytic enzymes to produce energy through an anaerobic mechanism.

In contrast, type IIb fibers produce ATP from glycolysis because of their high accumulation of glycogen, glycolytic enzymes, and low number of mitochondria. Type IIb fibers are also called fast twitch fibers because of their ability to produce great force in a short amount of time. Because force is produced by anaerobic glycolysis, muscle fatigue occurs after a short time when glycogen stores are depleted [7] [8].

1.1.2 Myogenesis

The formation of adult muscle tissue occurs through a process called myogenesis in which precursor cells, in the presence of certain stimuli, differentiate and fuse to

form mature tissue.

The myogenic process has been studied *in vitro* on isolated muscle cells of mice, rats, or humans, or with immortalized cell lines and consists of an ordered process that occurs in two different temporally separated stages called primary and secondary myogenesis.

Myoblasts are the precursor cells of muscle, these in the presence of proliferative stimuli replicate until the conditions for differentiation occur. *In vitro*, differentiation is induced by depriving myoblasts of proliferative factors.

The first phase of myogenesis sees myoblasts differentiate into more elongated structures called myocytes. The latter are able to migrate, adhere and interact with other myocytes in order to fuse generating a multinucleated structure called myotube. In the process of fusion myocytes appear and preferentially bind to the ends of already formed myotubes. Focusing on the myocytes migration previously mentioned, it was observed in different *in vitro* studies a change in cell motility during the differentiation process. If compared to myoblasts, it was seen that reduced motility of myocytes may promote cell-cell contact and so the subsequent fusion into myotubes. There were also observed several modifications within the structure of a cell that undergoes differentiation. Firstly, particular lamellipodia and filopodia extensions were observed in cells' contact regions to find other cells in the neighborhood that are ready to fuse [11] [12].

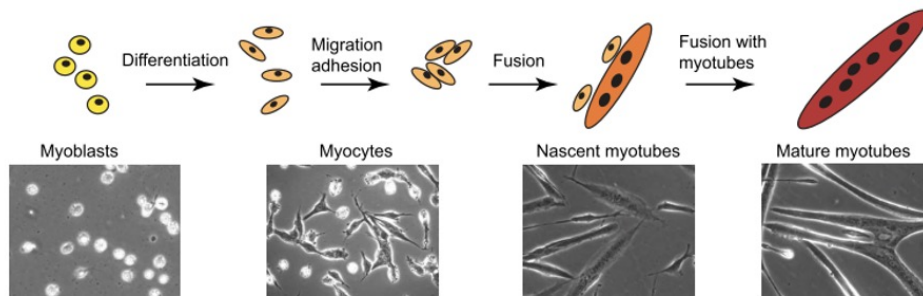


Figure 1.2: Schematic representation of the differentiation process from myoblasts to myotubes at top, representative images of *in vitro* cultures at bottom. Reproduced from Abmayr et al. [11]

This complex process, regulated by numerous factors including signaling molecules, genetic regulators, modifications of the cytoskeleton, etc., is the first step in the formation of muscle tissue. But this process of differentiation and fusion of myoblasts can also occur within mature muscle tissue, involving a third type of precursor cells, the satellite cells.

Satellite cells, located between the basal lamina that surrounds each fiber and the

plasma membrane of the myofiber, are usually in a quiescent state in adult muscles, but they can exit to this quiescent state in the presence of specific stimuli.

The activation of these cells occurs as a result of an immune response due to muscle degradation caused by physical or chemical trauma, which trigger a rapid necrotic process localized at the point of injury. Once out of quiescent state, satellite cells begin to proliferate, differentiate and fuse with existing fibers in order to repair and reunite the flaps of the injured area [11] [12] [13].

Activation depends on the interaction between satellite cells and the environment in which they are located, the niche. For example, the activation of satellite cells is not restricted to the area of the injury alone but occurs along with the entire muscle fiber, requiring the migration of the activated satellite cells [12].

This process gives the muscle self-healing capabilities but is also important for cellular turnover which makes possible the adaptation of the muscle and its performance to different physical and pathological conditions [11] [12][13][14].

Cell turnover is made possible by the simultaneous work of regeneration processes, through satellite cells, and protein degradation, via ubiquitin-proteasome system and autophagy [15].

The ubiquitin-proteasome system is required to remove damaged contractile proteins in response to changes in muscle activity. Autophagy, on the other hand, plays a fundamental role in the turnover of cellular components with the removal of other cellular components no longer functioning. These two aspects will be described in greater detail in the next chapter when the mechanisms that contribute to the loss of muscle mass will be examined specifically [15].

As explained below, these processes involved in cellular turnover are affected by the presence of oxidative stress.

1.1.3 Muscle alterations

Muscle alterations can be ascribed to several reasons (such as disease or disuse), and can either be transitory or permanent. Myopathy is the term comprising alterations of pathological origin. One of the main consequences of myopathies is manifested through the weakness of the skeletal muscles [16].

Diseases that affect skeletal muscles can be classified into three categories.

The first category comprehends the disorders of muscle metabolism. Oxidative phosphorylation is the aerobic process of cellular respiration in which the greatest amount of energy is synthesized in the form of ATP. Since ATP is needed to ensure the proper skeletal muscle contraction, patients with impaired oxidative metabolism are unable to sustain medium/long duration physical performance. Premature muscle fatigue is the main feature of these pathologies that involve muscle energy metabolism.

The second category concerns those disorders characterized by reduced muscle mass

due to necrosis or atrophy on a genetic basis, with the consequent replacement of the muscle mass with adipose and connective tissue. Examples of muscular dystrophies are Duchenne's and Becker's.

Both dystrophies are characterized by the absence of dystrophin. Dystrophin is a protein of the skeletal muscle filaments that supports the sarcolemma. It is clear that the total or partial lack of dystrophin causes damages to the sarcolemma with consequent weakness and atrophy of the muscle. Although the anaerobic processes of ATP synthesis appear to function properly, patients' physical performances are highly compromised due to the condition of muscle atrophy and weakness.

The third category of myopathies includes the disorders relative to muscle contraction. These disorders can result from intrinsic muscle dysfunction or due to abnormalities or damages in the central nervous system, motor nerves, or neuromuscular junction [17] [18].

This work will focus on muscle disorders related to the overproduction of reactive oxygen species. Particular attention will be given to the condition of muscular atrophy.

Skeletal muscle atrophy is defined as a decrease in the size of a tissue or organ due to the loss of organelles, cytoplasm, and proteins. It can be the result of disuse, denervation, systemic disease, or malnutrition. In all cases, the common features that lead to muscle loss are increased degradation of contractile proteins along with reduced protein synthesis.

Atrophy, as a consequence of muscle disuse, results in a decreased activity of motor neurons, a reduced protein synthesis rate, and an increased catabolic process with consequent loss of muscle mass and strength [8].

In particular muscle loss may be due to:

1. Inhibition of protein synthesis in favor of catabolic activity.
2. Increased muscle proteins-ubiquitin conjugations.
3. Increased protein degradation through autophagy and catabolic activities.
4. Increased production of certain signaling molecules, like cytokines and steroids, that may alter other signaling pathways involved in the protein synthesis and degradation [19].

These evidences about muscle protein degradation are also based on the observation of the slight and chronic imbalance of the autophagic process that contributes to the loss of muscle mass that occurs in the elderly, also called sarcopenia. During the ageing process, the abnormal regulation of the autophagy process interferes with the contractile properties of myofibers making them more susceptible to contraction-induced damage leading to muscle atrophy.

Peterson al. in their study have shown a correlation between the age of the individual, increased protein degradation, an increase in the accumulated oxidative stress, and cellular apoptosis.

It, therefore, appears that oxidative stress can contribute to the development and aggravation of muscle atrophy.

Reactive Oxygen Species can also influence muscle force. Myofilament proteins, such as myosin and troponin C, are targets of ROS and oxidation alter their structure and also affect their sensitivity to calcium which affect the proper muscle force production [15] [20] [21].

In the next sections, the correlation between oxidative-stress and muscle damage will be investigated in more detail by focusing on understanding which are the sources of free radicals within skeletal muscle, and the contribution of oxidative stress in the alteration of the aforementioned muscle degradation processes will be examined in greater detail.

1.2 Free Radicals and Oxidative stress

This second section deals with the condition of oxidative stress that occurs in skeletal muscles highlighting the sources, the possible causes and consequences.

First, is provided a brief overview of the problem with the definition of free radicals and oxidative stress. Then are listed the main sources of reactive oxygen species within the muscle tissue with a particular focus to the mitochondria as it is the most productive site. The discussion continues with the analysis of the cellular mechanisms that, influenced by the presence of reactive oxygen species, contribute to muscle degradation.

When the production of reactive oxygen species exceeds the antioxidant defense capabilities of the body, it is necessary to increase the defenses through the exogenous administration of antioxidant principles [4].

The section then concludes with an analysis of the mechanisms of antioxidant defense of biological systems and highlighting the problems of traditional low molecular weight exogenous antioxidant agents that lead to the adoption of a nanotechnological approach as an alternative solution to combat oxidative stress.

1.2.1 Free radicals

All atoms or molecules that contain one or more unpaired electrons are categorized as free radicals. The surplus of electrons gives them instability and high reactivity with many targets, such as biomacromolecules (lipids, nucleic acids, proteins etc.). [6].

Free radicals can be classified into two groups based on the element that represents the reactive center. Free radicals with oxygen as the reactive center, but also oxygen derivatives, are defined as reactive oxygen species (ROS). In contrast, free radicals with nitrogen as the reactive center are classified as reactive nitrogen species (RNS).

Radicals can come from external sources, but they can also be generated within cells. Generation of free radicals from external sources occurs through penetration into the body of substances such as environmental pollutants, heavy metals, chemical solvents, cigarette smoke, alcohol, or ionizing radiation. Once internalized, these substances are metabolized producing free radicals as by-products [22].

Instead, endogenous free radical generation can occur through enzymatic reactions or through other internal processes such as cellular respiration, inflammation, infection, cancer, intense exercise, or during aging. The two most common free radicals resulting from cellular mechanisms are the superoxide radical (O_2^-), resulting from an incomplete oxygen reduction process in electron transport systems or, as the nitric oxide (NO) that is the second main endogenous free radical, as a product of enzymatic reactions [6] [22].

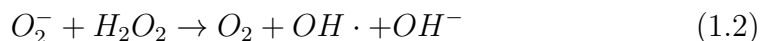
It is now presented a brief list of the most common free radicals produced within cells.

1. Superoxide radical (O_2^-): as mentioned earlier, the superoxide radical is the free radical most present in the body. It is generated as an intermediate product in several biochemical reactions by NADPH oxidase, and peroxidase. This radical is also largely produced as an immune response by inflammatory cells as a defense agent against foreign organisms.
Once formed, it can react with other substances such as nitric oxide, or oxidize/reduce biological materials, or be involved in a process of chain reactions that in turn generate other free radicals such as hydrogen peroxide (H_2O_2), hydroxyl radical (OH^-), peroxynitrite ($ONOO$), and hypochlorous acid ($HOCl$).
Compared to other free radicals, it is less reactive but has a long half-life that allows a good diffusion within the body [6] [22].
2. Hydrogen Peroxide (H_2O_2): it is a non-radical ROS resulting from some enzymatic reactions such as the dismutation of the superoxide radical by superoxide dismutase, which will be explained in more detail in this section. Hydrogen peroxide is weakly oxidizing, in fact it is not able to directly oxidize DNA and lipids but can contribute to the inactivation of some enzymes.
Although it is weakly reactive at high levels it can become cytotoxic because through the Fenton and Heber-Weiss reactions catalyzed by metals it is able to generate hydroxyl radicals [6].
3. Hydroxyl radicals (HO^-): as mentioned, it is generated via Fenton reaction

by H_2O_2 when it reacts with free iron ions or other transition metal.



It can be also generated through the Haber-Weiss process when superoxide and hydrogen peroxide react giving an oxygen molecule, an anion, and the hydroxyl radical in a reaction catalyzed by iron or copper ions.



Hydroxyl radical is the most reactive radical among those listed and because of this very high reactivity it damages the molecules that are close to the production site [6].

4. Nitric Oxide ($NO\cdot$): it is synthesized in many cell types from the amino acid L-arginine and it is involved in many physiological roles, for example it is a messenger required for the proper blood flow modulation. It is a weak reducing agent that reacts, as mentioned earlier, very rapidly with superoxide to produce peroxynitrite [6].
5. Peroxynitrite ($ONOO^-$): The reaction by which this radical is formed is the first reaction to occur when peroxynitrite interacts with the superoxide radical because this reaction occurs three times faster than the reaction of dismutation of the superoxide radical by superoxide dismutase.



Given the ease with which it can be generated, peroxynitrite can be highly dangerous because it is highly oxidizing and can damage DNA, proteins and thiol groups.[6]

As you can guess from the above free radicals inside biological systems can have a dual role, both beneficial, being involved cell processes like respiration, lipid synthesis and immune response, and harmful according to the concentration. When there is an imbalance between the production of reactive species and the body's ability to defend itself against oxidizing agents, a situation called oxidative stress arises.

In a highly oxidative environment, free radicals begin to oxidize biological macromolecules as lipid, nucleic acid, and proteins. For example, a high presence of hydroxyl radicals can cause lipid peroxidation, which through a series of other chain reactions can lead to the formation of cytotoxic and mutagenic agents. Oxidative stress damage to proteins causes conformational changes that result in a loss, or

impairment, of their function. DNA damage can cause mutagen formation or loss of genetic information.

Oxidative stress is not only a common feature of several diseases such as heart failure, muscle wasting, diabetes, cancer, and neurodegenerative diseases such as Parkinson's and Alzheimer's, but it can also be the cause of worsening and disease onset [22].

1.2.2 Free radicals sources in Skeletal Muscle

In this paragraph, the main free radical production sites within muscle tissue are presented.

As seen above ROS produced endogenously have a physiological function, in muscle tissue in particular they can act as signal molecules in regeneration processes and mitochondrial biogenesis. Excessive production of free radicals, however, can compromise normal cellular functioning by altering proteins, lipids and nucleic acids.

The generation of free radicals within the muscle tissue occurs as a result of physical stimuli such as intense exercise but also prolonged muscle disuse. From the literature [6] there is evidence of a high production of ROS following intense physical exercise especially in the liver and skeletal muscle. Even muscular disuse seems to cause an excessive production of free radicals and in particular, focusing on skeletal muscle, of superoxide ion.

Mitochondria appear to be the main source of free radicals within the muscle fiber. It appears that 2-5% of the total oxygen consumed by mitochondria during metabolic processes may be reduced to the form of superoxide ion [6].

Mitochondria are double membrane organelles involved in several cellular processes including metabolic processes, cell cycle regulation and apoptosis. They are extremely dynamic organelles as they are able to regulate cellular dynamics according to the stimuli provided, for example in response to an increased energy demand through biogenesis or in response to damaged cellular components they can program apoptotic processes [20]. Mitochondria consume oxygen to generate ATP through a process called oxidative phosphorylation (OXPHOS), which is accomplished through the tricarboxylic acid cycle (TCA) and the electron transport system (ETS). The ETS is a complex of five polypeptides located in the inner mitochondrial membrane (from complex I to complex V) that are responsible for accepting electrons instead, the TCA cycle has the task of generating the reduced form of NAD^+ and $FADH$ ($NADH$ and $FADH^2$).

The process begins when $NADH$ and $FADH^2$ donate electrons to the ETS. These electrons move through red-ox reactions along the chain of complexes generating an amount of energy that allows the translocation of hydrogen ions across the inner

mitochondrial membrane. At complex IV these electrons are donated to oxygen which is reduced to water.

This process is followed by the generation of a membrane potential and proton gradient, which is used to move back hydrogen into the mitochondrial matrix. It is through this backward movement through the last complex (complex V, also called ATP synthase) that leads to ATP synthesis [20].

During the electron movements described above, there is a likelihood of ROS being

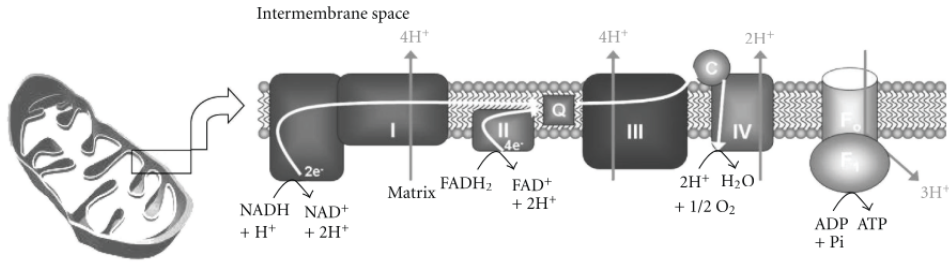


Figure 1.3: Schematic representation of the electron transport process during oxidative phosphorylation. Reproduced from Peterson et al. [20]

generated due to the possible release of electrons from the inner mitochondrial membrane. ETS complex I and complex III, in particular, are the main sites involved in the production of superoxide [6] [20].

It must be considered that the number of mitochondria in skeletal muscle tissue is the highest because of its need to produce a large amount of ATP required for muscle contraction, so muscle cells can be considered as highly productive sites of ROS [6] [20].

Reactive oxygen species are not only produced within the mitochondria, but also by the sarcoplasmic reticulum from the transverse tubule system and also through other internal mechanisms. An example is the production of ROS following a muscle injury event. The immune system responds to an injury by invading the area of damaged tissue with macrophages and phagocytosing cells. The latter during the regeneration process release ROS that can then induce oxidative stress and damage surrounding tissues [6] [22].

1.2.3 Oxidative damage in muscle tissue

If previous paragraphs mentioned the main sources of ROS in the muscle cell, the focus is now shifted on the oxidation-induced problems in muscle tissue with particular attention on the ROS-dependent mechanisms.

Focusing on the condition of muscle atrophy following disuse, demonstrations correlating elevated ROS production with the weakness and loss of muscle mass that characterizes this condition can be found in the literature [6] [15] [4] [21] [22].

This evidence relates high levels of oxidative stress within muscle tissue to muscle fiber degradation. Indeed, there are five different ROS-dependent mechanisms involved in protein synthesis or degradation in skeletal muscle. The presence of ROS affects the proper functioning of these mechanisms by causing an imbalance in the protein synthesis-degradation systems leading to a reduction in muscle mass. A list of ROS-dependent mechanisms involved in muscle degradation follows.

1. The ubiquitin-proteasome system (UPS) is considered one of the major protein degradation systems within the muscle cell. The role of UPS is to label, via ubiquitin (Ub) molecules, specific proteins that have been selected to be degraded by the E3 enzymes (ubiquitin ligase). The degradation of the selected proteins is carried out by a specific subunit of the UPS (the S26 subunit) [21]. The degradation activity of the UPS can be highly upregulated in pathological conditions and oxidative stress is one of the causes of this over-activation. High ROS concentrations can increase the production of the proinflammatory transcription factor NF- κ B (nuclear factor kappa B), which is involved in the regulation of specific UPS genes. In particular, in skeletal muscle, NF- κ B induces the expression of a specific E3 enzyme (MURF1) that targets myofibrillar proteins and other factors involved in the myogenic process. NF- κ B has also been found to induce an increase in the production of certain pro-inflammatory cytokines, like *TNF* - α , which also appear to be involved in the development of muscle atrophy.

This evidence correlates ROS with overexpression and dysregulated activity of critical UPS components, specifically increased conjugation between ubiquitin and muscle proteins that causes decreased muscle mass [15] [21].

2. The second muscle protein degradation system is represented by Calpains. These are proteases activated by the presence of high calcium cytosolic (Ca^{2+}) levels and, in skeletal muscles, they are involved in the flaking of target proteins.

As mentioned in the previous section, high levels of ROS in the sarcoplasmic reticulum cause an increase in the release of calcium by the latter. Being Calpains activation Ca^{2+} -dependent, a consequence of this excessive release of calcium leads to Calpains over-expression.

This dependence of Calpains expressions on ROS has been confirmed by some studies which report that both ROS levels and Calpains over-expression can be controlled through antioxidant treatments [6] [21].

3. Muscle loss can also be attributed to the inhibition or malfunction of anabolic processes in favor of the catabolic ones.

The anabolic process includes all mechanisms that, starting from small molecules, synthesize more complex molecules which will then be cellular components.

Protein synthesis begins when insulin-like growth factor (IGF1), activated through phosphorylation of its receptor (IGRF), activates an enzyme (PI3K enzyme) that in turn activates protein kinase Akt and thus mTOR, which is the gene responsible for protein synthesis in skeletal muscle.

IGF1 is a growth factor involved precisely in the maintenance of the rate of synthesis-degradation of proteins, in fact, in addition to activating the process of protein synthesis is also involved in the inhibition of protein degradation operated by UPS.

The presence of ROS can inhibit the protein synthesis process by affecting the pathways involved: it has been said that ROS increases the production of proinflammatory cytokines such as TNF-alpha, which is a small protein responsible for the alteration of the PI3K / Akt pathway. An alteration of the PI3K / Akt pathway causes the inhibition of the anabolic process and therefore protein synthesis.

This relationship between the anabolic process and ROS was also supported by different studies that claim antioxidant treatments are a way to prevent Akt inhibition [21].

4. A further effect of ROS overproduction is the alteration of the process by which non-functional or damaged cellular components are degraded. This physiological process is called autophagy.

Autophagy is a fundamental cell turnover process that eliminates the non-functioning cellular components by encapsulating them in a vesicle called the autophagosome. Autophagosomes are double-membrane vesicles that fuses with lysosomes to degrade the non-functional components contained inside.

The mechanisms by which this process is influenced by ROS are still unknown, but some evidence indicates that these two phenomena are related. Some studies report that if the autophagy process is over-regulated, the level of ROS will increase. On the other hand, other researchers show that it is the increase in ROS production that leads to unregulated autophagy. It is therefore possible to think about the existence of a double directionality that connects these two phenomena.

Other studies suggest also that some signaling pathways are involved in the alteration of the autophagy process due to ROS presence, and an example is the alteration of pathways that regulate the autophagosomal formation [21].

5. Reactive oxygen species trigger also the beginning of a vicious circle inside

the mitochondrial functioning.

Proper mitochondrial function depends on a number of mitochondrial processes such as biogenesis, remodeling and fusion, and finally degradation (mitophagy) [21]. It was shown [20] that the alteration of the mitochondrial life cycle can lead to a decreased ATP production and an increased production of free radicals.

Furthermore, when ROS oxidizes the respiratory chain and the mitochondrial DNA, they cause DNA mutations and other alterations of proper mitochondrial functioning. In this way, a vicious circle begins because, as just said, non-functional mitochondria are also highly ROS productive. It is therefore of great importance to have an efficient mitochondrial turnover via mitophagy to prevent excessive ROS production and also to degrade non-functional mitochondria [20] [21].

Based on what has been reported above [6] [15] [20] [21], it is possible to say that all of these mechanisms are involved in muscle loss and are influenced by the presence of high levels of reactive species.

It is therefore possible to summarize that muscle degradation as a result of muscle disuse is caused by the oxidative stress condition that occurs within skeletal muscle tissue. Oxidative stress is the cause of the dysregulated relationship between the synthesis and degradation of the contractile proteins that comprise and characterize skeletal muscle. The presence of high levels of ROS increases the activity of the two main processes involved in protein degradation: the ubiquitin-proteasome system and Calpain. In addition, ROS are involved in the inhibition of the anabolic process involved in protein synthesis, autophagy and mitochondria malfunction. The malfunction of these processes caused by OS, triggers a vicious circle in which the malfunction of these processes can lead to further production of free radicals. It is clear that a proper redox balance is highly important to maintain the integrity of muscle tissue.

Release of ROS during the abovementioned processes is normally neutralized by the antioxidant defenses of living organisms. If the amount of ROS becomes greater than the cell capabilities in ROS scavenging, the administration of antioxidants is the only solution to prevent muscle oxidative damage [22].

1.2.4 Antioxidant defense system

This paragraph is concerned with describing the main antioxidant mechanisms used by cells to maintain redox homeostasis, explaining that endogenous antioxidants can be classified into enzymatic and non-enzymatic agents.

Exogenous antioxidant agents can be introduced into the body through the diet.

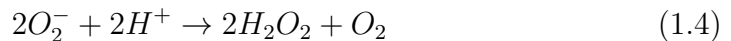
There are in fact many antioxidant principles of natural origin found in many foods. This section concludes by addressing the main issues related to antioxidant agents normally administered to counteract the condition of oxidative stress, which lead to take a nanotechnological approach as a solution to the problem.

An antioxidant is a molecule capable of preventing the oxidation of a substrate. Endogenous antioxidants are located both in cellular compartments such as organelles and cytoplasm, but also in the extracellular and vascular space.

Antioxidants act in a coordinated manner through different strategies to counteract the excessive production of free radicals. Among the different strategies to fight the reactive oxygen species (ROS), antioxidant enzymes act by catalyzing the reaction that transforms the reactive species into something less reactive. Instead, low molecular weight antioxidants, such as glutathione, uric acid and dietary antioxidant agents, act as scavengers by eliminating ROS [6].

A list of the major enzymes involved in counteracting excess reactive oxygen species is now presented.

1. Superoxide dismutase (SOD). It is the enzyme that protects against superoxide radicals (O_2^-) by dismutation in hydrogen peroxide (H_2O_2) and oxygen (O_2) [21] as indicated in the reaction below 1.4.



There exist three isoforms of SOD: SOD 1-2 and 3 located in the intracellular cytoplasmic compartment, in mitochondria, and the extracellular matrix respectively. The amounts of SOD present in skeletal muscle fibers differ among fiber types, and it has been shown that regular muscle exercise can promote SOD1 and SOD2 content in muscle fiber [6].

Abrigo et al. reports the result of an additional study showing a correlation between SOD1 deficiency and loss of muscle mass in mouse models indicating a possible involvement of this enzyme in muscle maintenance [21].

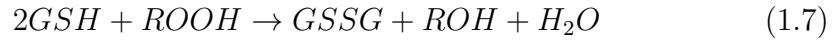
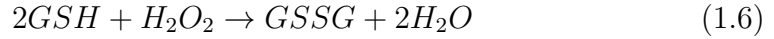
2. Catalase (CAT). Catalase is an enzyme present in the cytoplasm and mitochondria of muscle fibers that catalyzes, as indicate in the reaction 1.5, the breakdown of hydrogen peroxide to water and oxygen [6].



This enzyme uses iron as a cofactor, and enzymatic activity appears to be higher in oxidative myofibers when compared with fast glycolytic fibers. [21]

3. Glutathione peroxidases (GPX). It is a tetrameric enzyme with a higher affinity to hydrogen peroxide compared with Catalase [6]. GPX catalyzes the

reduction of hydrogen peroxide and also organic peroxides (ROOH) into water or ROH respectively via the oxidation of the Glutathione (GSH), which works as an electron donor and is oxidized to glutathione disulfide (GSSG).



Exist five types of GPXs that perform the same activity, but they differ in substrate specificity and localization within the cells. In all cases, given the functioning of GPX which requires GSH as an electron donor, it is important that cellular systems are able to regenerate GSH from its oxidized form GSSG. As for the other two enzymes, the content of GPX depends on the type of muscle fiber [6].

Together with the action of enzymatic antioxidants, another group of antioxidants acts to purify the cell from reactive oxygen species. They are called secondary or non-enzymatic antioxidants and some of the most non-enzymatic antioxidants of cells are bilirubin, uric acid, and coenzyme Q10 (ubiquinone). Among them, Glutathione (GSH) is the most important in the muscle fiber.

GSH is a tripeptide synthesized in the liver and transported to tissue by blood circulation. The concentration of GSH varies depending on the type of tissue, indeed, in tissue highly exposed to oxidant the concentration increases. GSH plays different roles as an antioxidant:

1. It can donate hydrogen to reactive spices.
2. It cooperates with the enzyme GPX to decompose hydrogen peroxide and organic hyperoxides.
3. It participates in the maintenance of the reduced state of other antioxidants like Vitamin C and Vitamin E.

Antioxidants can be uptaken also through alimentation. In this case, they are called dietary antioxidants and they are not synthesized by humans.

A few examples of dietary antioxidants are recalled in the following: the most studied is vitamin E, which is a lipophilic molecule synthesized from organisms that can be assumed through oils and seeds. More generally, the term vitamin E refers to 4 tocophenols and 4 tocotrienols. The antioxidant activity comes from the free hydroxyl group present on the structure. Being fat-soluble it resides in lipid membranes and lipoproteins and is therefore responsible for their protection against free radicals [6] [22] [23].

Vitamin C, also called ascorbic acid can scavenge some free radicals such as superoxide, and contribute also to the recycling process of vitamin E [6] .

Vitamin C is a water-soluble molecule that contains two hydroxyl groups disposed to donate an electron or a hydrogen atom from which derive the antioxidant capabilities.

Being water-soluble, vitamin C is found at high concentrations in tissues (2.5 mM), but it is also free in the bloodstream but at lower concentrations (from 20 to 85 μM). Vitamin C appears to have an excellent effect in protecting plasma lipids from free radicals, but being a reducing agent it may also have pro-oxidant activity. In fact, vitamin C, like hydrogen peroxide, can reduce transition metals through the Fenton reaction generating very reactive hydroxyl radicals (OH^\cdot). [6] [23] The carotenoids are lipid soluble antioxidants whose antioxidant capacity against superoxide ion and peroxidant derive from the particular structure composed of chains with conjugated double bonds. Being fat-soluble they too, like vitamin E, are located mainly in cell membranes [6].

Flavonoids are a class of polyphenolic compounds with functional hydroxyl groups able to scavenge free radicals or chelate metal ions. Flavonoids are polyphenolic compounds whose antioxidant properties derive from their ability to scavenge free radicals due to the particular conformational arrangement of functional hydroxyl groups. In particular, the configuration, the substitution and the total number of hydroxyl groups are the factors that determine the mechanisms of antioxidant activity of these compounds. In fact, flavonoids are involved in both scavenging and suppressing the production of reactive species [22]. Dietary antioxidants belong to the family of low molecular weight antioxidants and it is possible to consider vitamin C and vitamin E as important antioxidants to maintain redox homeostasis. Based on what said, antioxidants act through various mechanisms to prevent tissue oxidation by inhibiting the propagation or generation of free radicals. The effectiveness of an antioxidant lies in its ability to interfere with free radical chain reactions by donating an electron.

When the condition of oxidative stress is significant, it is necessary to intervene with the administration of antioxidant agents from outside. Current therapies involving the administration of low molecular weight antioxidants show some problems due to the short half-life of the antioxidant in the body, the lack of specificity of the target, and especially once neutralized a reactive species antioxidant activity ceases. These problems require administration of repeated doses to address the problem [4].

To overcome this problem, many studies are focusing on the development of nanotechnologies with antioxidant properties. Among the promising antioxidant nanotechnology solutions, this work will focus on cerium oxide nanoparticles [4]. Cerium oxide nanoparticles, also called nanoceria (NC), are highly biocompatible and are extremely interesting for their ability to mimic the activity of the two

enzymes superoxide dismutase and catalase. The characteristics and properties of these nanoparticles will be described in more detail in the chapter (Section 1.4).

1.3 Microgravity as mechanical stimulation to induce oxidative stress

Skeletal muscles easily adapt their morphology and cellular functions according to the variation of the stimuli and loads received [24].

Concentrating now on the loads exerted on the muscles, it must consider that all living beings have evolved by adapting to the presence of the constant load imposed by the force of gravity and it is clear that any slight alteration of this condition will cause alterations within the tissue [2].

Long periods of bed rest or immobilization are the conditions in which skeletal muscles suffer from the lack of load imposed by gravity. As presented in a previous section (Section 1.2.3), skeletal muscles suffer damage from the presence of reactive oxygen species following prolonged periods of inactivity. Another situation in which normal muscle loading is lacking is that experienced by astronauts during space travel. Several authors report a correlation between the loss of muscle mass that occurs upon return from space travel and the condition of oxidative stress [2] [3] [5].

The condition of weightlessness is called microgravity to indicate the value towards zero of the gravity vector [2]. This section will mainly focus on how the adaptation of biological systems to conditions of microgravity can induce changes in cell morphology and also in physiological processes.

The first subsection provides a list of the main devices used to simulate the microgravity condition in the laboratory. A more accurate description of the instrumentation used in this thesis project will be provided in Chapter 3 when the experimental set-up is described. In conclusion, since loss of muscle mass is the main problem detected after exposure to microgravity, the second subsection explains the changes observed in vitro on muscle cells after exposure to microgravity.

1.3.1 Devices to simulate microgravity conditions

In this section the main devices developed to simulate microgravity are examined. These devices are needed to overcome the problems due to practical difficulties, safety constraints but also the high costs encountered in conducting experiments in real conditions of microgravity in space [3][25].

These devices can be categorized into two groups: rotating walled vessels, and 2D

and 3D clinostats.

A first version of the rotating wall vessel (RWV) was developed by NASA with particular attention to fluid dynamics to try to minimize the generation of stress due to turbulence. It consists of a slowly rotating container filled with liquid into which cells fall constantly. The design of the device provides for maximizing the oxygenation of suspension cultures. The choice of rotational speed must be chosen appropriately to the weight of the suspended cells and the density and viscosity of the fluid. [26].

Among clinostats, an early version of the 2D clinostat is the rapid rotation clinostat (FRC). It consists of a series of rotating tubes with a millimetric diameter in which cell cultures are suspended. For correct functioning, the balance between fluid density, viscosity, and cell density is needed.

Studies with the FRC are limited at small samples because of the impossibility to make larger diameter tubes to avoid centrifugal forces generation that could damage cells. The rotation speed usually used space from 60 rpm to 90 rpm [26].

The 3D clinostat is another commonly used device. In this case, the machine is

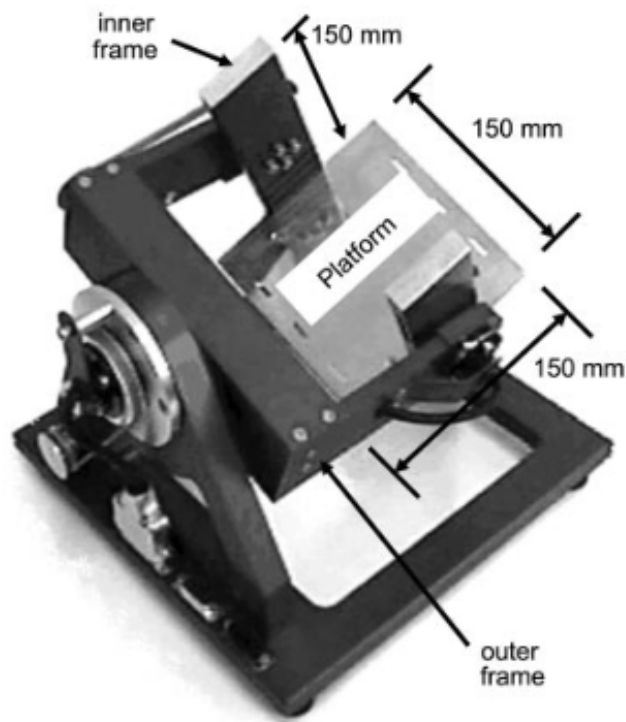


Figure 1.4: Random positioning machine components. Reproduced from S.J. Pardo et al. [27]

composed of two frames driven by two independent motors which ensure a smooth

speed rotation.

The subsequent development of this device consists of randomizing the direction of rotation of the two frames. The generated random motion gives the name of Random Positioning Machine (RPM) to this device.

The random positioning machine is composed, as shown in the Figure 1.4, of an external frame positioned perpendicularly to two parallel internal frames connected by a platform on which the sample is positioned. The two inner frames and the outer one are able to rotate independently in different directions and at different speeds to simulate the microgravity condition [26] [28]. The instrument is not able to remove the force of gravity but through the random movement makes sure that the sample placed on the central platform does not feel it. [27] Going into more detail, microgravity is generated through an algorithm that rotates frames randomly. The totally random movement allows for the continuous change of direction of the gravity vector from the point of view of the samples. These continuous changes of direction of the gravity vector allow obtaining an average of its value close to zero [29]. It is known from the literature that frames must rotate faster than the sample reaction time to prevent cells from feeling the influence of gravity if the gravitational vector points in a certain direction for long enough [26][25].

In order to achieve a good simulation of microgravity, it is essential to satisfy several constraints and find the most suitable experimental rotational conditions for the sample in question.

Correct positioning of the samples on the platform placed between the two inner frames is highly important to prevent side effects such as the generation of centrifugal accelerations. Centrifugal accelerations depend on the rotational speeds of the two frames and also on the position of the sample and provide exactly the opposite stimulus to the one we want to recreate with RPM. In an ideal condition where all cells are positioned in the center of rotation, the perceived centrifugal acceleration can be considered negligible [26] [29].

For this reason, also the RPM manual suggests that it is important to position the sample as close as possible to the center of rotation, possibly within a circumference with a radius of 22 mm. The constraint of having to place samples within this circumference leads to significant limitations in the size of samples that can be used.

Given the random rotation mode, the culture chambers must provide the ability to be sealed to prevent fluid leakage for the duration of the experiment. The need to seal filled culture chambers can lead to an additional stress due to the movement of air bubbles that can generate strange fluid movements causing shear stresses to the sample [29]. Therefore, the need arises to implement a good method to close the culture chambers to avoid trapping air bubbles inside during the sealing process and also to avoid as much as possible the formation of bubbles during rotation.

Another problem is the generation of turbulence within the fluid that can cause

shear stresses on the cells attached to the substrate. This problem can be solved by minimizing the volume of the culture chambers as much as possible.

The convenience of the RPM lies in its small size, which allows it to be placed inside an in vitro cell culture incubator, thus ensuring temperature, CO_2 level and humidity control [29].

In addition, the RPM allows three rotation modes. The first mode is the 2D

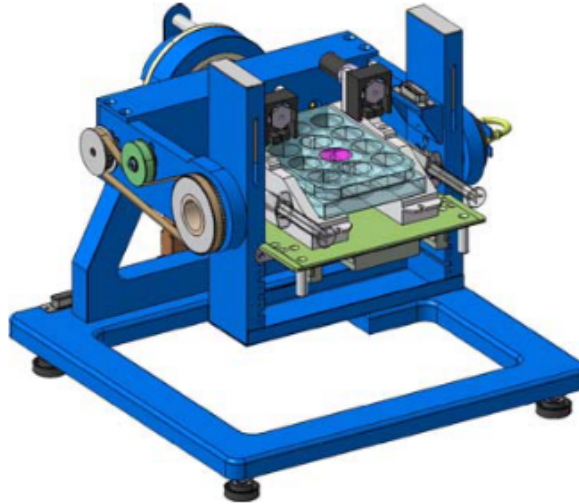


Figure 1.5: Schematic representation of the random positioning machine with samples placed on the central plate. Reproduced from A.G. Borst et al. [29]

clinostat mode in which only one of the two frames is set in motion and maintained at a constant speed. The second rotation mode is the 3D clinostat mode where the rotation of the second frame is added and the speed of both remains constant as well. However, this rotation mode does not guarantee symmetrical coverage of all possible orientations as it generates repetitive and predictable trajectories. As mentioned above to obtain a good simulation of microgravity, it is important that the biological system is unable to adapt to a condition of gravity, it is therefore necessary to introduce a random movement to fill all possible orientations. Therefore when the RPM is set to the random mode the two frames rotate in different directions, at different speeds ranging between a previously set minimum and maximum speed [29].

These devices are only suitable for simple biological systems such as cell cultures. Among the various limitations we find the difficult sample handling. Especially for RPM, sample preparation requires time, precision and manual dexterity. In addition, long-term experiments that require changing the spent cell medium are limited by the fact that such an operation is not possible without interrupting the

microgravity simulation. Imaging also cannot be performed without disrupting the continuity of the experiment.

Thus, among the various limitations and issues one can list the complicated sample handling, the number of usable samples that also limits the high data throughput, and most importantly the complicated fluid dynamics. The advantage of these devices lies in the fact that they can provide results to complete those obtained in the real condition of microgravity.

1.3.2 Effects of microgravity on muscle cells

Alterations at the level of the entire organism have been observed in astronauts returning from space and are comparable to conditions found in people suffering from degenerative diseases and also comparable to the aging process. It seems in fact that the effects of inactivity following space travel are similar to an increased aging process, with dysfunctions not only of the muscular system but also of the immune system, heart and bones [2].

A loss of muscle mass and strength is known to occur after only 5 days of spaceflight; during a short-duration space flight, the total loss is about 10-20% of the total muscle mass [1] [3]. The level of severity of this condition is highly dependent on the anatomical region and time of exposure to microgravity [5].

As seen in the previous section (1.3.2), muscle loss due to disuse is accompanied by the generation of high amounts of ROS. In this case, the production of ROS is not only due to muscular disuse but also to exposure to ionizing radiation that the spaceships are not able to shield. The intensity of the radiation depends on the proximity to the Earth and can generate reactive oxygen species within the tissues by radiolysis of water [3].

In the literature [1][2][5] there are several *in vitro* studies in simulated microgravity conditions aimed at finding solutions to problems related to the condition of oxidative stress that aggravates the level of atrophy.

The immortalized cell line of murine myoblasts (C2C12) is considered a good model for *in vitro* muscle testing because of its high proliferation rate and good ability to differentiate into myotube under appropriate culture conditions producing many proteins and mRNAs also present in the human muscle tissue [2].

Considering the results of the study conducted by D.Calzia et al, it seems that the proliferation rate of these cells is not affected by weightlessness. On the contrary, a positive proliferation rate was found in cells exposed to microgravity by using a random positioning machine. On the other hand, regarding the process of differentiation from myoblast to myotube, a delay in the process is observed when comparing cells exposed to microgravity with control cells left in normal gravity [2].

The more rapid proliferation of myoblasts was also found in another study where, however, microgravity was simulated with a 3D clinostat [1].

In three different studies [1][2][30] conducted on differentiated C2C12 cells, they showed the presence of oxidative stress, an increase in the expression of autophagy-related genes that exposure to microgravity, and alterations in parameters indicative of cellular metabolic status after exposure to simulated microgravity. In these three studies, the gravity condition was simulated with different instruments, leading to the suggestion of consistency in the data found.

Thus, the presence of oxidative stress [2], increased expression of genes related to autophagy and muscle atrophy [1][5][30], and reduced calcium content in the membrane probably due to increased calcium content in the intracellular space [2] are all findings in line with what was said in the previous chapter regarding ROS dependence of cellular mechanisms contributing to muscle loss. To confirm this possible connection between microgravity exposure and muscle loss, a research group compared the expression of the key mRNAs involved in protein synthesis and those in autophagy. They found an increased expression of autophagy markers and a low expression of those genes involved in protein synthesis [5].

In conclusion, in light of these precedent in-vitro studies about the effect of the absence of gravity on C2C12 cell line it is possible to summarize the following common effects:

1. The proliferation rate is not affected by microgravity but on the contrary, some studies report an increased rate if compared with cells in normal gravity condition.
2. The myoblasts' differentiation process seems to be slowed down.
3. The presence of higher levels of reactive oxygen species in the tissue was reported.
4. It was seen as a decreased protein synthesis due to the abnormal activation of the autophagy and catabolism processes.

It is therefore evident that muscle adaptation to the absence of gravity causes alterations in many cellular processes and the resulting muscle loss seems to be related to the excessive production of reactive oxygen species due to muscle disuse. Considering that oxidative stress is a common feature in different muscular pathologies, there is the need to develop accurate in vitro models to find solutions to prevent oxidative damage, not only for astronauts but also for patients on earth suffering from muscle atrophy.

1.4 Cerium oxide nanoparticles: a nanotechnological approach for the treatment of oxidative stress

Given the main causes of the oxidative stress condition, and given the problems of conventional antioxidant therapies, this last section aims to introduce a nanotechnological approach as a solution to the problem.

In the first subsection is briefly proposed the state of the art about nanotechnology with antioxidant capabilities to get to explain why the interest is posted on cerium oxide nanoparticles, also called Nanoceria.

After describing the characteristics and properties of cerium oxide nanoparticles, this introductory chapter concludes by describing the applications of Nanoceria already under study in the field of nanomedicine.

1.4.1 Antioxidant nanotechnologies: state of the art

Current therapies with low molecular weight antioxidants or the administration of free or encapsulated antioxidant enzyme show some limitations due to their short half-life within the organism and the lack of specificity to the target.

Another limitation of traditional antioxidants lies in the fact that once the reactive species has been neutralized, the antioxidant activity stops. This limitation requires the necessity to administrate more antioxidant doses to reach the target with the right concentration of antioxidants.

In light of these problems, many studies are focusing on the development of nanotechnologies with an antioxidant activity more similar to that of enzymes, where once one cycle of action is completed, another begins thus limiting the administrations.

Among the proposed solutions there are two types of synthetic antioxidant nanoparticles: nanoparticles used as transporters, loaded with natural antioxidants, and nanoparticles with their antioxidant activity [31].

An example understudy of the first type of nanoparticles includes the solid lipidic nanoparticles (SLN) that carry the antioxidant principle protecting it from blood clearance and keeping it in circulation for a longer time directing towards the specific target [32].

Akram Ahangarpour et al. [32] conducted a study with SLNs loaded with a naturally occurring antioxidant agent, Myricitrin, to evaluate the effects on type 2 diabetes mellitus. The nanoparticles were shown to improve the diabetic condition and hyperglycemia, the cause of free radical overproduction, both in vitro and in vivo.

On the other hand, examples of nanoparticles with intrinsic antioxidant capacity

are gold and silver nanoparticles.

All of these examples are under study for different applications and the treatment of different diseases. For example, AgNP have been tested to treat diabetes complications caused by oxidative stress, showing significant benefits in the scavenging of reactive oxygen species [33].

Another promising nanotechnology with antioxidant properties involves this time organic nanoparticles: polydopamine nanoparticles.

Polydopamine, is widely known for its adhesive properties but also seems to be a promising antioxidant agent. In the study performed by Xingfu Bao et al. [34] the ability of polydopamine to fight oxidative stress in dental diseases and reduce the inflammation process *in vivo* is shown.

Among the promising antioxidant nanotechnologies solutions, this work will focus on cerium oxide nanoparticles, also called Nanoceria.

Nanoceria is highly biocompatible and extremely interesting due to its ability to mimic the antioxidant capabilities of the two main antioxidant enzymes in the human body: superoxide dismutase (SOD) and catalase (CAT). The interesting feature lies in the particular crystal structure of the nanoceria that gives a biomimetic antioxidant activity that is regenerated at the end of the cycle of red-ox reactions [35].

1.4.2 Cerium oxide nanoparticles

Cerium oxide (CeO_2) is a rare earth compound that belongs to the lanthanide metals [36]. The resulting nanoparticles, Cerium oxide nanoparticles, also called Nanoceria (NC), exhibit at the nanoscale a particular crystal structure that confers interesting catalytic capabilities [37].

Indeed, at the nanoscale Nanoceria exhibit a cubic fluorite structure in which can coexist both the trivalent and the tetravalent state of cerium, Ce^{3+} and Ce^{4+} [38]. The presence of the trivalent state creates a charge deficit that is compensated by the presence of oxygen vacancies in the crystal structure.

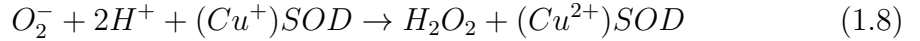
Oxygen vacancies provide active sites for redox reactions giving the nanoceria the ability to absorb and release oxygen molecules through the redox cycle between the Ce^{3+} and Ce^{4+} ion couple [36] [31].

This ability to rapidly change the valence state from trivalent to tetravalent thanks to the low reduction potential (1.52 V) [31] of the Ce^{3+} / Ce^{4+} pair, confers the nanoparticles high catalytic performances that allow the use in different fields of application from oxygen sensors, oxide fuel cells to ultraviolet absorbent [37] [31]. As for applications in the biomedical field, the nanoceria has aroused particular interest thanks to the Ce^{3+} / Ce^{4+} pair which confers the nanoparticles biomimetic properties [35].

The biomimetic activity concerns the activity of the two main antioxidant enzymes of biological systems, Superoxidismutase (SOD) and catalase (CAT).

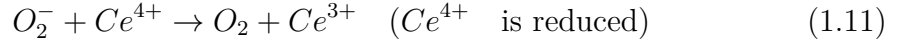
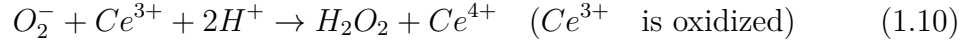
Nanoparticles with a high ratio of trivalent to tetravalent states, thus nanoparticles having a predominance of Ce^{3+} , are mimetic of SOD. The trivalent state of cerium (Ce^{3+}) acts by mimicking the SOD enzyme through the reduction of the superoxide ion (O_2^-) into H_2O_2 through a two-step catalytic dismutation reaction, while the nanoceria oxidizes from Ce^{3+} to Ce^{4+} [36] [31].

The SOD enzyme neutralizes O_2^- by removing or donating electrons to it as shown in the dismutation reactions below [36].



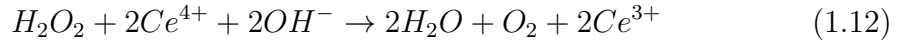
In the first step, SOD, by oxidizing, acts by removing an electron from O_2^- generating H_2O_2 . In the second step, the oxidized SOD donates an electron to a new O_2^- molecule by reducing and generating an O_2 molecule. This second step regenerates the reduced form of the SOD enzyme so that the ration cycle can start again [36] [31].

The mechanism of action of the nanoceria is similar to that just described. The process is made self-regenerating thanks to the redox couple Ce^{3+} / Ce^{4+} acting in a SOD-mimetic way [36].



Looking at these reactions, it is clear that high amounts of Ce^{3+} lead to an overproduction of many H_2O_2 molecules that are much more dangerous than O_2^- itself because reacting with metals through the Fenton reaction, they produce even more dangerous reactive species [36].

Therefore, the presence of the tetravalent state of cerium on the surface of the nanoparticle is necessary to neutralize H_2O_2 . The reduction from Ce^{4+} to Ce^{3+} induces the oxidation of H_2O_2 to molecular oxygen (O_2) and water as the activity of the enzyme catalase [36].



It is therefore important that the ratio between the Ce^{3+} and Ce^{4+} ions is adequate to avoid pro-oxidant effects due to a high Ce^{3+}/Ce^{4+} ratio and give the nanoparticles antioxidant and regenerative capabilities. It is the ability to interchange between the Ce^{3+} and Ce^{4+} state which makes the antioxidant properties of the nanoparticles

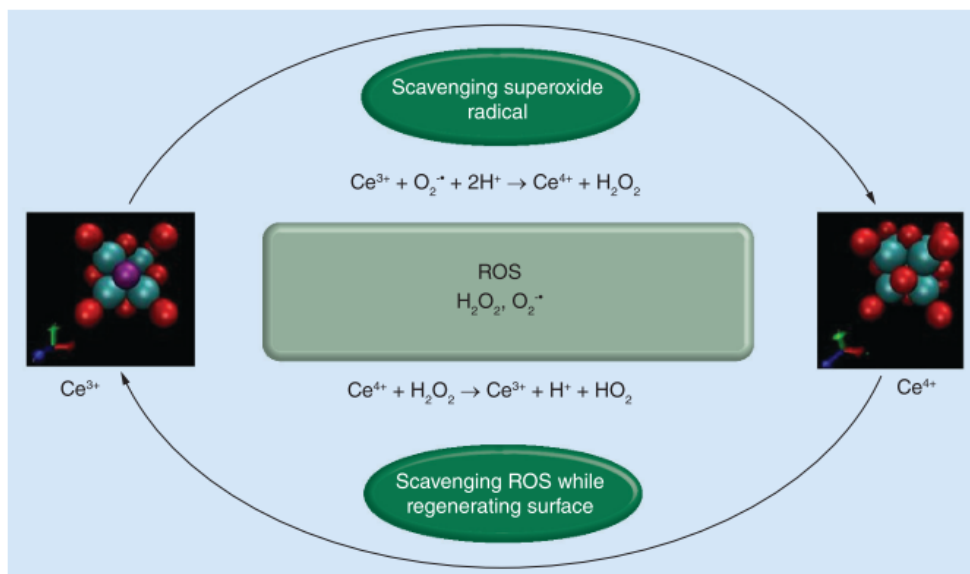


Figure 1.6: Schematic representation of the mechanism of action against free radicals of the nanoceria: ROS scavenging and surface regeneration properties. Reproduced from S.Das et al. [31]

regenerative [35][36].

Figure 1.6 shows a schematic representation of the mechanism of action against free radicals of the nanoceria comparing it with the situation of oxidative stress that occurs in the absence of antioxidant agents.

Since the antioxidant behaviour of the nanoceria, and thus its catalytic properties, depend critically on the purity of the reagents, the synthesis procedure, the functionalization of the NP, it is of great importance to evaluate the final application field to choose the most suitable synthesis method to obtain nanoparticles with the desired properties.

Cerium oxide nanoparticles, according to data in the literature [36] [38] [39], can be synthesized through several processes including aqueous precipitation, solvothermal methods, microemulsion, and sol-gel.

In any case, it is important to control the nucleation and growth rates, which are the two steps of the nanoparticle crystallization process that determine the final result of the synthesis. These two steps are controlled through the selection and concentrations of precursors, use of stabilizing agents, solvent type, reaction duration, reaction temperature, etc. Thus, by controlling the reaction parameters, it is possible to selectively produce cerium oxide nanoparticles with desired properties [36].

The size of the nanoparticles is a particularly important feature in the biomedical field as nanoparticles have to interact with biological components [38]. As the size decreases, the ratio between surface and volume increases changing the catalytic activity of nanocerium. Increasing the surface-volume ratio increases the number of oxygen vacancies on the surface that enhance oxygen movements and therefore the red-ox activity [38]. Smaller nanoparticles have higher Ce^{3+} concentrations than those with a larger size. Consequently, it is possible to say that the antioxidant capacity of cerium oxide nanoparticles is size-dependent [38].

Among the synthesis parameters, temperature is the one that most determines the size of the final products. The size of the nanoparticles increases with temperature and reaction time, in fact the synthesis of nanoparticles at high temperatures does not allow the production of homogeneous particles [31].

The morphology of nanoparticles is quite important to satisfy the biocompatibility requirement. In fact, nanoparticles with sharp edges can damage the membrane of the cells with which they interact [38].

The main problem with the use of nanocerium in the field of nanomedicine is its lack of stability in aqueous suspensions, and therefore in physiological environments, where nanoparticles tend to form aggregates [38].

When nanoparticles aggregate their size becomes larger and therefore the surface-to-volume ratio decreases giving the nanoparticles a lower antioxidant activity. In addition, when administered in vivo, the formation of nanoparticle aggregates could have side effects or even be toxic due to accumulation in organs such as the spleen and kidneys [39].

To overcome the problem of poor stability, surfactants are widely used today as stabilizing agents to coat nanoparticles and increase their stability in suspension. Compared to uncoated nanoparticles, the presence of a surface coating significantly changes the chemical composition of the surface and the surface electrostatic charge of the nanoparticles affecting their aggregation rate [39].

A further parameter to be considered to improve the stability of the nanocerium is the synthesis temperature. Low temperatures not only have an important effect in determining the size of the nanoparticles but also affect the stability of the final product. Indeed, when compared with nanoparticles synthesized at high temperature, those at low temperatures show a lower tendency to aggregate [38]. Due to the complex chemical structure of cerium oxide nanoparticles, based on the properties of sintered nanoparticles, beneficial effects have been observed, thus antioxidant, but also cytotoxic and pro-oxidant effect. As mentioned above, a high presence of the trivalent state on the surface of the nanoparticles can have beneficial effects, thus SOD mimetic, but also harmful effects leading to excessive production of ROS. This evidence, therefore, suggests that it is of considerable importance to accurately characterize the newly synthesized nanoparticles [36].

1.4.3 Cerium oxide nanoparticles applications in nanomedicine

The self-regenerating antioxidant properties of cerium oxide nanoparticles have attracted considerable interest in the biomedical field as they represent a promising strategy for the healing of numerous oxidative stress-related pathologies [38]. In vitro and in vivo experiments have been performed to evaluate the tolerability and antioxidant activity of cerium oxide nanoparticles in various ROS-related pathologies on different cell types such as cardiac, neuronal and stem cells [37] [31]. This section lists the potential developing applications of nanocerium in the field of nanomedicine.

As for neural cells, nanocerium is a promising protective agent that can be used to treat neurodegenerative diseases such as Parkinson's and Alzheimer's, but also to treat ischemias.

A study conducted by G.Ciofani et al. [37] on a representative model of dopaminergic cells (PC12 cell line) shows improved neural differentiation with longer neurites and increased dopamine secretion in cells treated with NC for three days. The antioxidant capacity of the nanocerium was evaluated by comparing cells incubated with a pro-oxidant agent and nanocerium and cells with the pro-oxidant alone. The amount of reactive oxygen species decreases by 20% in samples treated with cerium oxide nanoparticles, and a decreased level of basal ROS was also seen in cells not treated with the oxidant agent. In this study, the antioxidant properties of the nanocerium were also evaluated at the gene level where downregulation of the genes involved in the antioxidant defences was observed perhaps to compensate for the strong antioxidant effect due to the presence of the nanocerium [37].

Instead, a correlation between oxidative stress and adiposity was shown in a study conducted by A.Rocca et al. [35] in which it was found that ROS, acting as cellular messengers, are involved in the process of adipogenesis. It seems that the presence of reactive oxygen species promotes the maturation of adipocytes although the mechanisms by which this occurs are not yet clear.

The potential antioxidant effects of nanocerium was therefore studied to limit the differentiation of mesenchymal stem cells into adipocytes. A good interaction between cerium oxide nanoparticles and mesenchymal stem cells was found, demonstrated by the high internalization of the nanoparticles. At the gene level, down-regulation of all adipogenic genes was found in NC-treated cells compared to untreated cells. In particular, the reduced transcription of the *Creb1* gene required to induce adipogenesis is significantly downregulated. This gene is activated by the presence of reactive oxygen species, so the antioxidant activity of nanocerium seems to have a significant effect in limiting adipogenesis. It was also found that the activity of the main enzyme involved in the differentiation of mesenchymal cells into adipocytes (G3PDH) is markedly reduced when the nanocerium is administered to the cells inhibiting the adipocytes maturation. All these results confirm the antioxidant

activity of cerium oxide nanoparticles in the prevention of adipogenesis [35]. Another application in the field of nanomedicine sees the use of cerium oxide nanoparticles as an anti-cancer agent. In this case the pro-oxidant effects of these nanoparticles are exploited. Z. Diacoeasa et al. [40] showed a different interaction of nanoceria depending on the cell line used for in vitro studies. It seems that internalization is favored in the case of tumor cells treated with nanoceria. On the contrary, with healthy cells, the internalization seems to stop at the level of the cell membrane. Furthermore, comparing the amount of free radicals produced after treatment with nanoceria between tumor cells and healthy cells, an increase of free radicals was shown only in samples with tumor cells [40].

Other promising applications of cerium oxide nanoparticles under study concern:

1. Eyes diseases where the endogenous redox-defences produce a higher percentage of ROS.
2. In regenerative medicine where Nanoceria incorporated in scaffolds or used directly in wound healing can promote tissue regeneration reducing the ROS produced during cell growth and differentiation.
3. Nanoceria has also a protective activity against radiation toxicity. Radiation is widely used for the treatment of circumscribed tumours. The problem with this type of treatment lies in the inability to differentiate malignant from healthy tissue, so the tissues adjacent to the tumour are damaged by radiation.

Given the potential, problems and possible negative aspects of the use of these nanoparticles as antioxidant agents in the field of nanomedicine, this thesis work aims to investigate whether this type of nanoparticles can guarantee the maintenance of conditions/performance of muscle tissue in conditions of muscle discharge, such as weightlessness.

Chapter 2

Aim of the project

In the literature, changes in gravity conditions are known to be associated with increased production of reactive oxygen species within muscle tissue [2] [3] [4] which motivates the elaboration of antioxidant countermeasures of compelling need in order to enable long-term human permanence in altered gravity condition.

Therefore, this thesis project was carried out with two main objectives: the evaluation of the interaction between cerium oxide nanoparticles and muscle cells under simulated microgravity conditions and then the assessment of the magnitude of oxidative stress induced by simulated microgravity to investigate the potential antioxidant effect of nanocerium.

The first objective consisted into the elucidation of the interaction between cerium oxide nanoparticles and muscle cells in simulated microgravity conditions. To the purpose, cerium oxide nanoparticles were synthesized and characterized by using different techniques, including DLS, XPS, TGA and TEM. In particular, the antioxidant property of the nanocerium was evaluated through a direct and an indirect method. The direct method was based on a colorimetric assay and photometry for expression of the antioxidant capacity of cerium oxide nanoparticles in terms of an analogue of Vitamin E, as a reference antioxidant. The indirect method involved cell culture. The antioxidant capacity was assessed directly on the cells, maintained at normal gravity, after the administration of a pro-oxidant stimulus.

The internalization of the nanoparticles was evaluated after checking that the induced stimulus and the chosen experimental setup were suitable for cell survival. A cell viability test was then performed, both on cells treated with nanocerium and not, after 48 hours of exposure to simulated microgravity.

Finally, the interaction between the cells and the material was evaluated both by confocal microscopy and by spectroscopy analysis.

The second objective of this project was to investigate whether the nanocerium can reduce or prevent the oxidative stress induced by the stimulus imposed by the

random positioning machine (RPM). Therefore, once the internalization of the nanoparticles in simulated microgravity was confirmed, several experiments were carried out to evaluate the extent of the oxidative stress induced by the simulated microgravity and to evaluate the antioxidant capacity of nanoceria.

Chapter 3

Materials and Methods

This chapter reports on all the reagents, materials, methodologies and instruments used to carry out the project. All the techniques adopted for the synthesis and characterization of cerium oxide nanoparticles, the cell culture techniques, the microgravity experimental setup (i.e., the tools to simulate weightlessness), and the experiment performed are described. The chapter also presents a description of experiments performed to investigate the interaction between cerium oxide nanoparticles and muscle cells in microgravity.

3.1 Materials

3.1.1 Chemicals

The reagents used in the synthesis of cerium oxide nanoparticles (NC) are ethylene glycol (*Fluka analytical*, 99.5%), ammonium hydroxide solution (*Carlo Erba Reagents*, 30% ammonia solution), cerium (III) nitrate hexahydrate ($Ce(NO_3)_3 \cdot 6H_2O$) (*Sigma-Aldrich*). Nanoparticle stabilization in aqueous medium was conducted with fetal bovine serum-FBS (*Gibco*).

The reagents used to determine the antioxidant capacity of the nanoceria are part of the ‘Total antioxidant Capacity Assay kit’ (*MAK187*, *Sigma-Aldrich*) which contains: Cu^{2+} solution (*MAK187A*, *Sigma-Aldrich*), assay-diluent (*MAK187B*, *Sigma-Aldrich*) and Trolox Standard (*MAK187D*, 1 μ M, *Sigma-Aldrich*). To prepare the Trolox standard solution Dimethyl sulfoxide-DMSO was used.

Polydopamine nanoparticles were synthesized in the IIT lab by another group as indicated in their work [41].

To compare the antioxidant capacity of NC with natural antioxidants, ascorbic acid, curcumin and resveratrol (*Sigma-Aldrich*) were used to prepare aqueous solutions. Cells were cultured in high glucose Dulbecco’s Modified Eagle’s Medium (DMEM)

(*Gibco*, 4.5 g glucose) enriched with 10% fetal bovine serum (FBS), 1% penicillin and streptomycin (PS) (*Gibco*, *Pen-Strep*) and 1% sodium pyruvate (*Gibco*).

To fabricate the cell culture chambers suitable to 3D clinorotation, a Versalaser (*Universal laser system -TBH*), polydimethylsiloxane (PDMS) (*SYLGARD 184-DOWSYL*), and CorelDRAW software were used.

To process cells, a Dulbecco's Phosphate Buffered Saline (PBS), (*Gibco*) solution with and also without Calcium and magnesium was used.

To perform cytotoxicity tests and evaluate the percentage of nucleic acids present in the samples, the PicoGreen assay was used.

Tert-butylhydroperoxide-TBH (7.7 M) was used as a pro-oxidant agent.

CellROX Green Flow cytometry assay kit (*ThermoFisher Scientific*) was used to assess the extent of oxidative stress in live cells.

3.1.2 Cell lines

The immortalized cell line of murine myoblasts (C2C12 cell line) and primary human skeletal myoblasts (HSkM) were used for *in vitro* studies as skeletal muscle models.

3.1.3 Instruments

For cerium oxide nanoparticles synthesis, a magnetic stirrer equipped of a thermal couple for temperature control was used.

For nanoparticles characterization, Zeta-Sizer Nano (*Malvern Instruments, Malvern*) was used to measure nanoparticles size and z-potential.

To measure the absorbance peak in the antioxidant assay, a spectrophotometer (*Victor3, PerkinElmer*) was used.

To simulate the microgravity condition a random positioning machine (RPM) (*Airbus*) was used.

For flow cytometry analysis, the CytoFLEX (*Beckman Coulter*) flow cytometer was used.

3.1.4 Materials

Petri dishes were used to propagate cell cultures and to obtain the cell adhesion surface to be inserted into the homemade circular culture chambers.

Thermanox slides treated for cell culture were used to cover the bottom of the homemade PDMS cell culture chambers.

PCR films (*BIORAD*) were used to seal off the homemade PDMS cell culture

chambers.

3.2 Synthesis of cerium oxide nanoparticles

This section describes the process adopted for the synthesis of cerium oxide nanoparticles (nanoceria, NC) and the coating strategy used to improve the stability of the nanoparticles in the solution.

Several methods to synthesize cerium oxide nanoparticles are reported in the literature, such as electro-thermal, microemulsion, hydrothermal etc [36] [38] [39]. In general, a soluble precursor of cerium, containing the Ce^{3+} ion, oxidizes to cerium oxide (CeO_2), containing the Ce^{4+} ion.

In this work, cerium oxide nanoparticles were synthesized by direct precipitation. Chemical precipitation is commonly used as a method for producing nanoparticles [39]. The precipitation of solid nanoparticles occurs as a product of the reaction between the cerium precursor salt and a base.

Ethylene glycol was used as a synthesis cofactor in the NC synthesis. It has the advantage of increasing the solubility of inorganic salts and is therefore used to control the homogeneity of the reaction.

The direct precipitation synthesis process was adapted from the literature (Caputo et al. [39]). This process was conducted as described in the following:

1. 7.8 ml of ethylene glycol (99.5 %) was mixed with 92 ml of deionized water (MQ water) in a round-bottomed flask placed on a magnetic stirrer to maintain the reaction temperature at 50 °C.
2. Once the reaction temperature was reached, 5.16 g of Cerium(III) nitrate hexahydrate ($Ce(NO_3)_3 \cdot 6H_2O$) were added to the solution.
3. Direct precipitation of ceria salts was induced using ammonia as a strong base: 4.7 ml of ammonia solution (30%) were added dropwise to the reaction while maintaining agitation between 200 and 300 rpm for 1 hour. Earlier ammonia addition provokes a change in color towards yellow. At the end of the reaction time, the color of the reaction product was light grey.
4. Three washing cycles were then carried out with ultrapure water by centrifugation until a neutral pH was reached in the supernatant. To promote nanoparticle precipitation, centrifugation was performed for 20 minutes at 7983 RCF at low temperature (4°C).

As mentioned in the previous chapter (1.4.2), the temperature is the synthesis parameter that mostly influences the antioxidant properties of the final product.

To investigate the influence of this parameter the synthesis of nanoceria was carried out both at 50 °C and 80 °C.

The obtained cerium oxide nanoparticles were freeze-dried overnight, weighed with precision balance and subsequently resuspended by sonication (8 W, with a Bandelin tip sonicator) in ultrapure water at a concentration of 10 mg/ml for 2 min. The obtained nanoparticle dispersion was stored at +4°C until use.

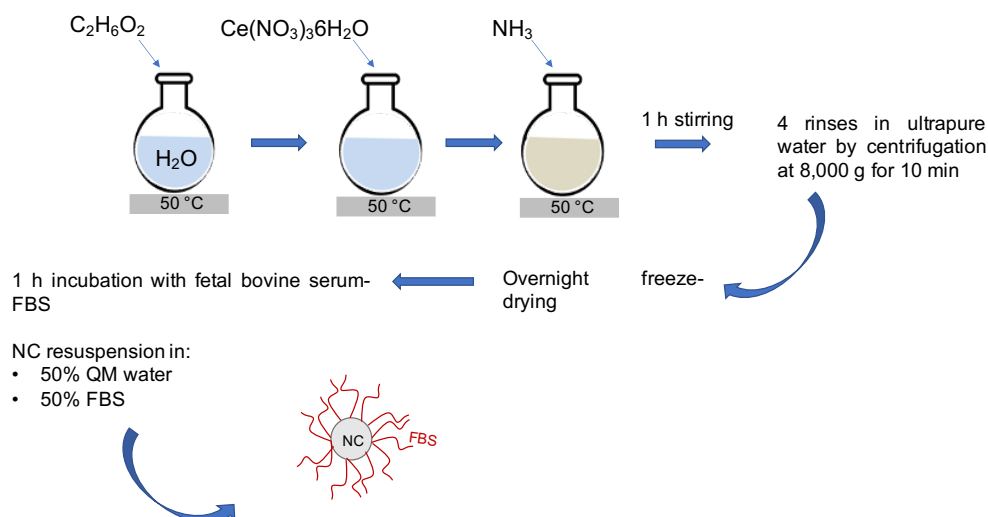


Figure 3.1: Schematic representation of the synthesis and coating process of cerium oxide nanoparticles by direct precipitation using ethylene glycol as reaction cofactor.

As mentioned in the previous chapter (1.4.2), cerium oxide nanoparticles in water solution undergo undesired aggregation and precipitation. To prevent this, nanoparticle dispersion was stabilized by 30 min incubation with FBS under mild shaking (100 rpm). This incubation ensured that the proteins contained in the serum were adsorbed on the surface of the nanoparticle.

3.3 Nanoparticle characterization

This section deals with the characterization performed on cerium oxide nanoparticles.

Characterization of the nanoparticles was performed by the techniques described in the Appendix A. Size and Z-potential value were evaluated by using dynamic light scattering, whereas the chemical composition was evaluated by using X-ray photoelectron spectroscopy. Characterization was performed both on IIT-synthesized

nanoparticles and on commercial nanoparticles (*Sigma-Aldrich*) for comparison.

3.3.1 Transmission electron microscopy (TEM)

At the end of the synthesis process, nanoparticles were imaged by TEM with the support of the IIT Electron Microscopy Facility in Genoa.

TEM imaging was conducted on 1 μM nanoceria dispersions in different aqueous media:

1. Uncoated NC dispersed in ultrapure water.
2. FBS-coated NC dispersed in ultrapure water.
3. FBS-coated NC dispersed in ultrapure water added with 10% FBS.

3.3.2 X-Ray Diffraction (XRD), X-Ray Photoelectron Spectroscopy (XPS) and Thermogravimetric Analysis (TGA)

Nanoceria samples underwent extensive characterization in terms of chemistry, crystallinity and thermal analysis with the support of the IIT Materials Characterization Facility in Genoa. To the purpose, 1 mg of freeze-dried nanoparticles (both uncoated and FBS-coated) were prepared.

Chemical composition was assessed with XRD and XPS analyses on uncoated particles. Thermal analysis was conducted on both uncoated and FBS-coated nanoparticles with TGA.

XRD analysis was performed with a Rigaku SmartLab X-ray diffractometer. Diffraction patterns were collected in Bragg-Brentano geometry over an angular range (2theta) between 20° and 100°, with a step size of 0.02° and 0.05°. Measurements were conducted at room temperature, using a zero-diffraction silicon substrate.

XPS analysis was performed with a *KratosAxisUltra^{DL}* spectrometer (*Kratos Analytical Ltd.*) using a monochromatic Al K source ($h = 1,486.6$ eV) operated at 20mA and 15kV. Wide scans were performed with a pass-energy of 160 eV and energy step of 1 eV, while narrow scans were conducted with a pass-energy of 10 eV and energy step of 0.1 eV. The Kratos charge neutralizer system was used for all measurements. Spectra were analyzed with CasaXPS software (Casa Software, Ltd., version 2.3.22).

TGA analysis was conducted with a TA instruments Q500 thermogravimetric analyser under a nitrogen flux with a 50 ml/min flow rate. The samples were analyzed by equilibrating the temperature at 30°C for 5 min to stabilize the weight and then heating ramps of 5 °C/min up to a maximum temperature of 1000 °C were performed. For the analysis, 5.84 mg of nanoceria were used.

3.3.3 Size and Zeta Potential measurements

This section describes the characterization performed with Zeta-Sizer Nano (*Malvern Instruments, Malvern*) by measuring the hydrodynamic diameter, the polydispersion index (PDI) and the zeta potential by dynamic measurement of light scattering (DLS).

Measurements were performed at physiological temperature (37 °C) and an NC concentration of 100 $\mu\text{g/ml}$ for all samples.

The evaluation of the size distribution was carried out under the conditions listed below:

1. Uncoated nanoparticles in ultrapure water (MilliQ).
2. Coated Nanoparticles suspended in MilliQ water.
3. Coated nanoparticles suspended in MilliQ water enriched with 10% FBS.
4. Coated nanoparticles suspended in DMEM cell culture medium enriched with 10% FBS.

The same dispersions were used for the measurement of the Z potential, except for the last one. The rich composition of conductive species of dispersion 4 indeed hindered a correct measurement of nanoparticle surface charge.

For all the listed conditions, the measurement of the size of the nanoparticles was performed on 1.5 ml samples in cuvettes for the DLS analysis. For each sample, the instrument was set to perform four readings and each reading was composed by an automatic number of runs based on the goodness of the sample.

Zeta potential measurements were conducted with 0.7 ml samples positioned in special electrode-provided cuvettes enabling the quantification of the difference in potential between the nanoparticle surface and their liquid dispersant. In this case, three runs of measurements were performed, each one with at least 10 readings.

The long-term colloidal stability of cerium oxide nanoparticle dispersions was also evaluated. To the purpose, measurements were done every two days for two weeks on both nanoparticles maintained at normal gravity and in microgravity. In both cases, the cuvettes were fully filled with nanoparticle dispersions and were sealed to prevent medium oxidation, in order to precisely to mimic the experimental conditions applied to cell cultures during spaceflight.

3.4 Total antioxidant capacity

Nanoceria antioxidant capacity was quantified photometrically by using a colorimetric test relying on Cu^{2+} ion reduction. To the purpose, the Total Antioxidant

Capacity Assay kit MAK187 from Sigma-Aldrich was used. This assay provides the antioxidant capacity of the substance tested in Trolox equivalents (number of moles, n.mol). Trolox is a vitamin E analogue and is used in this assay as a control condition.

A standard curve was obtained by preparation of a 1 mM Trolox solution in 20 μ l of DMSO and 980 μ l of ultrapure water and following dilutions as recommended by the manufactures. To obtain the standard curve, 0, 10 and 20 μ l of 1mM Trolox standard were diluted with ultrapure water up to a volume of 100 μ l. A working copper solution was prepared by performing a 1:50 v/v dilution of the Cu^{2+} -containing stock with the provided Assay Diluent.

The antioxidant capacity was investigated for:

1. 10 mg NC IIT synthesized at 80 °C
2. 1 and 5 mg NC IIT synthesized at 50 °C
3. 10 mg NCsigma (Sigma-Aldrich)
4. 10 μ g of polydopamine nanoparticles synthesized in the IIT lab by another group.
5. 2 mg of natural antioxidants: Ascorbic Acid, Curcumin and Resveratrol.

Each sample (standard, nanoparticles and soluble antioxidants) was incubated with 100 μ l of the copper working solution for 90 min at room temperature in the dark. At the end of the incubation time, samples were centrifuged in order to precipitate nanoparticles that could interfere with absorbance reading with a Victor X3 photometer, and supernatant were collected and underwent absorbance measurement at 570 nm. Each sample was assayed at least in duplicate.

3.5 Microgravity simulation: experimental set-up

This section describes the experimental setup to study the interaction between cells and nanoparticles under mechanical unloading. A random positioning machine - RPM (*Airbus*) was used as a platform to simulate microgravity by 3D clinorotation.

As shown in the Figure 3.2, the instrument core consists into two frames capable of rotating independently at different speeds and in different directions to simulate microgravity. The inner frame presents a central plate working as a sample holder. A controller and a laptop computer equipped with a dedicated software complete the setup.

Correct positioning of the samples on the central plate is critical to the prevention



Figure 3.2: Random positioning machine - RPM (Airbus RPM2.0).

of the generation of undesired acceleration loads. The latter depend on the rotation speeds of the two frames, as well as on the position of the sample in space and time. Based on the RPM features, a clinorotation of constant speed up to 30 deg/s is expected to generate negligible centrifugal accelerations within a sphere of 22 mm radius, placed at the center of rotation of the two RPM frames. This geometrical parameter significantly limited the number of samples that could be positioned on the sample holder of the RPM inner frame. 3D clinorotation imposed

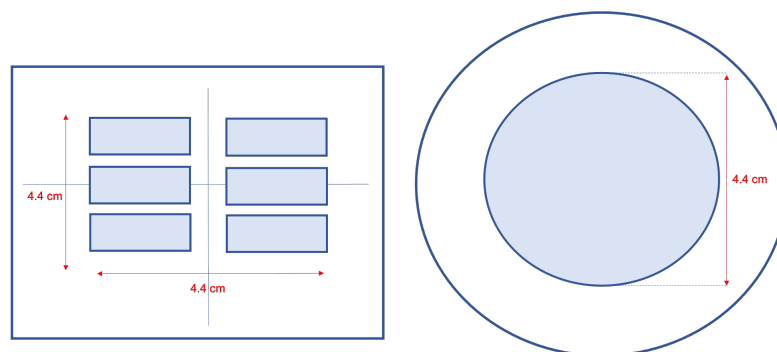


Figure 3.3: Schematic representation of the design of the mold for silicone cell culture vessels for simulated microgravity studies.

the fabrication of cell culture vessels to be fully sealed in order to prevent 1) liquid spills and 2) air bubble trapping, that could impart noxious shear stresses on the cultures. To satisfy these requirements, a fast prototyping method leveraging on laser cutting with a VersaLaser TBH cutter (50 W) was used, Laser cutting (100% power, 1.5% speed) was applied to the fabrication of molds for silicone casting. Molds were designed with CorelDRAW software, and they were obtained by cutting Plexiglas pieces of desired shape (22 x 11 x 5 mm parallelepipeds, or cylinders with 22 mm radius and 5 mm height) and by properly anchoring them to plastic Petri dishes (Figure 3.3).

Cell culture vessels were then obtained by casting polydimethylsiloxane-PDMS (silicone base mixed with curing agent with 20:1 w/w ratio) on the molds of the desired geometry (mono-or multi-compartmentalized), and by promoting cross-linking for 1 h at 60°C. The same fabrication method was also applied to prepare vessels for static cell culture, suitable to biocompatibility studies.

Cell culture vessels were sterilized by exposure to UV rays for 20 min, and then were filled with polymeric substrates, that is Thermanox rectangular slides or polystyrene circular substrates obtained by laser cutting of tissue culture Petri dishes.

After cell seeding and complete filling of the cell culture vessels with cell culture medium (see also the next section), the vessels were sealed with the adhesive PCR film (*BIORAD*) taking care not to leave any air bubbles inside.

The vessels intended for exposure to simulated microgravity were then placed on the RPM, positioned in an incubator set at 37°C, at the centre of the inner frame and anchored with a normal paper adhesive tape. An equal number of samples were used as controls and maintained under the same conditions (wells filled with medium and sealed) at normal gravity.

From now on, for convenience, the abbreviation $s - \mu g$ will be used to refer to the simulated microgravity condition, and 1g to indicate the normal gravity control condition.

3.6 Cell culture

To investigate the interaction between cells and nanoceria in the simulated microgravity regime with the RPM, two cell typologies were used: the immortalized cell line of murine myoblasts (C2C12 cell line) and primary human skeletal myoblasts (HskM).

C2C12 cells were cultured in proliferative DMEM medium with high glucose content (4.5 g/l) containing 10% FBS, 1 mM sodium pyruvate, 2 mM L-glutamine, and 100 U/ml penicillin-100 $\mu g/ml$ streptomycin.

HSkM cells were cultured in low glucose (1 g/l) phenol red-free DMEM proliferative medium containing 10% FBS, 1 mM sodium pyruvate, 2 mM L-glutamine, and 100 U/ml penicillin-100 $\mu\text{g/ml}$ streptomycin.

Cell cultures under regular proliferative conditions were incubated at 37 ° C under 5% CO₂ atmosphere in Petri dishes or 75 cm^2 culture flasks.

For clinorotation experiments, a cell culture medium added with 25 mM HEPES was used for pH buffering in the absence of carbon dioxide. Nanoceria dispersions in complete medium were obtained by taking into consideration a 10%FBS carry-over due to the nanoparticle coating.

3.6.1 Cell sub-culture and freezing

Subcultures were obtained by resuspension of cells and subsequent seeding at a desired cell density with the following procedure. The same procedure was applied for the preparation of aliquots of cells for long-term refrigerated storage (freezing). To harvest the cells in culture, the exhausted culture medium was removed from the Petri dish and a rinse was performed with calcium-free and magnesium-free phosphate buffered saline-PBS to remove any traces of serum that could hinder activity of the enzyme necessary to cell resuspension. 2 ml of trypsin were then added to each Petri dish and kept in the incubator at 37 ° C for 2 minutes to promote enzyme action and cells detachment from the substrate. To deactivate trypsin and remove cells from the Petri, 10 ml of fresh medium were added. Then, the cell suspension was removed from the Petri dish and centrifuged for 5 minutes at 2500 rpm (600 g) in a 15 ml tube. The supernatant obtained following centrifugation was removed and the cell pellet was resuspended in 1 ml of fresh medium. Cells were thus subcultured by distribution into higher number of cell culture containers, or processed for freezing at -20°C.

Cell freezing was conducted by mixing 50 μl of DMSO for cryoprotection, 450 μl of the obtained cell suspension and 500 μl of FBS in a 2 ml cryotube, and by stowing the cryotube in a -80 °C freezer. For longer term cryopreservation, cultures were stored in liquid nitrogen vapors.

Cell subculture for experiments with nanoparticles or under simulated microgravity was performed by cell counting in order to achieve a desired cell density on the substrates. C2C12 counting was performed with an automatic counter (Millipore Scepter) equipped with a 60 μm cut-off count probe. The cell suspension was diluted (usually 1: 100 or 1: 1000) in a culture medium without phenol red in order not to interfere with the reading by the probe. The detected cell number was multiplied by the dilution factor used to obtain the number of cells contained in 1 ml. The volume necessary to seed a certain cell number was obtained by a simple proportion with the obtained total number of cells/ml.

Automated cell counting could not be performed with HSkM due to the larger size

than the probe cut-off. In this case, count was performed with a Burker chamber. 10 μl of the cell suspension obtained by pellet resuspension were infiltrated under the appropriate slide on the Burker chamber. At the optical microscope, the Burker chamber shows an incised square grid, made up of 9 smaller squares, each one containing 16 square regions useful to cell counting. Cell number can be obtained by visually counting cells present in at least 4 of the smaller squares. The number of cells per ml is then obtained by multiplying the average of the counted values with a factor of 40000.

Cell seeding was performed on substrates conditioned with cell culture medium by incubation at 37°C for at least 1 h and replenished with fresh cell culture medium (500 μl of fresh medium in rectangular wells, and 6 ml for the circular ones). A typical volume of 200 μl and 1 ml of cell suspension was used for cell seeding depending on the size of the substrate. Experiments with nanoparticles and under simulated microgravity were typically performed at 12-24 h from cell seeding, by providing the cultures with HEPES-added medium.

3.7 Cytotoxicity tests on C2C12 cell line

In order to identify the safest concentration of nanoceria to be used for internalization studies, five different concentrations were tested on cells maintained both in normal gravity and under simulated microgravity by clinorotation at 20 deg/s. The following concentrations of nanoceria were tested: 0, 100, 200, 500, 1000, 2000 $\mu\text{g/ml}$.

Cells were seeded at a density of 5,000 cells/cm^2 on Thermanox slides positioned at the bottom of PDMS vessels.

Nanoparticle administration and simulated microgravity effects were qualitatively assessed with an optical microscope in phase contrast mode at 24 h. Through the visual analysis on the appearance of the cells, 100 and 200 $\mu\text{g/ml}$ NC concentrations were selected for following quantitative analysis.

For the second experiment, cells were seeded at the same density and the rotation speed of the RPM was set on the same value. This time the effects of microgravity exposure were analyzed after 72 hours of exposition. In these experiments, both commercial nanoceria and the nanoceria we synthesized (NC IIT).

After 72 hours, the cells were processed and prepared for the PicoGreen assay to assess the number of nucleic acids present in the samples.

3.7.1 Pico-Green assay

This paragraph describes the procedure used to evaluate the nucleic acid content of the samples after exposure to simulated microgravity. The nucleic acid content of the samples was measured by using the PicoGreen kit following the manufacturer's

instructions. A fluorescent dye binds selectively to the nucleic acids of the lysed cells. It is, therefore, possible to determine the number of cells present in the analyzed sample by measuring fluorescence intensity with a spectrophotometer (Victor3, PerkinElmer). An excitation wavelength of 485 nm was used to measure fluorescence. Based on the detected fluorescein intensity, and through a calibration curve obtained from samples with a pre-determined number of cells, it was possible to determine the number of cells present in the sample of interest.

After 72 hours of exposure to simulated microgravity on the RPM, cells were trypsinized, centrifuged at 12,000 g for 5 min, and the pellet was lysed in ultrapure water by three cycles of freezing-thawing. disrupt nuclei and to enable nucleic acid staining.

The calibration curve was obtained by measuring the fluorescence of three samples with known cell numbers (10,000, 30,000 and 60,000 cells). Once the samples were lysed, a 96-well black plate was loaded with the amounts of reagents as described in the manufacturer's instructions. Once the plate was loaded with 50 μ l of buffer solution, 25 μ l of cell lysate and 75 μ l of Picogreen reagent. Picogreen reagent was added to each well using a multiple-precision pipette.

Samples were thus incubated for 10 min by shaking at 160 rpm (protected from light) prior to fluorescence reading. This analysis allowed the choice of the most appropriate concentration of nanoceria to perform the following internalization experiments .

3.8 Evaluation of oxidative stress extent in cells

This paragraph describes the experiments performed to assess the extent of oxidative stress in muscle cells. Exploratory experiments were conducted with mouse C2C12 cells maintained at normal gravity and by staining cultures with CellROX Green dye. The latter can have toxic effects on the cultures, and therefore may determine overestimation of the percentage of stressed cells. First, oxidative stress evidences were collected by incubating cells with increasing concentrations of CellROX Green dye. Then, oxidative stress was induced with a pro-oxidant agent and cell staining with CellROX Green dye. The percentage of cells positive to staining was assessed by flow cytometry. Later on, experiments were conducted to quantify the extent of RPM-induced oxidative stress. Focus of this investigation was on primary cells, human skeletal myoblasts, for their relevance to NC application in human spaceflight.

3.8.1 Flow Cytometry

Flow cytometry is a technique that allows analysis of cells in suspension. A flow cytometer can simultaneously measure some morphological parameters of

single cells deriving from the interaction with a laser beam. The scattered and/or fluorescent light signals deriving from the interaction with the cells are read by detectors (photodiodes or photomultiplier tubes) and converted into electronic signals which are analyzed by special software. Through a constant flow, the instrument aligns cells in a row and brings them to the counting chamber where they will be analyzed. Every single cell analyzed is considered as an "event". The analysis provides both information on the dimensions and on the morphological (e.g. roughness) and internal characteristics of the cells based on how the light is scattered. The size of the cells derives from the measurement of the scattering of visible light coming from the frontal direction (therefore called Forward Scatter or FSC); instead, the internal roughness of the cell derives from the measurement at 90 ° (Side Scatter or SSC). The fluorescence parameter allows to obtain additional information and it is measured after cell staining thanks to a directly proportional relationship between the quantity of fluorochrome and the intensity of the emitted fluorescence.

In this project flow cytometry analysis was performed to investigate oxidative stress in cell cultures. CellROX Green Flow cytometry assay kit was used to assess the presence of oxidative stress in live cells. CellROX is a fluorogenic probe that oxidizes in the presence of reactive oxygen species.

To perform flow cytometry analysis the following procedure was followed for all the completed experiments.

1. The exhaust medium was removed from the wells of the culture chambers and a rinse was performed with PBS free of calcium and magnesium.
2. 300 μ l or 1ml of trypsin for the rectangular wells and the bigger circular wells were used respectively. Cells were incubated under trypsin for 3 minutes.
3. Resuspended cells were centrifuged for 5 min at 700 g by setting a low temperature (4°C).
4. Once the supernatant was removed, cells were resuspended in PBS enriched with calcium and magnesium.
5. 100 μ l were used as a control to assess baseline fluorescence with the flow cytometer.

Staining with CellROX at different concentrations was performed by suitable dilutions of the 2.5 mM stock in PBS with Ca^{2+} and Mg^{2+} , and by incubating cells with the staining solution for 15 min in the dark.

3.8.2 Assessment of cells oxidative stress level: C2C12 cell line

To evaluate the behavior of muscle cells in response to a pro-oxidant stimulus and assess the potential beneficial effect of nanoceria, two experiments were conducted in normal gravity with C2C12 cells. The oxidative stimulus was provided using a pro-oxidant agent, tert-butyl hydroperoxide (TBH). The hypothesis underlying these experiments concerns the ability of cerium oxide nanoparticles to decrease oxidative stress.

To validate this hypothesis, C2C12 cells were seeded at a density of 20,000 *cells/cm*² in a proliferative medium added with 25 mM HEPES and after 24 hours of adhesion, they were exposed to increasing concentrations of TBH, without gas exchange with the environment (cultures sealed with film as described in section 3.5).

TBH concentrations were: 0, 10, 50, 100, 1000 μ M and were obtained by proper dilution of the 7.7 M stock solution.

Flow cytometry analysis by staining cells with CellROX Green was performed at three different observation times (1h, 6h and 24h) to evaluate the percentage of CellROX Green-positive cells. With this preliminary experiment, it was possible to choose the concentration of TBH more suitable to induce oxidative stress over 24 h of observation.

In the second experiment, three different concentrations of nanoceria were considered: 0 μ g/ml (control condition), 100 and 200 μ g/ml.

In a second experiment, three different concentrations of nanoceria in complete proliferative medium were considered: 0 μ g/ml (control condition), 100 and 200 μ g/ml.

The test was performed both on cells not treated with TBH to verify the absence of pro-oxidant effects induced by the administration of the nanoceria, and on cells treated with the selected TBH concentration to verify the antioxidant effects of the nanoparticles. Nanoparticles were administered at 24 h from cell seeding and the pro-oxidant stimulus was applied at 24 h from NC administration.

These experiments were performed with 18 well- homemade cell culture plates.

3.8.3 Assessment of cells oxidative stress level: HSkM cell line

Based on the results achieved with mouse myoblasts, experiments were also performed with human myoblasts under simulated microgravity.

The goal of these experiments was to find the right combination of cell density, RPM rotation speed, and observation times to be able to induce a significant level of oxidative stress on cells without causing cell apoptosis.

Flow cytometry analysis by staining cells with CellROX Green was performed

at three different time points (1 h, 6 h and 24 h) to evaluate the percentage of CellROX Green-positive cells.

The following constant rotation speeds were tested: 20, 25 and 30 deg/s. Then, random speed mode (8-20 deg/s, 5 s shift) was also explored in an attempt at improving nanoparticle internalization. This mode imparts different speeds to the two RPM frames. A total of 4 different conditions were tested to find the most suitable condition to induce a significant level of oxidative stress.

3.9 Study of interaction between muscle cells and Nanoceria in simulated microgravity

This section deals with the evaluation of the interaction between muscle cells and nanoceria. To the purpose, three different techniques were applied.

Inductively coupled plasma-optical emission spectrometry (ICP-OES) was used as a quantitative analysis to evaluate the amount of internalized nanoparticles. With the same aim, flow cytometry was performed. For qualitative analysis, cells were stained by cytochemistry and underwent confocal microscopy imaging.

For each test performed, four experimental conditions were evaluated: samples in normal gravity with and without administration of nanoceria, and samples in microgravity always with and without administration of nanoceria.

3.9.1 Inductively coupled plasma-optical emission spectrometry (ICP-OES)

To quantitatively assess the extent of nanoparticle internalization, ICP-OES was performed at the IIT Materials Characterization facility on samples obtained after clinorotation in two different regimes. At the end of the experiments, the cells were harvested and pelleted, and the pellet was frozen and shipped for analysis.

The experiment was conducted in large, monocompartment PDMS cell culturing vessels (3 cm radius, 4 mm height) to ensure collection of at least 280,000 cells for ICP-OES analyses and for minimization of cell culture medium volume in comparison to traditional flasks for cell culture, that should be completely filled to prevent shear stresses to act on cells. A cell culture volume of 13 ml was used during the experiment described in the following.

A total of 12 plates were used to perform this experiment, three for each experimental condition. The experimental conditions are four:

1. Samples not treated with nanoceria, kept at normal gravity.
2. Samples not treated with nanoceria, exposed to simulated microgravity.

3. Samples treated with nanoceria, kept at normal gravity.
4. Samples treated with nanoceria, exposed to simulated microgravity.

The experiment was conducted with C2C12 cells seeded at a density of 10,000 *cells/cm²*.

Nanoceria was administered at 24 hours from seeding at a concentration of 100 $\mu\text{g/ml}$.

After cell culture medium replacement, the cultures were sealed and placed in the incubator (normal gravity condition) and on the RPM (simulated microgravity condition) for a 48 h incubation. This experiment was performed twice.

3.9.2 Flow Cytometry to evaluate NPs internalization

A preliminary quantitative assessment of nanoparticle internalization was conducted. In this case, the technique of cytofluorimetry was used to assess nanoparticle internalization. As explained in section 3.8.1, the flow cytometer can simultaneously measure several morphological parameters of individual cells resulting from interaction with a laser beam. The analysis provides both information on the size and morphological (e.g., roughness) and internal characteristics of the cells based on how the light is distributed after the interaction.

In this case, no staining was performed, but a scattering threshold was set to be able to intercept the cells that internalized the nanoceria.

3.9.3 Cytochemistry

To perform confocal microscopy imaging, cell samples underwent a staining process consisting of 5 steps: cells fixation, permeabilization, saturation of aspecific sites of interaction with fluorophore carriers, staining with fluorophore carriers and final washing.

Before cell fixation, Thermanox slides with cells attached were placed in 6-well plates and washed twice with PBS with calcium and magnesium to remove traces of serum.

Paraformaldehyde (4% solution in PBS) was used as a fixative. Fixatives act on the protruding amine groups creating stable bridges. Fixation was conducted with 1.5 ml of cold fixative at 4°C for 20 min.

After this incubation time, the fixative was removed through two washes with PBS with calcium and magnesium. A solution of 0.1% Triton in PBS was then added to open pores on the cell membrane and facilitate interaction with the fluorophore carriers. Incubation was performed for 15 min.

Saturation was performed to maximize the signal-to-noise ratio, thus maximizing specific fluorescein and minimizing background fluorescence. A 10% goat serum in

PBS solution (1.5 ml) was used for 1h saturation.

To mark the cytoskeleton, fluorophore-conjugated phalloidin was used. Phalloidin is a bicyclic peptide belonging to a family of toxins isolated from fungi. Phalloidin selectively binds with high affinity to F-actin. The utilized phalloidin is labelled with Alexa Fluor 488 fluorophores (*AF488, ThermoFisher Scientific*).

Diamidino-2-phenylindole (DAPI) was used to mark cell nuclei due to its high selectivity for DNA. A staining solution was then prepared with 10% goat serum in PBS, with phalloidin and DAPI diluted 1:100. 1.5 ml of staining solution was added to each well and the samples were incubated for 45 min in the dark.

At the end of the incubation, two final washes with PBS with calcium and magnesium were performed, and the samples were provided with fresh PBS for storage at 4°C until imaging at the confocal microscope.

Chapter 4

Results and Discussions

This chapter reports and discusses the results obtained in the experiments performed for this experimental thesis. The chapter begins with the results related to the characterization of cerium oxide nanoparticles and the evaluation of their antioxidant capabilities. Then, the results obtained in preliminary experiments aimed at evaluating nanoceria cytocompatibility and at establishing the most suitable concentration for administration for following experiments are described. The results concerning the study of the interaction of nanoceria with skeletal muscle cells are reported upon application of 3D clinorotation in order to simulate microgravity by a random positioning machine (RPM). The results of test aiming at assessing possible oxidative stress imposed by clinorotation to two skeletal muscle cell models are finally reported.

4.1 Nanoceria characterization

This first section reports all the results collected by nanoparticles characterization, which was carried out both on nanoparticles synthesized in the IIT laboratory (thereafter termed NC IIT) and on commercial nanoparticles (thereafter termed NC Sigma), considered as controls since used in past experimental activities at IIT.

4.1.1 TEM imaging

Figure 4.1 shows TEM images of uncoated and coated IIT nanoceria samples. Imaging was performed on 1 mM NC dispersions. The top panel refers to the uncoated IIT samples, whereas the one to the coated nanoparticles, dispersed in 10% fetal bovine serum (FBS) dilution in ultrapure water. Both images show nanoparticles with average size of 8 nm, rough surface and moderate aggregation.

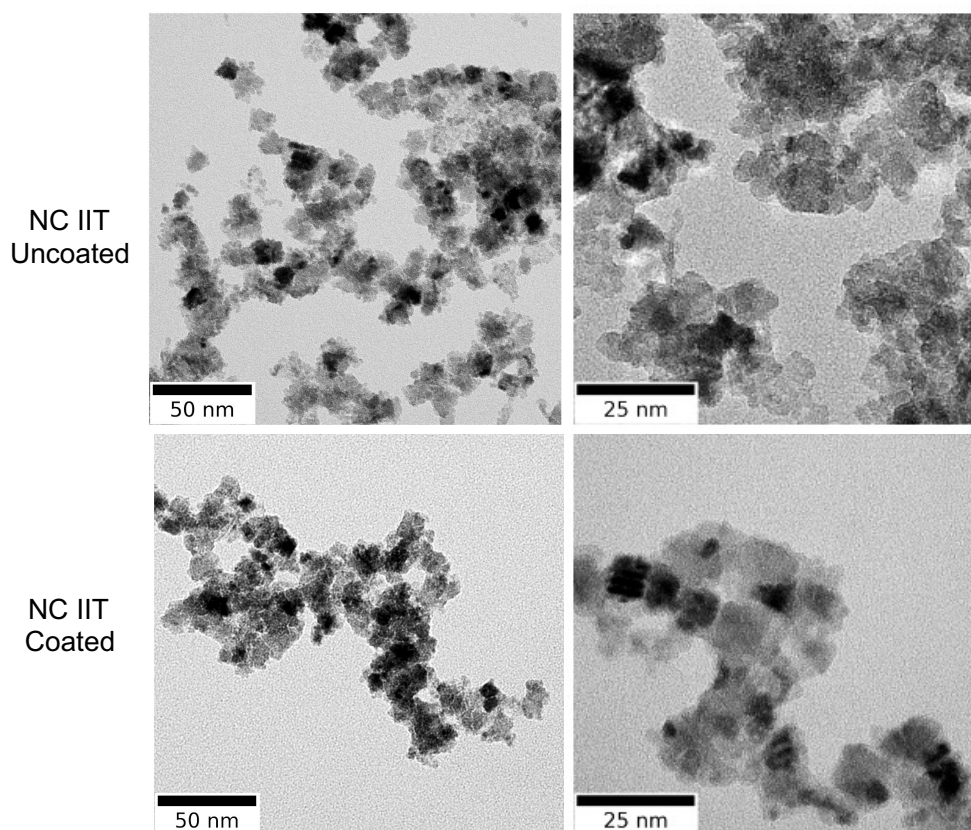


Figure 4.1: Images from Transmission electron microscopy at two different magnifications. Uncoated NPs are reported in the three images on the top, and coated NPs on the bottom.

4.1.2 X-Ray Photoelectron Spectroscopy (XPS)

In this paragraph, the results obtained through the X-ray Photoelectron Spectroscopy (XPS) characterization technique regarding the chemical composition of cerium oxide nanoparticles are reported and discussed.

The wide scans (with binding energies from 0 to 1000 eV) confirmed the expected chemical composition of both NC IIT and NCsigma samples. The obtained spectra are reported in Figure 4.2, and show a characteristic peak attributable to Ce3d at about 883 eV in the spectrum for the IIT sample (shown in blue) and at about 882 eV in the commercial one (shown in red).

The main differences between IIT NC and Sigma NC consist into the occurrence of

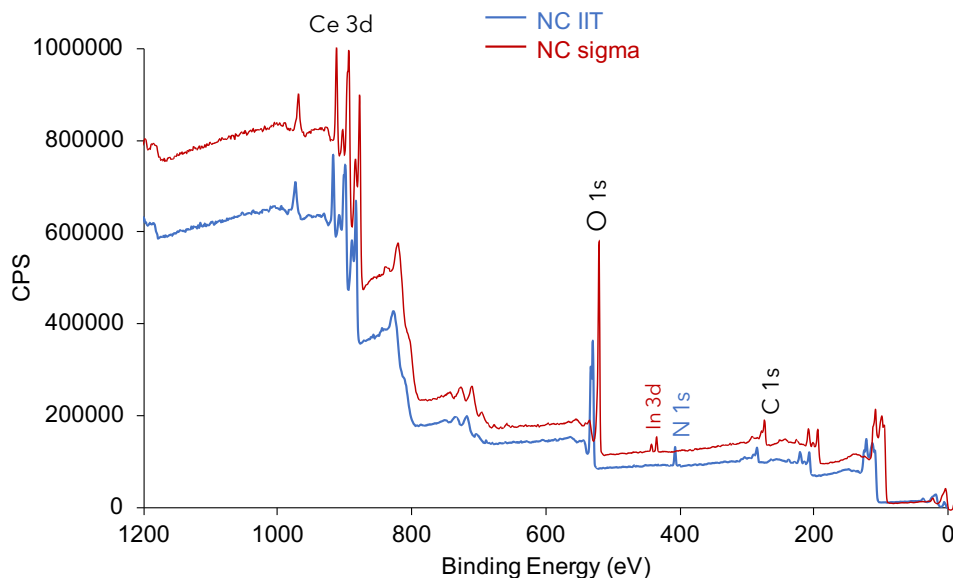


Figure 4.2: Wide scans obtained by XPS technique.

NC IIT	Position (eV)	A%	NC Sigma	Position (eV)	A%
O 1s	530	62.9	O 1s	592.3	63.3
C 1s	285.0	11.9	C 1s	284.3	16.6
Ce 3d	883.0	19.0	Ce 3d	882.3	19.5
N 1s	407.0	7.2	In 3d	444.3	0.6

Table 4.1: Atomic percentages and peaks' positions detected via XPS

the N1s peak at approx. 407 eV in the IIT sample and the presence of In 3d peak at approx. 444 eV in the NCsigma sample, respectively ascribable to synthesis reagents and to the substrate used for the analysis. Besides these differences, the two spectra are very similar.

Peak positions and atomic percentages are shown in Table 4.1.

It is known from the literature ([36]) that the ratio of Ce^{3+}/Ce^{4+} sites on the nanoparticle surface greatly influences the enzymatic antioxidant activity of the nanoceria. In general, nanoparticles with high amounts of the trivalent state of Cerium, ranging from 40% to 60%, appear to have enzymatic antioxidant activity more similar to that one of Superoxide Dismutase (SOD). On the other hand, NC with high amounts of Ce^{4+} , from 70% to 80%, seem to better mimic the enzymatic activity of the catalase enzyme (CAT). Therefore, nanoceria with high levels of Ce^{3+} and a high Ce^{3+}/Ce^{4+} ratio on the surface appear to be more efficient O_2^-

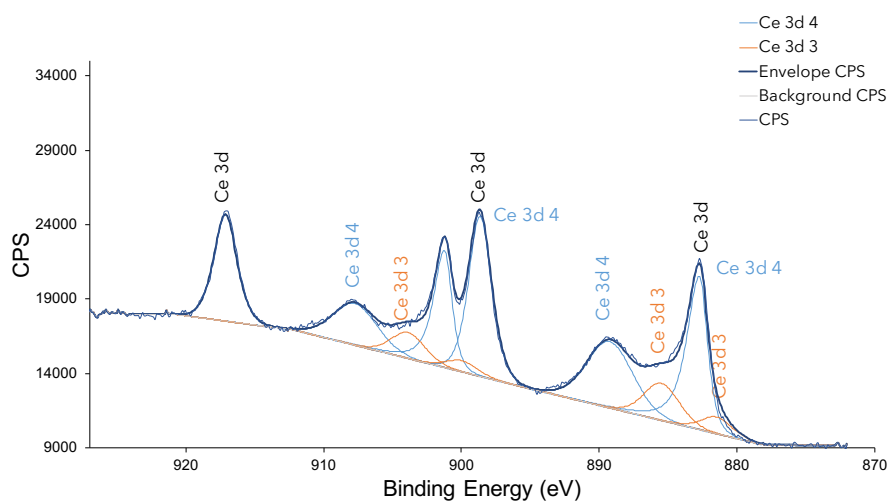


Figure 4.3: High resolution scan of the Ce 3d region of the NC IIT sample.

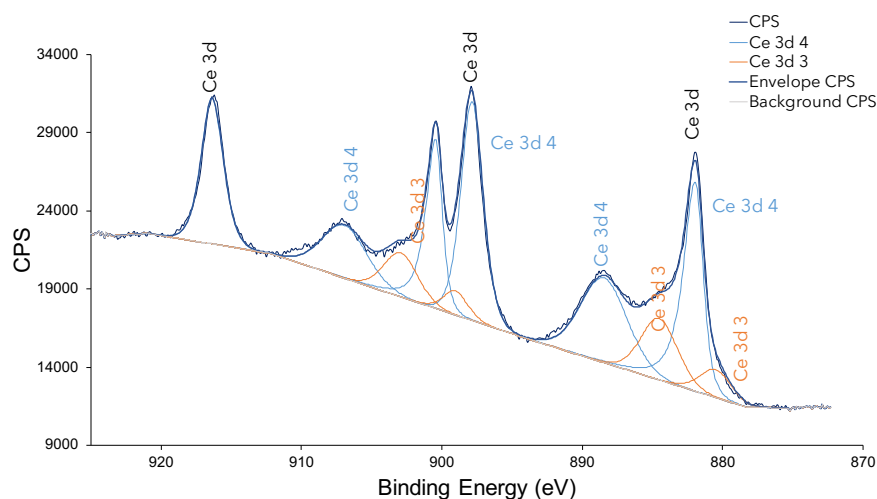


Figure 4.4: High resolution scan of the Ce 3d region of the NCsigma sample.

scavengers then nanoparticles rich of Ce⁴⁺ state. Being highly SOD-mimetic, these nanoparticles neutralize the O_2^- ion by converting it to H_2O_2 and O_2 through a catalytic dismutation reaction. However, high levels of H_2O_2 are potentially more dangerous for cells than high levels of O_2^- , because H_2O_2 is involved in the generation of even more damaging free radicals from interaction with metals. The co-existence of both cations is therefore needed on the surface to counteract H_2O_2 overproduction [36].

XPS analysis enabled the quantification of the two oxidation states by Ce 3d peak deconvolution: Figure 4.3 and Figure 4.4 show the high-resolution scans of the Ce

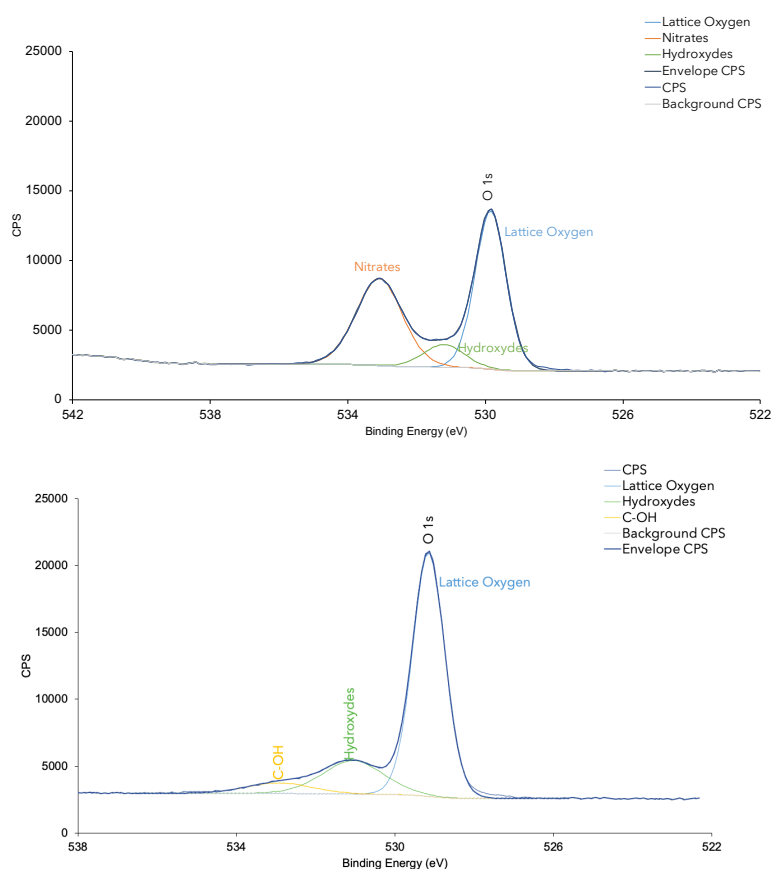


Figure 4.5: High resolution spectra of the oxygen peaks. On the top, the peak of oxygen detected in the NC IIT sample and below the peak detected in the NCsigma sample.

3d peaks of both NC IIT and NCsigma samples. The peaks relative to the trivalent state, in the NC IIT sample, were found at binding energy values of 885.47 eV, 881.47 eV, 903.87 eV, 899.97 eV. Instead, the peaks relative to the trivalent state at 882.73 eV, 889.23 eV, 917.13 eV, 901.23 eV, 907.73 eV, 898.63 eV.

From the ratio between the areas subtended by the peaks, it was possible to deduce values of about 15% for the trivalent state, and 85% for the tetravalent state, promising the exertion of a satisfactory antioxidant activity by NC IIT, comparable to the values obtained for the NCsigma sample [37].

High-resolution spectra for the other species are also shown in Figure 4.5 and Figure 4.6.

A remarkable difference was found between the two samples in the oxygen peak assignment. The NC IIT sample shows an intense oxygen peak (O 1s) at about 533 eV different from the position detected for the NCsigma.

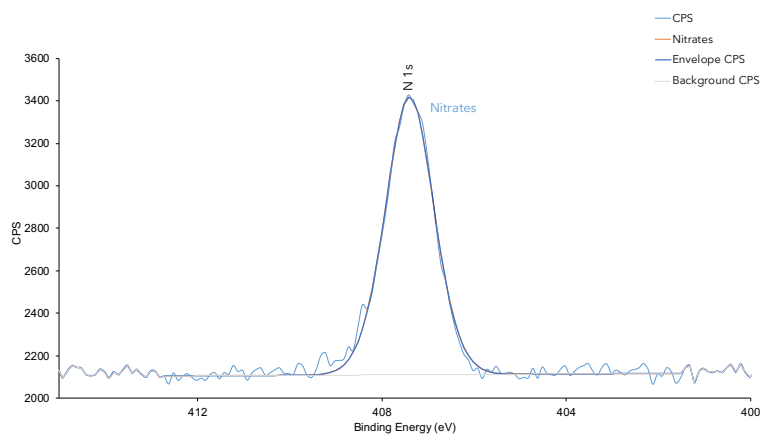


Figure 4.6: High resolution scan of the N 1s region of the NC IIT sample.

The assignment of the O 1s peak at 533 eV is confirmed by observing the presence of the N 1s peak at about 407 eV in the NC IIT sample and not present in NCsigma, and likely due to a chemical shift induced by the presence of nitrogen. The carbon spectra of the two samples were also evaluated and were used to calibrate the energy scale through the location of the main carbon peak.

4.1.3 Size and Zeta Potential measurements

In this paragraph, the results obtained through the dynamic light scattering (DLS) technique regarding the size and the Z potential of cerium oxide nanoparticles are reported and discussed. The main objective of this analysis was to evaluate the colloidal stability of the nanoparticles obtained through the synthesis process described in the previous chapter, and compare them with that one of commercial nanoparticles. Table 4.2 reports the results of hydrodynamic diameter measurement obtained from both NC IIT samples and from NCsigma samples.

The DLS revealed a peak indicating a size of approximately 220 nm, with a polydispersity index of 0.28 for the coated NC IIT suspended in the complete cell culture medium. The obtained polydispersity index indicates a good homogeneity of the cerium oxide nanoparticles.

The values shown in the table were calculated from the distribution of data shown in Figure 4.7, where the position of the peaks indicates the size of the nanoparticles, the intensity indicates the number of molecules having that size and the width indicates variability. The presence of a single intensity peak indicates the goodness of the analysis. The presence of less intense peaks for larger or smaller dimensions

Sample	Size (d.nm)	PdI
NC IIT uncoated in MQ	157.2 ± 6.8	0.32
FBS-coated NC IIT in ultrapure water	239.4 ± 14.5	0.22
FBS-coated NC IIT in 10% FBS	225 ± 17.7	0.31
FBS-coated NC IIT in complete proliferative medium	218.8 ± 16.4	0.28
NC Sigma uncoated in MQ	182.4 ± 7.12	0.20
FBS-coated NC Sigma in ultrapure water	274.0 ± 14.0	0.22
FBS-coated NC Sigma in 10% FBS	285.5 ± 9.0	0.23
FBS-coated NC Sigma in complete proliferative medium	296.5 ± 8.7	0.23

Table 4.2: Hydrodynamic radius (Size d.nm) and polydispersity index (PdI) obtained in different experimental conditions. The results are reported as the mean and standard deviation of four measurements made on the samples.

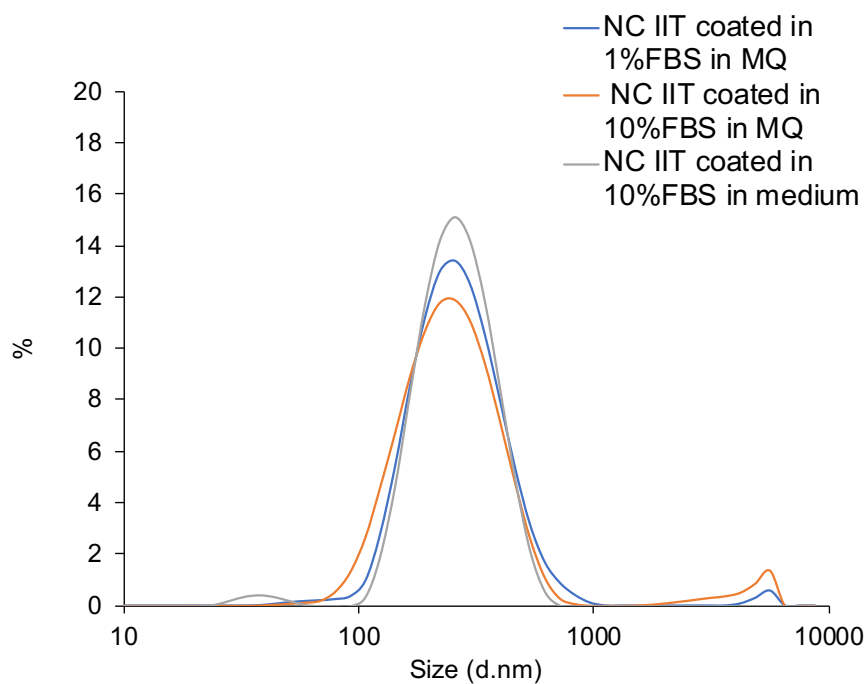


Figure 4.7: Size distribution data of FBS-coated NC IIT

indicates aggregates of nanoparticles or the presence of proteins or impurities in the solution.

DLS technique was also used to assess the short-term stability of nanoceria. The value of the Z-potential was evaluated in three different conditions: uncoated and coated NC in ultrapure water and coated NC in 10% FBS in ultrapure water. The

results obtained are reported in Table 4.3. Also, in this case the results are reported as the average and standard deviation of three different readings.

As stability is a fundamental requirement for applications in the biomedical field,

Sample	Zeta Potential (mV)
NC IIT uncoated in ultrapure water	37.6 ± 0.8
FBS-coated NC IIT in ultrapure water	-21.2 ± 0.6
FBS-coated NC IIT in 10% FBS	-15.3 ± 0.7
NCsigma uncoated in ultrapure water	38.5 ± 2.6
FBS-coated NCsigma in ultrapure water	-12.1 ± 1.8
FBS-coated NCsigma in 10% FBS	-15.9 ± 0.8

Table 4.3: Z Potential values obtained in different experimental conditions. The results are reported as the mean and standard deviation of three measurements made on the samples.

the long-term stability of the nanoparticles was also evaluated.

Both size and Z-potential values were monitored over two weeks (measurements carried out every two days) on nanoparticles maintained in normal gravity and those exposed to simulated microgravity on Random Positioning Machine (RPM). Table 4.4 and Table 4.5 report the average value of the dimension and the Z-Potential of the samples. The standard deviation refers to the seven measurements and was therefore calculated to highlight the variability of the dimensions detected in the different days of analysis.

As indicated by the low value of the standard deviation, coated nanoparticles

Size (d.nm)	Normal Gravity	Microgravity
Uncoated NC in MQ	140.9 ± 7.2	Low quality
FBS-coated NC in MQ	184.8 ± 9	205.8 ± 9
FBS-coated NC in complete proliferative medium	280.0 ± 17.0	294.5 ± 5.0

Table 4.4: Long-term stability monitored at normal gravity and under simulated microgravity: size measurements.

maintain stability over this period. As could be expected, the stability of uncoated nanoparticles was lost within the first fourth days. Further measurements were not reliable due to the very poor quality of the sample. For this reason, the values of the size of the uncoated nanoparticles in microgravity, and of the Z potential for both conditions (1g and $s - \mu g$) were not reported in the tables.

Figure 4.8 shows the trend of the Z potential value over the 14 days. High variability is seen for the uncoated nanoparticles. While for the coated NC, for the two gravity

Size distribution Data (d.nm)	Normal Gravity	Microgravity
Uncoated NC in MQ	Low quality	Low quality
FBS-coated NC in MQ	-13.6 ± 0.7	-13.7 ± 0.7

Table 4.5: Long-term stability monitored at normal gravity and under simulated microgravity: Z Potential.

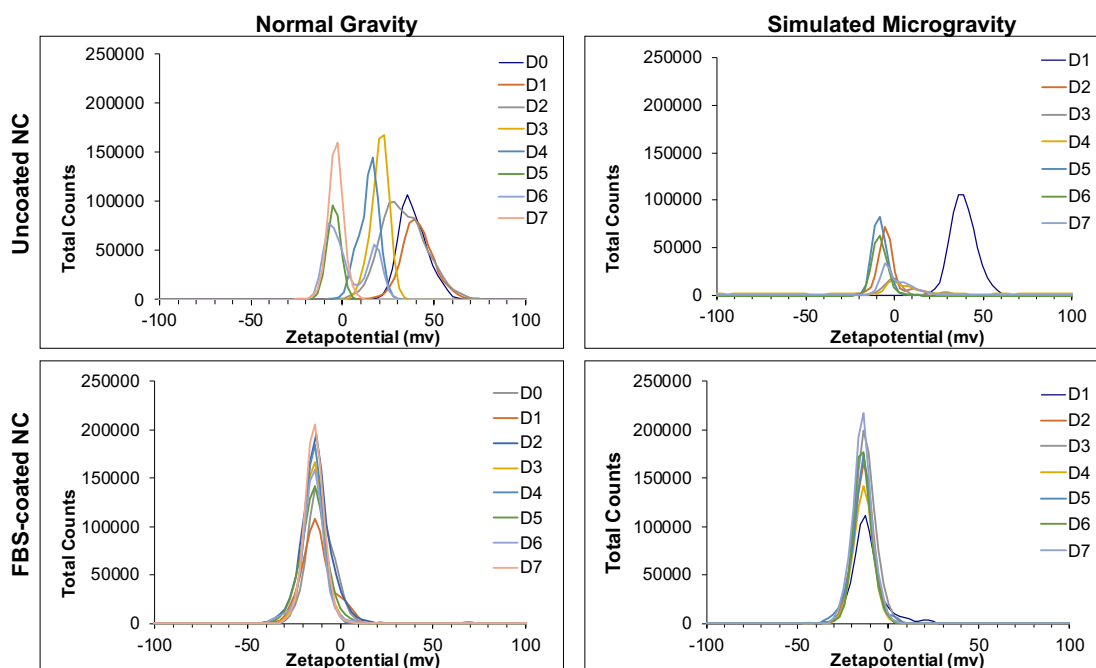


Figure 4.8: Z-Potential distribution data of the long-term stability monitoring.

conditions the recorded value remains constant over the seven readings.

4.1.4 X-Ray Diffraction (XRD) analysis

In this third paragraph, the results obtained through X-Ray Diffraction (XRD) are reported and discussed concerning the chemical nature and the crystalline structure of the synthesized nanoparticles and of the commercial ones.

The XRD confirms for both samples the presence of a single crystalline phase, namely the cubic CeO₂, with fluorite structure.

Figure 4.9 reports the two diffractograms of the analyzed samples, and shows that they overlap to the CeO₂ pattern from the Inorganic Crystal Structure Database, thus confirming the expected chemical composition of the synthesized nanoparticles,

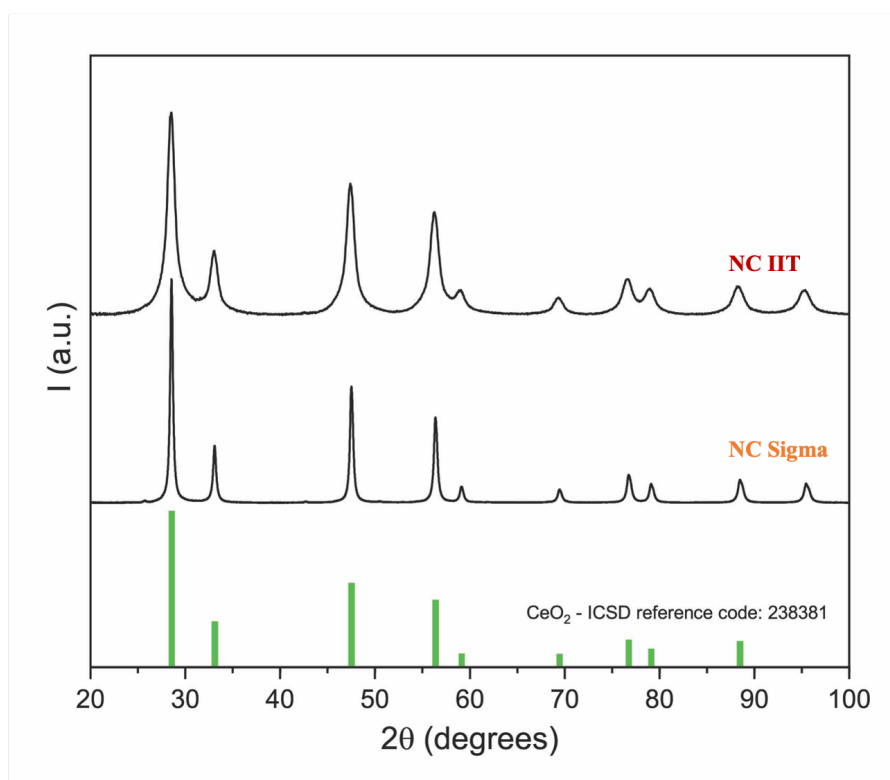


Figure 4.9: Spectrum obtained by XRD analysis: NC IIT at the top, NC sigma in the center.

in agreement with what was found by XPS analysis.

Table 4.6 reports quantitative data obtained by XRD analysis, demonstrating differences in nanoparticle crystallite size and lattice strain, likely ascribable to the synthetic method.

Sample	Crystallite Size [nm]	Lattice strain [%]
NC IIT	8.6	0.261
NCsigma	29.0	0.0664

Table 4.6: Crystal size and strain values obtained from XRD analysis.

4.1.5 Thermogravimetric analysis (TGA)

This paragraph reports and discusses the results obtained by thermogravimetric analysis (TGA).

Figure 4.10 shows the obtained thermograms over the 0-1000°C range. Quantitative data are reported in Table 4.7, were are reported the characteristic temperatures associated with significant weight loss resulting from the location of peaks detected in the first derivative of the TGA curve.

Table 4.7 clearly show that significant weight losses occurred at different temperatures for uncoated and FBS-coated nanoparticles, with FBS-coated nanoparticles undergoing a significantly higher overall weight loss than uncoated nanoparticles, obviously due to the degradation of the protein coating.

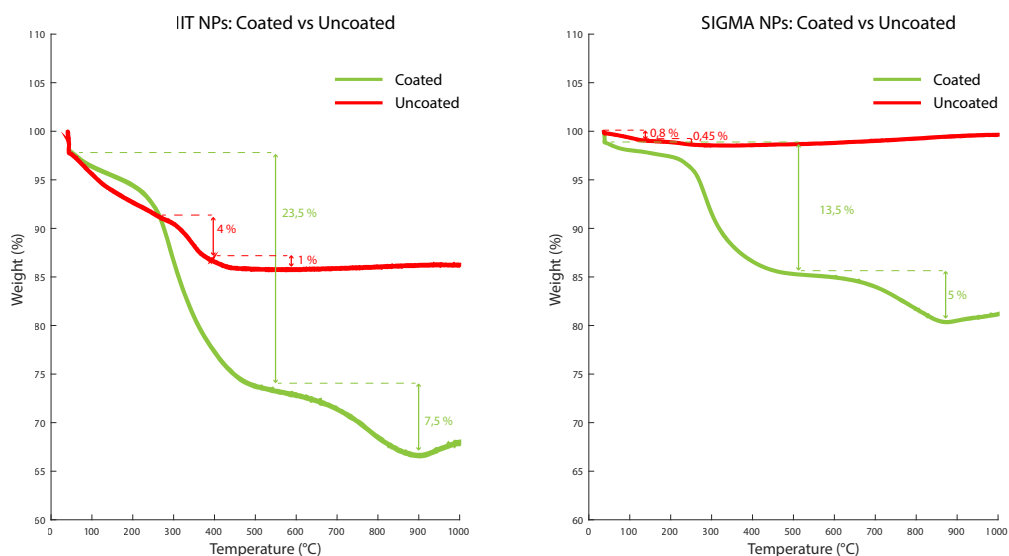


Figure 4.10: Comparison of TGA curves of coated (green line) and uncoated (red line) NPs.

Sample	1 st peak		2 nd peak	
	Critical Temperature (°C)	% weight loss	Critical Temperature (°C)	% weight loss
FBS-coated NC IIT	280	23.5%	796	7.5%
FBS-coated NCsigma	277	13.5%	820	5%
NC IIT uncoated	335	4%	412	1%
NCsigma uncoated	104	0.8%	221	0.45%

Table 4.7: Critical temperatures and weight loss percentages of uncoated and coated NPs derived using the TGA curves.

The results obtained on uncoated nanoparticles are comparable with the data found in the study by F.Caputo et al used as a reference for the synthesis protocol. In their study, the first mass loss of the uncoated nanoparticles is reported before

the temperature of 200 °C with a mass loss rate of 0.5%, while in the second region, between 200 and 400 °C, the mass loss rate is 4%. These results are not too far from those obtained for both tested samples but still more similar to the commercial sample.

According to their article [39], the first region seems to be associated with the volatilization of residual solvents and water absorbed by the material. In contrast, the second mass loss could be associated with the degradation of residual ethylene glycol. Another study by Diaconesea et al. reports a 7% of weight loss before 200 °C always due to the volatilization of water molecules, and a second region (3% of weight loss) between 250 and 300 °C associated with the exothermic effect of un-reacted nitrate decomposition [40].

4.2 Photometry for quantification of nanoparticle antioxidant capacity

This paragraph discusses the results obtained during the evaluation of the antioxidant capabilities of cerium oxide nanoparticles.

For this purpose, an assay capable of detecting the antioxidant capacities of the

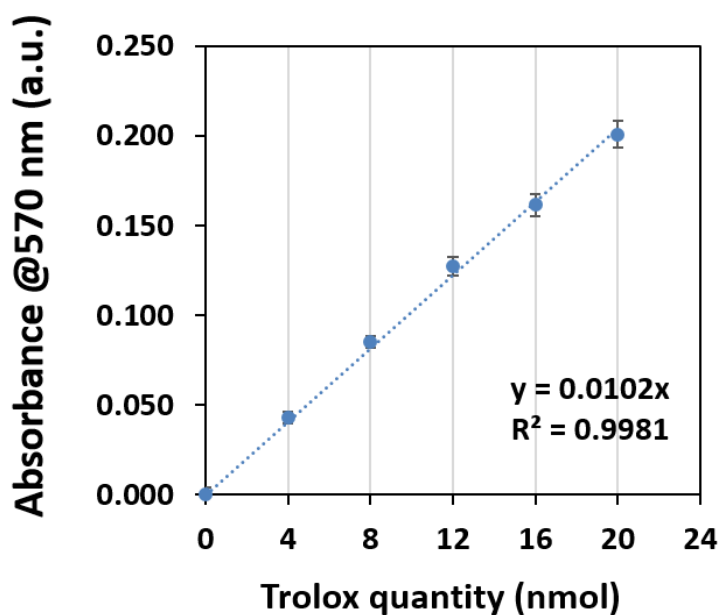


Figure 4.11: Calibration curve for Trolox standard in antioxidant capacity quantification assay.

tested substances was used. The assay relies on copper ion reduction and on a colorimetric probe producing a color change towards purple, the intensity of which directly correlates to the antioxidant capacity of the substance tested.

Trolox, an analogue of vitamin E, was used as a standard for the obtainment of a

Samples: Natural Antioxidants	Trolox Equivalents (n.mol)
NC IIT	235.0
NC sigma	0.1
PDNPs	7200.0
Curcumin	0.1
Resveratrol	5.4

Table 4.8: Antioxidant property of nanoparticles and soluble compounds (in Trolox equivalents).

calibration curve that was later used to known antioxidant capacity of nanoparticles. For this reason, the results regarding the antioxidant capacity are expressed as the number of mol of Trolox equivalents.

Antioxidant property of both NC and PDNPs was quantified upon proper dilution of the stock dispersions, and it was compared to that one of some soluble antioxidant compounds. The assay calibration curve based on dilutions of Trolox is reported in Figure 4.11. As shown in Table 4.8 (where all data refer to 1 mg of antioxidant), nanoparticles had a higher antioxidant property (expressed in Trolox equivalents) than soluble antioxidants. Ranking based on antioxidant property is therefore as follows: commercial NC < curcumin < ascorbic acid < resveratrol < IIT-synthesized NC < PDNPs.

4.3 Cytotoxicity tests

To evaluate possible NC cytotoxic effects, five different concentrations of nanoparticles dispersions were tested on both C2C12 cells and HSkM.

C2C12 myoblasts show comparable viability at all concentrations tested of nanopar-

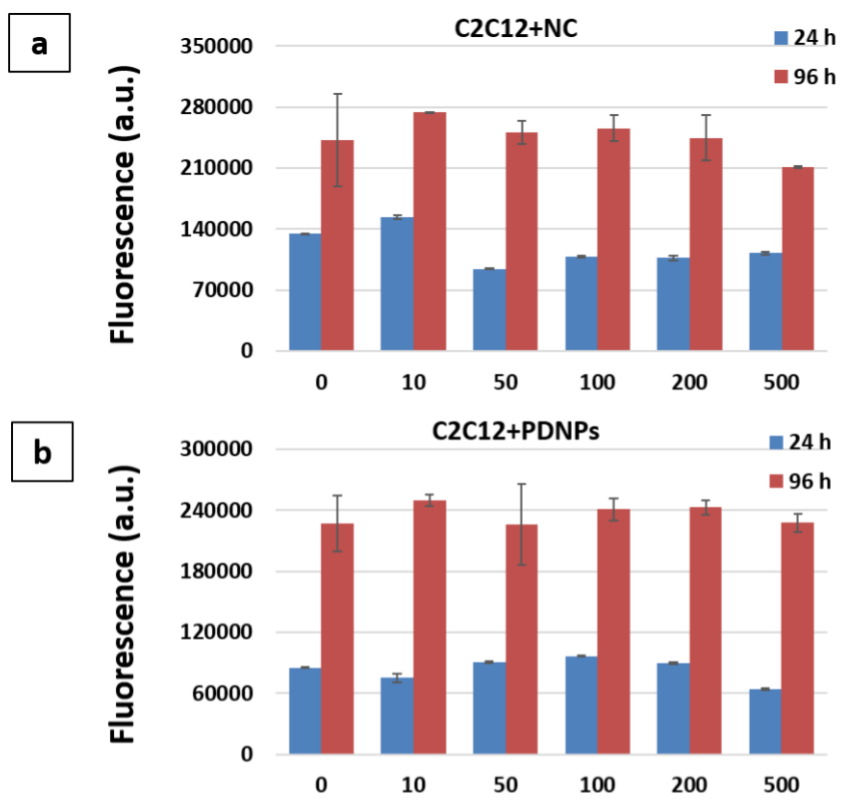


Figure 4.12: Biocompatibility test of increasing concentrations of NC (a) and PDNPs (b) with proliferating C2C12 myoblasts. Fluorescence is associated to ds-DNA content of the cultures.

ticles (NC and PDNPs), both after 24 h and 96 h of incubation. The cell population undergoes regular proliferation at all concentrations tested of nanoparticles, denoting high biocompatibility of both NC and PDNPs on the selected mouse cell model (Figure 4.12).

Figure 4.13, HSkM show comparable viability in the presence of all NC concentrations tested at 24 h from nanoparticles administration. The cell population undergoes regular proliferation up to 200 $\mu\text{g}/\text{ml}$ NC. Myoblasts have comparable viability within a smaller concentration range of PDNPs compared to NC, with proliferation occurring correctly only at the lower PDNP concentration tested,

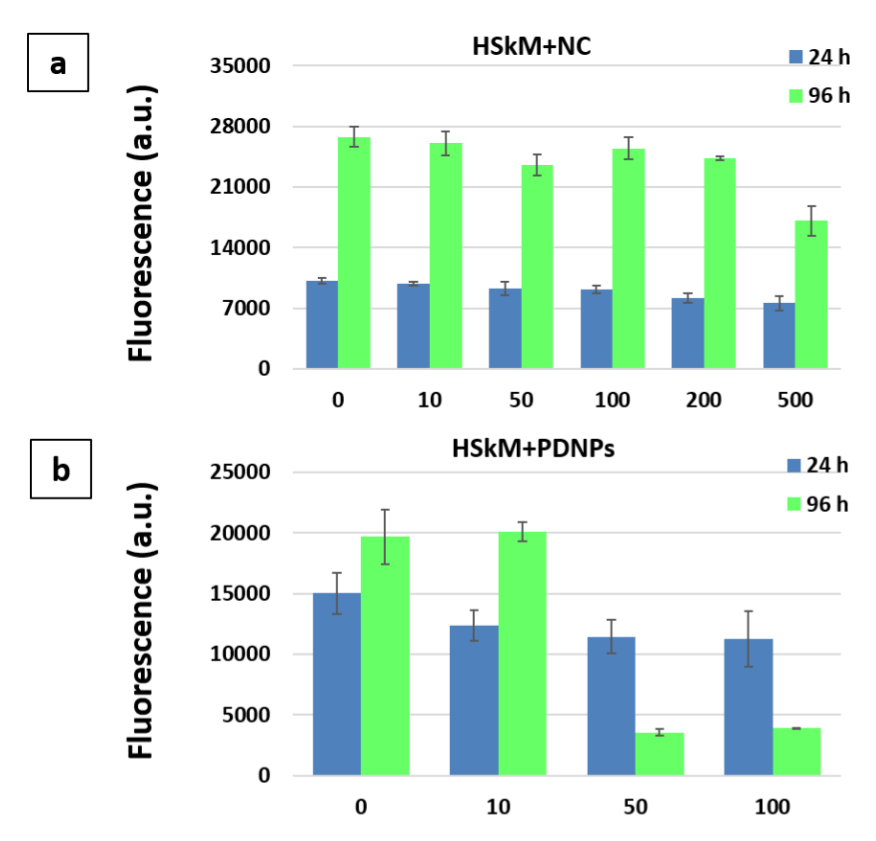


Figure 4.13: Biocompatibility test of increasing concentrations of NC (a) and PDNPs (b) with proliferating HSkM. Fluorescence is associated to ds-DNA content of the cultures.

for reasons yet to be ascertained. Biocompatibility tests motivated further experiments with the following concentrations: 0, 100 and 200 $\mu\text{g/ml}$ for NC, and 0, 10 and 50 $\mu\text{g/ml}$ for PDNPs. C2C12 myoblasts (seeded at a density of 5,000 cells/cm^2) were used to perform an exploratory experiment aiming at assessing qualitatively (by phase contrast microscopy imaging) and quantitatively (by fluorometry upon ds-DNA staining) synergic effects of nanoparticle administration and 3D clinorotation.

Figure 4.14 reports phase contrast microscopy images of cultures treated with increasing concentrations of NC, with regular morphology and adherent to the substrate, after exposure to both normal gravity and simulated microgravity. Samples treated with nanoparticles during 3D clinorotation are characterized by lower amounts of precipitated nanoparticles than samples kept in static conditions, suggesting lower cellular internalization of nanoparticles under simulated microgravity.

Figure 4.15 shows results of fluorescence detection after ds-DNA staining, sug-

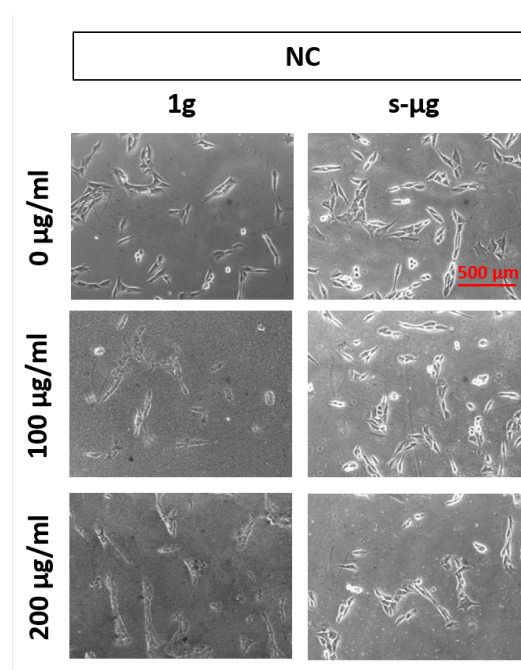


Figure 4.14: Representative phase contrast microscopy images of C2C12 cell cultures after 24 h of exposure to increasing concentrations of NC and to simulated microgravity (20 deg/s).

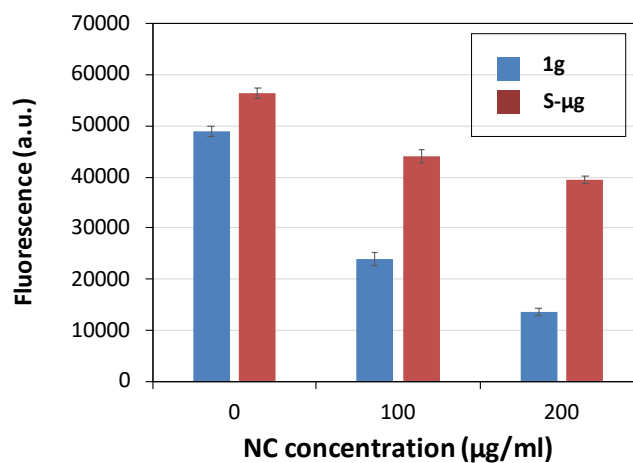


Figure 4.15: Biocompatibility test of increasing concentrations of NC and simulated microgravity with proliferating C2C12 myoblasts. Fluorescence is associated to ds-DNA content of the cultures.

gesting comparable response of NC-treated C2C12 cells to untreated ones under

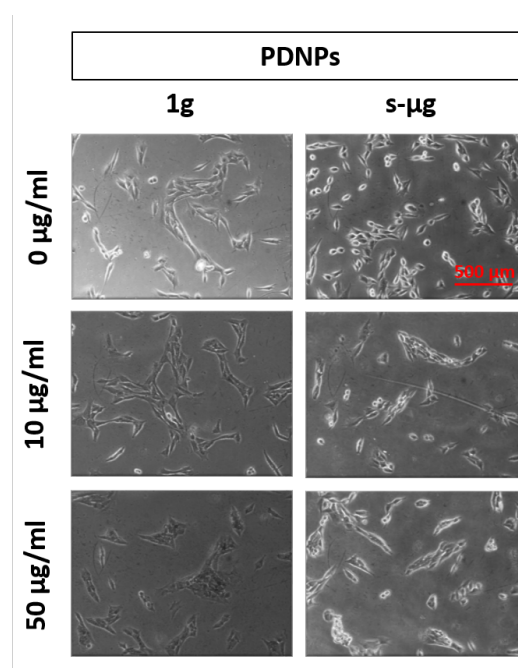


Figure 4.16: Representative phase contrast microscopy images of C2C12 cell cultures after 24 h of exposure to increasing concentrations of PDNPs and to simulated microgravity (20 deg/s).

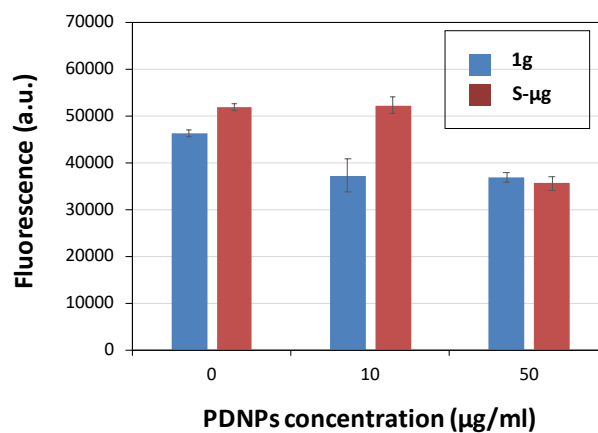


Figure 4.17: Biocompatibility test of increasing concentrations of PDNPs and simulated microgravity with proliferating C2C12 myoblasts. Fluorescence is associated to ds-DNA content of the cultures.

3D clinorotation, whereas cells in static conditions seem to show an increasingly

lower viability depending on NC concentration. This evidence is in contrast to the results reported in Figure 4.12 a, but in agreement with what is shown in Figure 4.14: further investigations may prove if this resulted from irregular nanoparticles coating with FBS or from re-use of contaminated cell culture vessels.

Figure 4.16 reports phase contrast microscopy images of cultures treated with increasing concentrations of PDNPs, with regular morphology and adherent to the substrate, after exposure to both normal gravity and simulated microgravity. Figure 4.17 shows results of fluorescence detection after ds-DNA staining, suggesting comparable response to PDNP administration and to 3D clinorotation.

4.4 Study of NC internalization under simulated microgravity

In this paragraph, results related to the study of the interaction between cerium oxide nanoparticles and muscle cells under simulated microgravity are reported. To study the nanoparticle internalization within cells several analytical techniques including transmission electron microscopy, inductively coupled plasma mass spectrometry (ICP-MS), flow cytometry, confocal microscopy, Raman confocal microscopy, etc. are reported in the literature [42].

Of these, TEM and confocal microscopy are the most widely used because they have a good spatial resolution but have time consuming. ICP has the advantage of providing quantitative results, but it is a destructive technique, not easily accessible and applicable only with inorganic particles, with chemical composition different than the cellular one [42].

Flow cytofluorometry is a promising strategy used for the evaluation of internalized nanoparticles. The device is capable of measuring light scattering and fluorescence of single events (e.g., cells or particles) in flow. The instrument records both forward and side scattering. These two vary depending on the particle size and complexity (intracellular density), respectively. Internalization of nanoparticles into cells results in increased side scattering. Therefore, side scattering can be used to quantify the uptake of nanoparticles into cells. [42].

In this work, the internalization of the nanoparticles was evaluated by three different methods, two quantitative methods (ICP-OES and flow cytometry), and one qualitative method (confocal microscopy). The reported results were obtained with three different techniques by exposing mouse myoblasts (C2C12) to the simulated microgravity condition for 48 hours.

Figure 4.18 shows the histogram for the preliminary experiments performed on cells maintained at normal gravity with two different concentrations of Nanoceria, 100 $\mu\text{g/ml}$ and 200 $\mu\text{g/ml}$.

For flow cytometry analysis after microgravity exposure, cells were seeded in the PDMS culture chambers with the six wells. After 48 hours from the onset of microgravity exposure, the cells were processed as described in Chapter 3 and prepared for analysis.

Figure 4.19 shows the images acquired with the microscope at the end of the experiment. Cell morphology is good in both cases and no substantial differences are noted between the experimental conditions. No particular differences in NC precipitate are evident when comparing the two experimental conditions.

The graph in Figure 4.20 shows the percentage of events (cells) that produce side scattering intensity greater than the set detection threshold.

Again, the condition without nanoceria (indicated in the graph with 0 $\mu\text{g/ml}$ NC) is

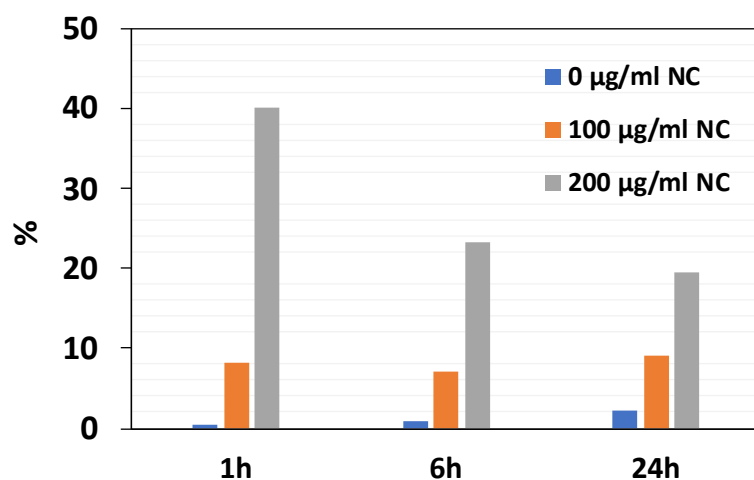


Figure 4.18: Study of the internalization of cerium oxide nanoparticles carried out with three different concentrations. Results from flow cytometric analysis, referred at three different observation times and cells maintained at normal gravity.

used as a control in both the gravity conditions. The percentage of events detected at the normal gravity for cells treated with 100 $\mu\text{g/ml NC}$ (condition indicated as 100NC in the graph) is in line with that found in the previous experiment (about 15%).

Looking at the results obtained from samples exposed to microgravity instead, no differences are noted between the condition with nanoceria and the control condition without NC. From this result, it, therefore, appears that there is very modest NC internalization in the conditions tested.

A qualitative confocal microscope analysis was also performed. As shown in Figure 4.21, nanoparticles could be detected in close proximity to nuclei only in the cultures exposed to normal gravity for 48 h. After application of constant speed mode for microgravity simulation instead, no signal from NC could be noted. These results motivated the utilization of the RPM in random speed mode.

The samples exposed to 8-20 deg/s rotation underwent quantitative analysis through ICP-OES. The collected data are reported in Figure 4.22, where the vertical axis is in logarithmic scale for better data visualization. Cerium concentration amounted to values of 0.003 and 0.005 ppm for untreated samples exposed to normal gravity and microgravity conditions, respectively. Cerium concentration instead was of 22.5 ppm and 1.6 ppm for treated samples exposed to normal gravity and microgravity conditions, respectively. These data are in agreement with flow

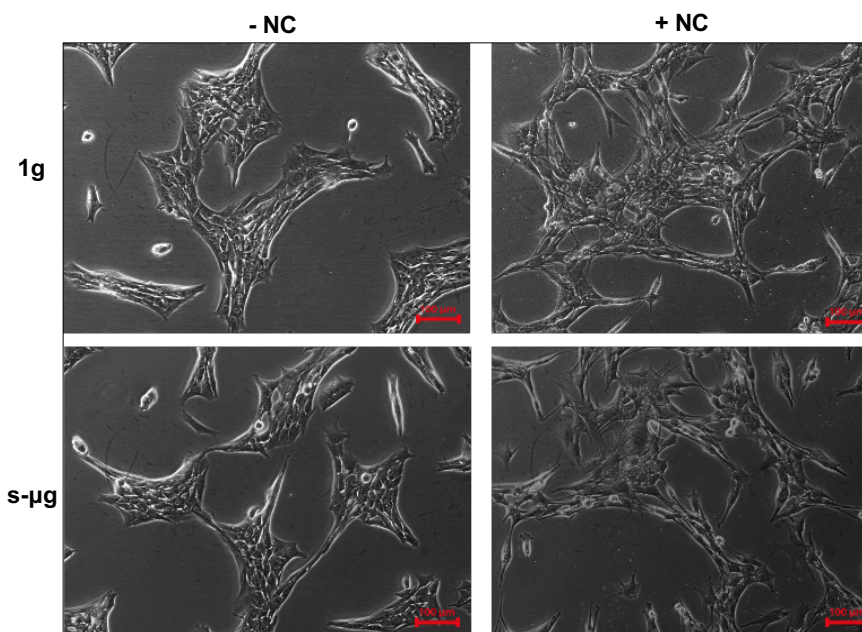


Figure 4.19: Microscope images of C2C12 cells acquired after 48h of microgravity exposure. Control condition at normal gravity (1g) top, cells exposed to microgravity shown instead in bottom images. The images in the left column refer to the condition without Nanocerium (-NC) and those on the right to the condition with Nanocerium (+NC).

cytometry data and indicating that internalization successfully occurred in the tested simulated microgravity conditions, although its entity was modest.

Altogether, these data suggest that the interaction between NC and cells under the tested simulated microgravity conditions is limited, and this might affect oxidative stress alleviation under mechanical unloading, although ameliorating cellular tolerance to nanoparticles.

Interestingly, a study conducted by Z. Diaconeasa et al. demonstrates that internalization of nanocerium occurs differently depending on the cell type. In their study [40], they observed that NC internalization is favored with tumor cells, while with normal cells it seems to be minimal. In fact, regarding normal cells, most of the nanoparticles were detected at the cell membrane level.

Based on the obtained results, alternative experimental protocols, including NC administration at least 24 h prior to cell exposure to simulated microgravity may be explored.

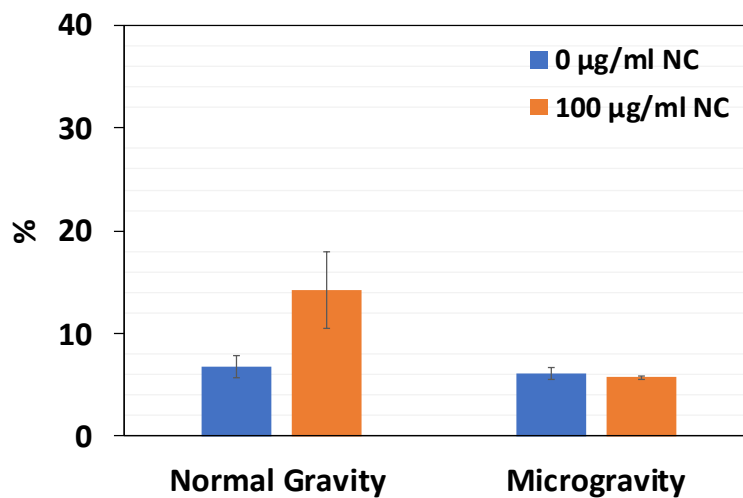


Figure 4.20: Histogram relative to the percentage of internalized Nanoceria obtained by flow cytometry: comparison between the conditions of normal gravity and microgravity.

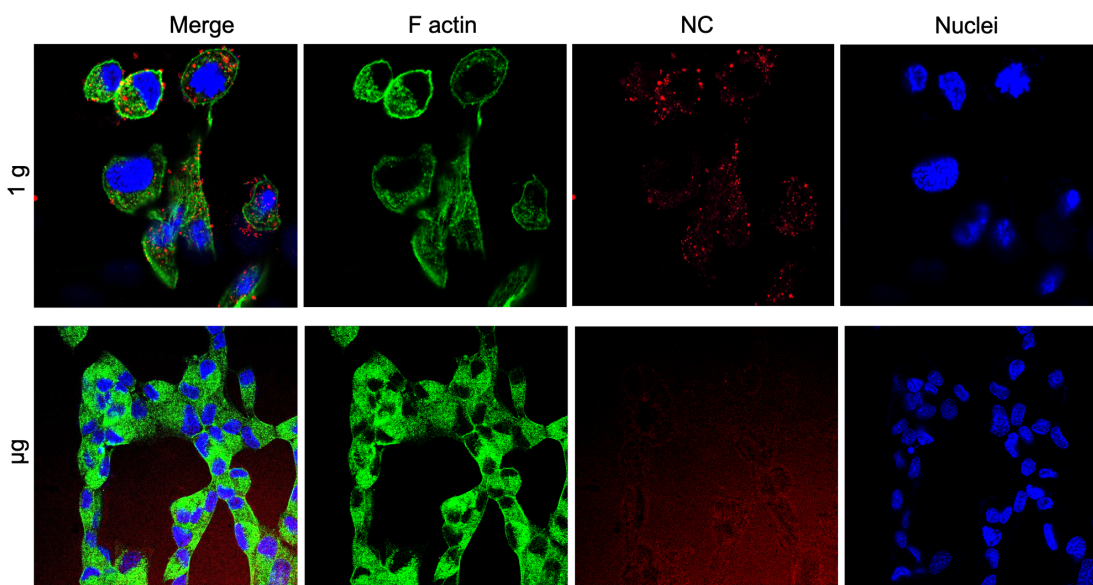


Figure 4.21: Images obtained by confocal microscopy. The top images refer to normal gravity condition, while the bottom images refer to microgravity condition.

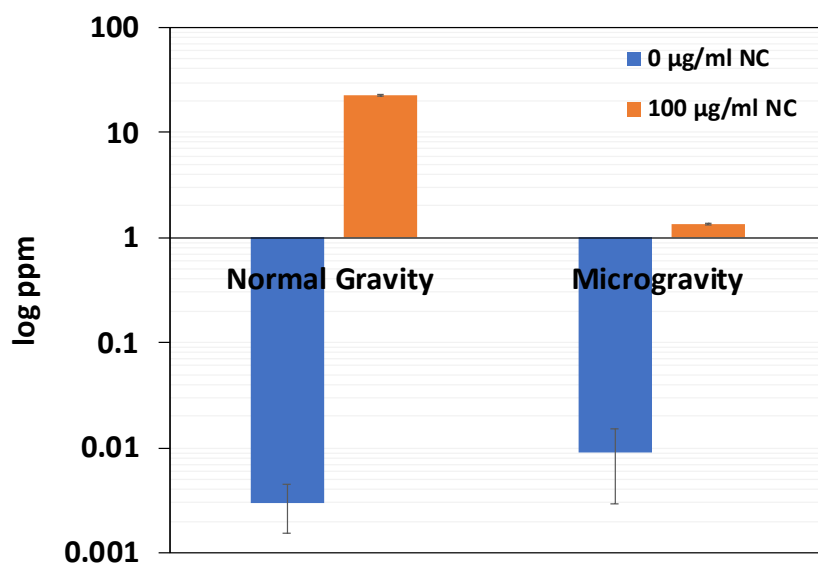


Figure 4.22: Histogram for the percentage of internalized nanoceria obtained by ICP-OES: comparison between the conditions of normal gravity and microgravity.

4.5 Evaluation of oxidative stress induced by microgravity simulation

Research aiming at quantifying the extent of oxidative stress potentially induced by the applied simulated microgravity protocols were also conducted by flow cytometry. Optimization tests were performed in order to find the right quantity of oxidative stress probe, and combinations of RPM rotation speed, observation time, and cellular status (proliferative vs. differentiative) suitable to testing possible protective effects from nanoparticles against oxidative stress.

Quantification of the extent of oxidative stress was performed by using a fluorescent probe, CellROX green dye, selective for ROS detection.

Preliminary testing was performed on a fixed number (100,000) of C2C12 cells

100,000 cells	0 μM	1 μM	2.5 μM
C2C12	8 %	15 %	48 %
HSkM	5 %	20 %	67 %

Table 4.9: Preliminary investigation on myoblast response to increasing concentrations of CellROX Green dye for quantification of ROS^+ -cells by flow cytometry.

and HSkM with increasing concentrations of CellROX Green dye. This testing was

conducted by cell staining and flow cytometry in the absence of any pro-oxidant stress. CellROX Green dye can indeed have toxic effects on cells, thus determining an overestimation of pro-oxidant chemical species in the cultures, i.e. percentage of stressed cells upon treatment. Results of this testing are reported in Table 4.9, clearly showing that the most suitable concentration of reagent to following experimental activities is $1 \mu M$.

To verify if nanoparticles were able to exert an antioxidant activity in cultures,

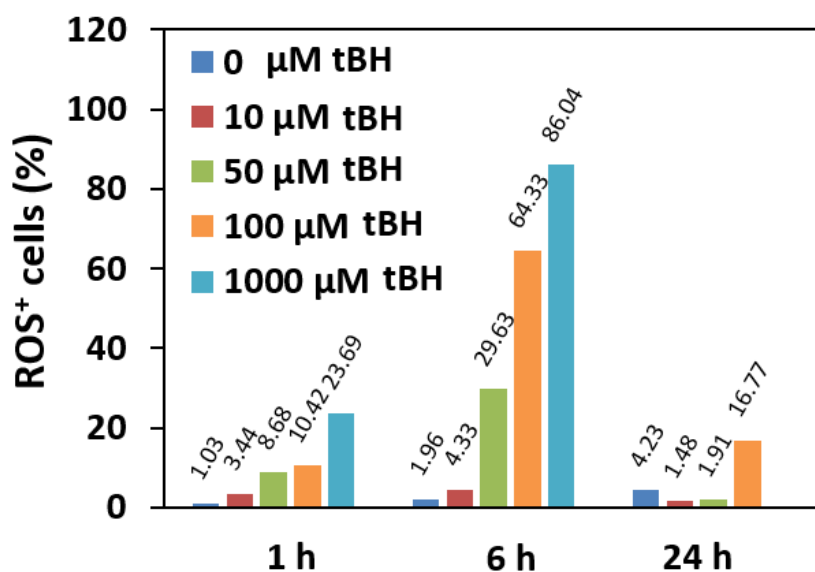


Figure 4.23: Preliminary testing of C2C12 cell response to a pro-oxidant insult provided through tBH administration.

a preliminary flow cytometry experiment was performed with C2C12 myoblasts (seeded at a density of $10,000 \text{ cells}/\text{cm}^2$) and with increasing concentrations of tert-butyl hydroperoxide-tBH (0, 10, 50, 100 and $1000 \mu M$), as a pro-oxidant agent. ROS^+ cells were quantified at 1, 6 and 24 h from tBH administration.

As show in Figure 4.23, the percentage of cells positive to staining at the lower TBH concentration tested ($10 \mu M$) is almost comparable to the control condition. By observing the results obtained for the increasing concentrations (higher than $50 \mu M$), at the three instants of time, a significant increase in oxidative stress is noted only within 6 h from tBH administration. At 24 h from tBH administration, a reduction in the percentage of cells positive to CellROX Green dye is evident. At the highest tBH concentration tested ($1000 \mu M$, red bar), all cells were found dead after 24 h and therefore could not be analyzed. After 24 h of exposure to the concentrations of $50 \mu M$ and $100 \mu M$ tBH, a very low percentage of cells positive

to CellROX Green dye was found, suggesting possible cellular adaptation to the condition of stress.

Antioxidant activity of NC was tested in the presence of a pro-oxidant insult

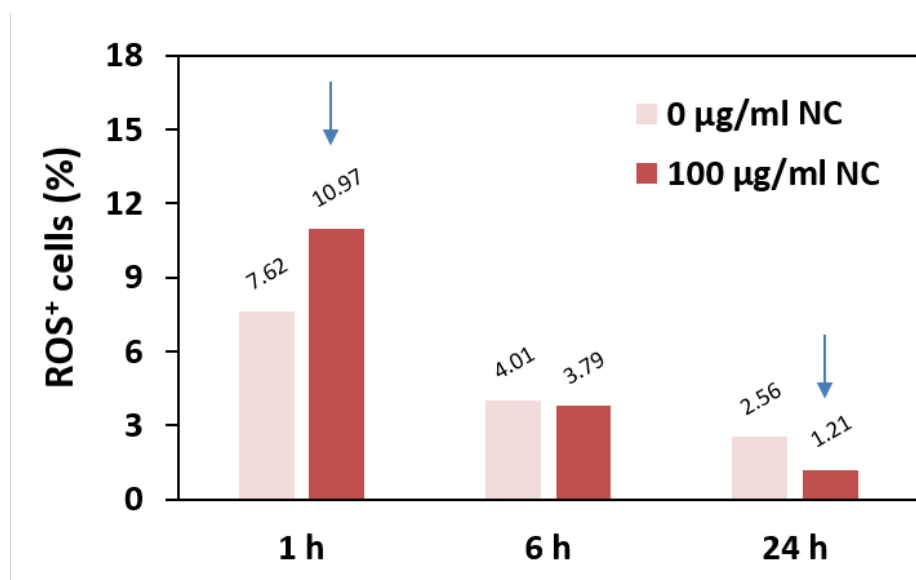


Figure 4.24: Effects of NC administration on C2C12 myoblasts exposed to a pro-oxidant agent at different time point from tBH administration.

provided through tBH administration to the cultures. To the purpose, myoblasts were processed as follows: 10,000 C2C12 *cells/cm*² seeding followed by 24 h incubation, 100 µg/ml NC dispersion administration followed by 24 h incubation, tBH administration followed by 1-6-24 h incubation, staining with CellROX Green dye and flow cytometry. Figure 4.24 shows the result of this investigation, showing a moderate increase of the percentage of *ROS*⁺ cells at 1 h from tBH administration in NC-treated cells: this seems to suggest that NC may exacerbate early oxidative stress induced by tBH for reasons yet to be ascertained. However, the percentage of *ROS*⁺ cells treated with NC at 24 h is half of that one of untreated cells, denoting mitigation of the oxidative stress imparted by tBH administration at a later time of investigation.

After evaluating the cellular response to a known stimulus, the results obtained by using the random positioning machine are reported. Several trials were performed to find the best experimental condition evidencing high levels of oxidative stress in the cultures.

Graph in Figure 4.25 shows the results obtained on C2C12 cells. The graph reports the percentage of cells positive to CellROX green after 24 h and 72 h of 3D clinorotation at 25 deg/s. It is evident that the percentage of cells affected by oxidative

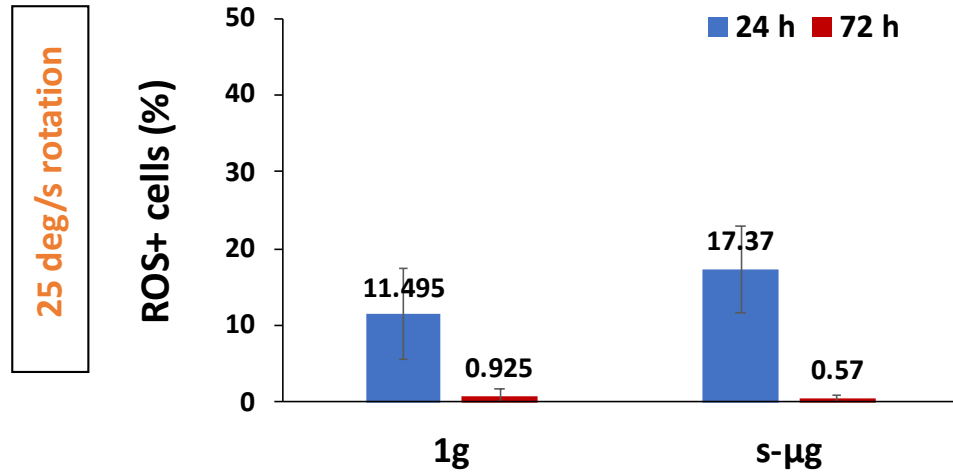


Figure 4.25: RPM-induced oxidative stress on C2C12 cell line after 24 and 72 h of exposure. 3D clinorotation at 25 deg/s.

stress decreases over time: this result supports what has been previously observed with the experiment performed with tBH as a pro-oxidant stimulus regarding C2C12 cell high adaptability to a stress condition.

4.5.1 Evaluation of oxidative stress induced by microgravity simulation: HSkM cell line

HSkM were also tested under constant speed mode for microgravity simulation and resulting data are reported in Figure 4.26. As shown in Figure 4.26, a constant speed of 20 deg/s was successful at inducing a modest oxidative stress in the cultures after 24 h of 3D clinorotation.

Based on the results shown in Figure 4.26, further experiments were conducted by 3D clinorotation useful to microgravity simulation at 20 deg/s. This speed proved to be extremely successful at generating a significantly high oxidative stress in early differentiating HSkM cultures seeded at a density of 20,000 *cells/cm*², kept for 48 h under low serum medium, and finally exposed to simulated microgravity for 24 h. As shown in Figure 4.27a (evidenced by red arrows in phase contrast optical microscopy images), human myoblasts underwent fusion into elongated myotubes, that were retained also after 24 h of clinorotation.

The number of *ROS*⁺ cells reported in Figure 4.27b approximated 60% after 6

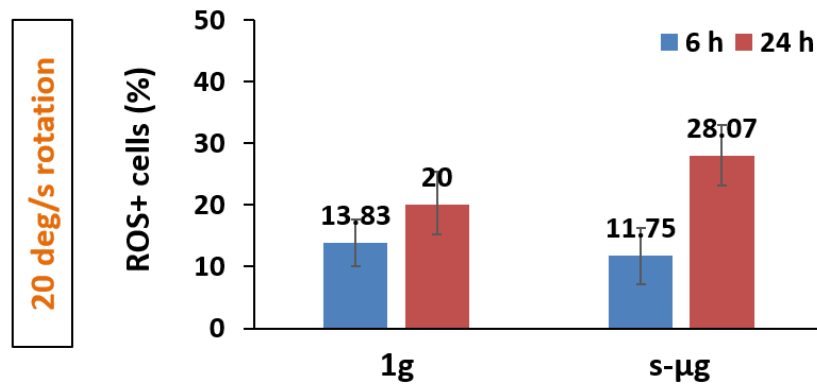


Figure 4.26: Investigations of the effects of different 3D clinorotation speeds on C2C12 cell cultures in terms of oxidative stress.

h and 40% after 24 h of 3D clinorotation, suggesting the deployment of innate oxidative stress response in the cultures, as also found in proliferating mouse myoblasts under simulated microgravity.

Another test was performed on HSkM exposed to random motion mode and data were reported in Figure 4.28. This graph refers to random change of the speeds of both RPM frames between a minimum and maximum speed of 8 and 20 deg/s, respectively.

In this case, data suggest a role of NC in oxidative stress alleviation only at 24 h, which therefore represents a fundamental time point for future studies.

In summary, only modest evidence of oxidative stress was detected for both cell lines, that is mouse C2C12 myoblasts and human skeletal myoblasts, under proliferative conditions, but very significant results were obtained with human skeletal myoblasts under differentiation in the tested conditions of simulated microgravity. Observation times and rotation modes appeared to be critical for oxidative stress assessment: these parameters will be carefully taken into consideration for future studies.

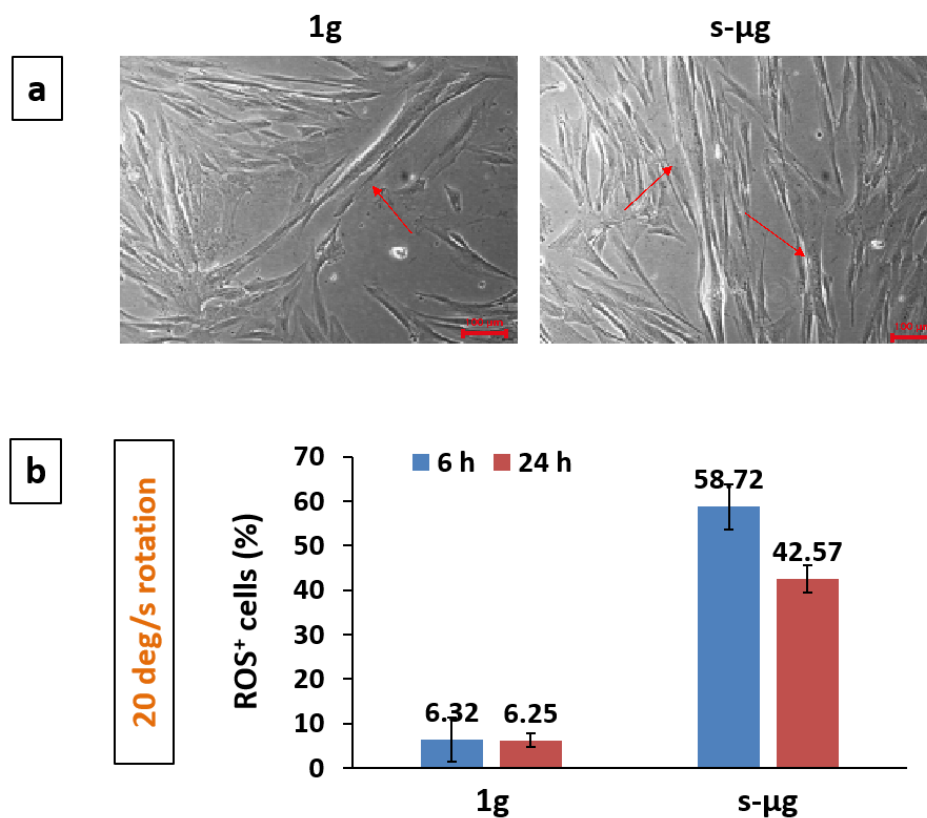


Figure 4.27: Representative images of phase contrast optical microscopy of early differentiating HSkM (a), and investigation of the effects of constant speed 3D clinorotation at 20 deg/s on HSkM cultures in terms of oxidative stress (b).

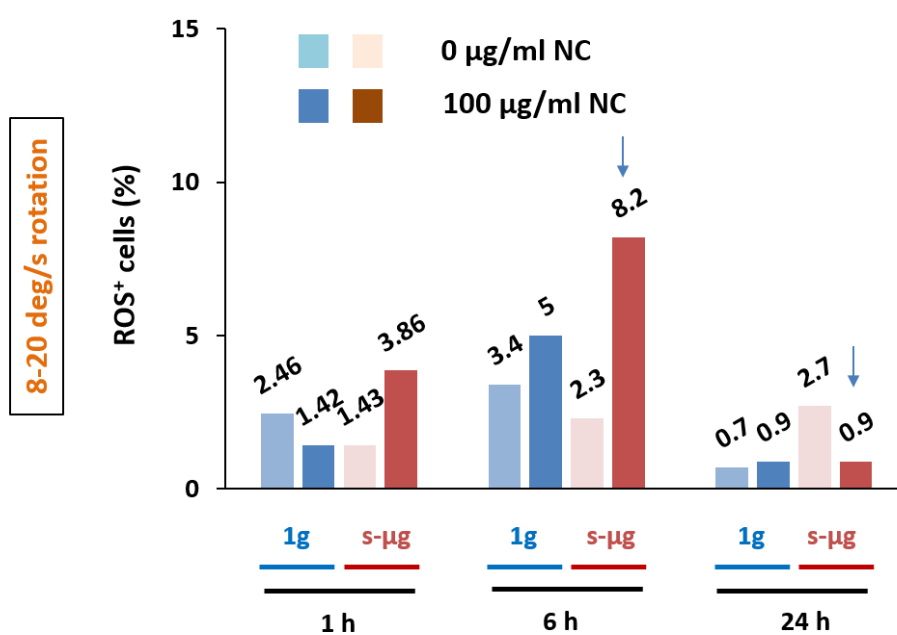


Figure 4.28: Investigation of the effects of random speed 3D rotation at 8-20 deg/s on HSkM cultures in terms of oxidative stress.

Chapter 5

Conclusions

This Master Degree Thesis work consisted into synthesis, characterization and application to skeletal muscle cell cultures of cerium oxide nanoparticles (also termed nanoceria), with focus on cell/nanomaterial interaction under simulated microgravity conditions. Nanoceria indeed represents a promising nanotechnological approach to counteract oxidative stress induced by mechanical unloading, with the final goal of enabling muscle mass and function maintenance in several conditions, including spaceflight.

In this Thesis work, cerium oxide nanoparticles were synthesized by direct precipitation and then characterized by several independent techniques, showing chemical composition, size and stability suitable for in vitro experimentation. In particular, antioxidant property was quantified and found to be higher than that one of commercial nanoparticles with same chemical composition. Then, biocompatibility studies with increasing concentrations of nanoparticles were conducted demonstrating high viability and proliferative capability of skeletal muscle cell cultures even at high concentrations. Simulated microgravity was also applied to the cultures through 3D clinorotation, enabling identification of conditions suitable to cell proliferation and demonstration of evidences of oxidative stress.

In agreement with the literature, simulated microgravity applied to mouse myoblasts was found to promote cell proliferation: this evidence deserves further studies for its possible relevance to muscle tissue engineering applications. Moreover, constant speed clinorotation associated to early differentiation of human myoblasts demonstrated onset of a significant level of oxidative stress suitable for studying of antioxidant effects of nanoceria. Studies conducted on cultures simultaneously exposed to nanoparticles and microgravity conditions demonstrated a low internalization of the nanomaterials. This suggests the opportunity of further studies exploring administration of higher concentrations of nanoparticle dispersions or pre-incubation of cultures with nanoparticles before clinorotation application. Future studies will aim at assessing antioxidant effects of nanoceria under simulated

microgravity enabling muscle cell feature retention or promotion.

Appendix A

Nanoparticles characterization techniques

This chapter is concerned with describing the characterization techniques, and the principles upon which they are based, used in this project to characterize cerium oxide nanoparticles. As mentioned in the previous chapter, cerium oxide nanoparticles can have both beneficial, antioxidant and antibacterial effects and harmful, pro-oxidative effects due to the complex chemical structure. A high presence of the trivalent state on the surface of the nanoparticles can have beneficial effects, thus mimicking SOD and harmful effects leading to excessive ROS production. [36] This evidence, therefore, suggests that it is of considerable importance to characterize the NC at each new synthesis.

In this work, the newly synthesized NC was characterized by comparing it to already well-characterized reference material. Commercial cerium oxide nanoparticles provided by SigmaAldrich were chosen as the reference material.

The techniques of X-Ray photoelectron spectroscopy (XPS), dynamic light scattering (DLS), X-Ray diffraction (XRD), thermogravimetric analysis (TGA) and TEM will be described.

The XPS analysis was used to evaluate the chemical composition of the nanoparticles and then to know the ratio of the Ce^{3+} and Ce^{4+} couple, to make sure that the synthesized nanoparticles could potentially be antioxidants and not the other way around.

DLS was used to measure the hydrodynamic radius, the polydispersity and the Z potential of the nanoparticles to evaluate the stability under the conditions of use. The XRD analysis was used to evaluate the crystalline structure of the nanoparticles and the TGA was performed to evaluate material behavior when subjected to thermal heating.

A.1 X-Ray photoelectron spectroscopy (XPS)

This section describes the technique of X-ray photoelectron spectroscopy (XPS), explains what the underlying principle is, how the XPS spectrum is obtained, and how it is interpreted.

The XPS is a qualitative and quantitative technique, is non-destructive and allow the detection of all elements except for H and He [43].

The physical principle on which this characterization technique is based is the release of electrons from the sample under test by the photoelectric effect [43].

When a photon with characteristic energy ($h\nu$) interacts with an atom, there is a possibility that it interacts with electrons in the atomic orbital. During the photon-electron interaction, the total energy of the photon is transferred to the electron. As the energy of the photon is higher than the binding energy of the electron, the electron is released from the atom through the photoelectronic effect with a specific kinetic energy [43].

The fundamental equation that underlies this technique and allows the identification of the elements present in a sample is the following:

$$E_b = h\nu - E_k$$

where E_b is the electron's binding energy, $h\nu$ is the photon's energy (h is the Planck's constant, ν is the X-Ray frequency), and E_k is the specific kinetic energy of the released electron.

By measuring the kinetic energy of the released electrons, it is possible to calculate the electron's binding energy. Binding energies are typical for each element and in this way it is possible to identify the elements that compose the sample under examination.

Then, an X-ray source irradiates the sample to be analyzed at known energy. A fraction of the electrons released from the sample surface is detected by a kinetic energy analyzer. The final result is a spectrum in which the intensity of the peaks is reported as a function of binding energy. The intensity of the peaks is equal to the number of electrons detected with the same kinetic energy, while the position of the peak (hence the binding energy) identifies the element.

The qualitative analysis to identify what are the elements that make up the sample under analysis is done through a wide scan (resolution from 0 to 1000 eV). It is also possible to make a semi-quantitative analysis of the elements through a high-resolution scan, in this case, it is possible to get information on chemical bonds through chemical shifts and calculate the area subtended to the peaks to assess the percentage atomic concentration. To evaluate the percentage of atomic concentration, it is necessary to consider the background emission, the mean free path, and the detector transmission. The percentage of atomic species present in the sample is calculated by comparing the intensity detected for that species with

the sum of the other species' intensities. [43]

A.2 Dynamic light scattering (DLS)

This section briefly describes the characterization technique of the dynamic light scattering (DLS) technique that in this project was used to measure the hydrodynamic radius, polydispersity, and Z-potential of nanoparticles.

The dynamic light scattering (DLS) technique is widely used to study specific properties of molecules in solution, such as size and homogeneity.

DLS technique is based on the detection of light scattered by the sample under investigation: the instrument irradiates the solution containing the nanoparticles with a beam of monochromatic light that upon interaction is scattered in all directions depending on the size and shape of the nanoparticles. The intensity of the scattered light is recorded by a particular detector to obtain information about the dimensions of the nanoparticles.

Nanoparticles in solution move by Brownian motion that depend on the size of the nanoparticles themselves, the temperature, and the solvent's viscosity. This movement of the nanoparticles causes changes in the intensity of the scattered light. These intensity variations are measured and processed to derive the hydrodynamic size of the macromolecules in that, the intensity of the scattered light is proportional to the square of the particle volume. [44]

Therefore by observing the movements of the nanoparticles in time it is possible to obtain information on their size because the nanoparticles move much more slowly than the solvent molecules and therefore if observed in different time instants, define similar positions. To verify the rapidity of the fluctuations, the instrument software uses an autocorrelator that correlates fluctuations in light intensity with time.

The DLS, by evaluating the size of the nanoparticles, also allows verifying their stability. For biomedical/pharmaceutical applications, it is important to evaluate the stability of nanoparticles in a physiological environment to avoid the formation of nanoparticles aggregates.

In addition to this great advantage, the DLS is a non-destructive technique, requires the use of little material, allows to perform analysis on many samples of different nature dispersed in different solvents at different temperatures. However, it is necessary for the transparency of the solvent and thorough cleaning of the cuvettes used to contain the solution.

Another constraint concerns the sample concentration. The signal recorded by the detector depends on the size but also the concentration of the nanoparticles in the solution. It is, therefore, necessary to select the most appropriate concentration to

perform the analysis and have good reliability of the reading. Temperature, also, is a parameter that greatly influences the analysis; it is, therefore, important to keep the temperature constant during the recording.

As the hydrodynamic radius measured by DLS is larger than the actual radius, it is also useful to compare the obtained size with other imaging techniques such as SEM and TEM, also to verify the goodness of the measurement, as aggregates or dust particles can disturb the size determination when the nanoparticles under analysis are smaller. [45] [44]

The DLS instrument was also used to measure the surface charge of nanoparticles. Determination of the zeta potential is critical to assess the stability of nanoparticles in solution and avoid aggregates. Through the measurement of zeta potential, the surface charge of the nanoparticles is estimated. The particles must have a repulsion force such that aggregation caused by Van Der Waals attraction forces is avoided. A large value (in absolute value) of the measured zeta potential indicates good stability. Usually, when the measured value is greater than 15-20 mV, in absolute value, the nanoparticle suspension can be considered stable. [46]

The Z potential is measured as the difference in the potential's value of the double layer of charge that forms on the surface of the suspended nanoparticles. It is determined by measuring the speed of movement of the nanoparticles towards the electrode of the measuring cuvettes in the presence of an external electric field. [47]

A.3 X-Ray diffraction (XRD)

This section describes the principles of the X-Ray diffraction technique, a characterization technique used to study the crystalline structure of nanomaterials. It is possible to measure the size and the shape of small crystalline regions because the wavelengths of the X-Ray, from 0.2 to 10 nm, are of an order of magnitude comparable to the interatomic spaces of the crystal. [48]

When the atomic structure of a crystalline material is irradiated with an X-ray beam, it causes constructive and destructive interference from the scattered X-ray beam. The set of interferences generates a unique spectrum for each element that has different peaks, known as Bragg diffraction peaks.

Indeed, the diffraction of x-rays by a crystal is described by the Bragg law indicated below:

$$2d\sin(\theta) = n(\lambda)$$

The equation relates the wavelength of the incident rays (indicated with λ), and the space between atoms in the crystal (understood as the perpendicular distance between pairs of adjacent planes and indicated with the letter d in the equation).

θ is the angle of incidence or Bragg angle, and n is the reflection index.

Then the rays generated by the diffraction are detected and processed to obtain, by varying the angle between source, sample and detector (over a 2 range, usually from 10 to 100 degrees [49], a spectrum with characteristic peaks for each material. The XRD peaks, therefore produced by the constructive interference of the X-ray beam diffused at specific angles, have an intensity determined by the atomic positions within the lattice planes. Hence, one can think of the XRD spectrum as an "imprint" of the periodic arrangement of the material's atoms.[50]

Thus, the XRD spectrum of a crystalline material has well-defined peaks at specific scattering angles, on the contrary, an amorphous material that is not characterized by the periodic and ordered arrangement of the atoms, has a spectrum having a maximum intensity extended for different angles of dispersion.

With this technique, it is also possible to know the average crystal size. The crystal dimension can be calculated from the amplitude, then from the total amplitude to half the maximum intensity of the reflection peak (beta) using the Scherrer equation:

$$t = k(\lambda)(\beta)\cos(\theta)$$

where K is the Scherrer constant and represents the shape of the nanoparticles. [48]

A.4 Thermogravimetric Analysis (TGA)

This section describes the principles of the thermogravimetric analysis technique (TGA) that was used to monitor the changes of the mass of the samples as a function of the temperature and time.

TGA is a thermoanalytical technique where the sample is placed on an electronic balance at high precision located in a furnace. The temperature inside the furnace is controlled through an apposite temperature controller programmed to heat the sample to a maximum temperature through several heating ramps. [51]

The TGA technique is commonly used to evaluate the loss of mass of a sample due to several possible causes as oxidation, decomposition, and loss of volatile.

The result of this analysis is a plot, the TGA thermal curve, in which is represented the percentage of weight loss as a function of the temperature. In the curve, it is possible to observe a first decomposition of the sample which continues up to an elevated temperature where a considerable percentage variation of the weight is observed. At high temperatures, uniformity of the curve is noted which corresponds to the crystallization temperature of the material. [52]

From the TGA curve, it is possible to extrapolate the point, and therefore the temperature, at which the mass loss begins. Another extrapolation useful to

characterize the material refers to the peak of the first derivative of the thermal curve. This peak is called the inflection point and indicates the point where the greatest change in weight of the sample is perceptible. The thermal curve of the TGA is therefore quite important to evaluate the behaviour of a material subjected to heating and therefore understand if the sample is thermally degrading through the loss of mass or is undergoing an oxidation process indicated instead by a mass gain. [53]

The purpose of the analysis is undoubtedly to evaluate the thermal heating behaviour of nanoparticles, but through this technique, by observing the degradation of the material at different temperatures we can get more information about the composition of the nanoparticles [53].

Bibliography

- [1] «Simulated Microgravity». In: *Encyclopedia of Neuroscience* 1.2019 (2008), pp. 3700–3700. DOI: 10.1007/978-3-540-29678-2_5411 (cit. on pp. 1, 23, 24).
- [2] Daniela Calzia, Laura Ottaggio, Alessandro Cora, Giorgia Chiappori, Paola Cuccarolo, Enrico Cappelli, Alberto Izzotti, Sara Tavella, and Paolo Degan. «Characterization of C2C12 cells in simulated microgravity: Possible use for myoblast regeneration». In: *Journal of Cellular Physiology* 235.4 (2020), pp. 3508–3518. ISSN: 10974652. DOI: 10.1002/jcp.29239 (cit. on pp. 1, 19, 23, 24, 32).
- [3] Charles Harding, Jon Takemoto, and Elizabeth Vargis. «In Vitro Modeling of Microgravity-Induced Muscle Atrophy and Spaceflight Radiation». In: *NASA Space Grant Consortium* (2016), pp. 1–11 (cit. on pp. 1, 19, 23, 32).
- [4] Giada Graziana Genchi, Andrea Degl’Innocenti, Alice Rita Salgarella, Ilaria Pezzini, Attilio Marino, Arianna Menciacchi, Sara Piccirillo, Michele Balsamo, and Gianni Ciofani. «Modulation of gene expression in rat muscle cells following treatment with nanoceria in different gravity regimes». In: *Nanomedicine* 13.22 (2018), pp. 2821–2833. ISSN: 17486963. DOI: 10.2217/nnm-2018-0316 (cit. on pp. 1, 8, 12, 18, 32).
- [5] Charles P. Harding and Elizabeth Vargis. «Muscle Atrophy Marker Expression Differs between Rotary Cell Culture System and Animal Studies». In: *BioMed Research International* 2019 (2019). ISSN: 23146141. DOI: 10.1155/2019/2042808 (cit. on pp. 1, 19, 23, 24).
- [6] 2005 Et al. «NIH Public Access». In: *Bone* 23.1 (2008), pp. 1–7. ISSN: 15378276. DOI: 10.1002/cphy.c100054.REACTIVE. arXiv: NIHMS150003 (cit. on pp. 1, 8–13, 15–18).
- [7] Philip M. Hopkins. «Skeletal muscle physiology». In: *Continuing Education in Anaesthesia, Critical Care and Pain* 6.1 (2006), pp. 1–6. ISSN: 17431824. DOI: 10.1093/bjaceaccp/mki062 (cit. on pp. 2–4).

- [8] Callahan AL. McCuller C Jessu R. «Physiology, Skeletal Muscle». In: (2020) (cit. on pp. 3, 4, 7).
- [9] Varacallo M. Dave HD Shook M. «Anatomy, Skeletal Muscle». In: (2021) (cit. on p. 3).
- [10] Andrea Bonetto and Lynda Bonewald. «Bone and Muscle». In: Jan. 2019, pp. 317–332. ISBN: 9780128132593. DOI: 10.1016/B978-0-12-813259-3.00016-6 (cit. on p. 4).
- [11] Susan M. Abmayr and Grace K. Pavlath. «Myoblast fusion: Lessons from flies and mice». In: *Development* 139.4 (2012), pp. 641–656. ISSN: 09501991. DOI: 10.1242/dev.068353 (cit. on pp. 5, 6).
- [12] C. Florian Bentzinger, Yu Xin Wang, and Michael A. Rudnicki. «Building muscle: molecular regulation of myogenesis.» In: *Cold Spring Harbor perspectives in biology* 4.2 (2012), pp. 1–16. ISSN: 19430264. DOI: 10.1101/cshperspect.a008342 (cit. on pp. 5, 6).
- [13] Jennifer E. Morgan and Terence A. Partridge. «Muscle satellite cells». In: *The International Journal of Biochemistry Cell Biology* 35.8 (2003), pp. 1151–1156. ISSN: 1357-2725. DOI: [https://doi.org/10.1016/S1357-2725\(03\)00042-6](https://doi.org/10.1016/S1357-2725(03)00042-6). URL: <https://www.sciencedirect.com/science/article/pii/S1357272503000426> (cit. on p. 6).
- [14] Malea Murphy and Gabrielle Kardon. *Origin of vertebrate limb muscle: The role of progenitor and myoblast populations*. Vol. 96. 2011, pp. 1–32. ISBN: 9780123859402. DOI: 10.1016/B978-0-12-385940-2.00001-2 (cit. on p. 6).
- [15] Paolo Bonaldo and Marco Sandri. «Cellular and molecular mechanisms of muscle atrophy». In: *DMM Disease Models and Mechanisms* 6.1 (2013), pp. 25–39. ISSN: 17548403. DOI: 10.1242/dmm.010389 (cit. on pp. 6, 8, 12, 13, 15).
- [16] David A. Chad. «Neuromuscular Disorders, Overview». In: *Encyclopedia of the Neurological Sciences*. Ed. by Michael J. Aminoff and Robert B. Daroff. New York: Academic Press, 2003, pp. 494–500. ISBN: 978-0-12-226870-0. DOI: <https://doi.org/10.1016/B0-12-226870-9/00844-3>. URL: <https://www.sciencedirect.com/science/article/pii/B0122268709008443> (cit. on p. 6).
- [17] Haller RG. Lewis SF. «Skeletal muscle disorders and associated factors that limit exercise performance». In: (1989) (cit. on p. 7).
- [18] Edens MA. Noto RE Leavitt L. «Physiology, Muscle». In: (2021) (cit. on p. 7).

- [19] Ting Liu, Lingyun Zhang, Donghyun Joo, and Shao Cong Sun. «NF- κ B signaling in inflammation». In: *Signal Transduction and Targeted Therapy* 2.April (2017), pp. 1–9. ISSN: 20593635. DOI: 10.1038/sigtrans.2017.23 (cit. on p. 7).
- [20] Courtney M. Peterson, Darcy L. Johannsen, and Eric Ravussin. «Skeletal muscle mitochondria and aging: A review». In: *Journal of Aging Research* 2012 (2012). ISSN: 20902204. DOI: 10.1155/2012/194821 (cit. on pp. 8, 11, 12, 15).
- [21] Johanna Ábrigo, Alvaro A Elorza, Claudia A Riedel, Cristian Vilos, Felipe Simon, Daniel Cabrera, Lisbell Estrada, and Claudio Cabello-Verrugio. «Role of Oxidative Stress as Key Regulator of Muscle Wasting during Cachexia». In: *Oxidative Medicine and Cellular Longevity* 2018 (2018). Ed. by Rodrigo Franco, p. 2063179. ISSN: 1942-0900. DOI: 10.1155/2018/2063179. URL: <https://doi.org/10.1155/2018/2063179> (cit. on pp. 8, 12–16).
- [22] Gabriele Pizzino, Natasha Irrera, Mariapaola Cucinotta, Giovanni Pallio, Federica Mannino, Vincenzo Arcoraci, Francesco Squadrito, Domenica Altavilla, and Alessandra Bitto. «Oxidative Stress: Harms and Benefits for Human Health». In: *Oxidative Medicine and Cellular Longevity* 2017 (2017). ISSN: 19420994. DOI: 10.1155/2017/8416763 (cit. on pp. 9, 11, 12, 15, 17, 18).
- [23] Sungbin Im, Tae Gyu Nam, Sang Gil Lee, Young Jun Kim, Ock Kyoung Chun, and Dae Ok Kim. «Additive antioxidant capacity of vitamin C and tocopherols in combination». In: *Food Science and Biotechnology* 23.3 (2014), pp. 693–699. ISSN: 12267708. DOI: 10.1007/s10068-014-0094-4 (cit. on pp. 17, 18).
- [24] Gianni Ciofani, Leonardo Ricotti, Jacopo Rigosa, Arianna Menciacchi, Virgilio Mattoli, and Monica Monici. «Hypergravity effects on myoblast proliferation and differentiation». In: *Journal of Bioscience and Bioengineering* 113.2 (2012), pp. 258–261. ISSN: 13891723. DOI: 10.1016/j.jbiosc.2011.09.025. URL: <http://dx.doi.org/10.1016/j.jbiosc.2011.09.025> (cit. on p. 19).
- [25] Simon L Wuest, Stéphane Richard, Sascha Kopp, Daniela Grimm, and Marcel Egli. «Simulated Microgravity: Critical Review on the Use of Random Positioning Machines for Mammalian Cell Culture». In: *BioMed Research International* 2015 (2015). Ed. by Jack J W A Van Loon, p. 971474. ISSN: 2314-6133. DOI: 10.1155/2015/971474. URL: <https://doi.org/10.1155/2015/971474> (cit. on pp. 19, 21).
- [26] Daniela Grimm et al. «Growing tissues in real and simulated microgravity: New methods for tissue engineering». In: *Tissue Engineering - Part B: Reviews* 20.6 (2014), pp. 555–566. ISSN: 19373376. DOI: 10.1089/ten.teb.2013.0704 (cit. on pp. 20, 21).

- [27] Steven J. Pardo et al. «Simulated microgravity using the Random Positioning Machine inhibits differentiation and alters gene expression profiles of 2T3 preosteoblasts». In: *American Journal of Physiology - Cell Physiology* 288.6 57-6 (2005), pp. 1211–1221. ISSN: 03636143. DOI: 10.1152/ajpcell.00222.2004 (cit. on pp. 20, 21).
- [28] Jack J.W.A. van Loon. «Some history and use of the random positioning machine, RPM, in gravity related research». In: *Advances in Space Research* 39.7 (2007), pp. 1161–1165. ISSN: 02731177. DOI: 10.1016/j.asr.2007.02.016 (cit. on p. 21).
- [29] A. G. Borst and Jack J.W.A. Van Loon. «Technology and developments for the random positioning machine, RPM». In: *Microgravity Science and Technology* 21.4 (2009), pp. 287–292. ISSN: 09380108. DOI: 10.1007/s12217-008-9043-2 (cit. on pp. 21, 22).
- [30] Hyun Wook Ryu, Sang Hun Choi, Sim Namkoong, Ik Soon Jang, Dong Hyun Seo, Inho Choi, Han Sung Kim, and Junsoo Park. «Simulated microgravity contributes to autophagy induction by regulating AMP-activated protein kinase». In: *DNA and Cell Biology* 33.3 (2014), pp. 128–135. ISSN: 15577430. DOI: 10.1089/dna.2013.2089 (cit. on p. 24).
- [31] Soumen Das, Janet M. Dowding, Kathryn E. Klump, James F. McGinnis, William Self, and Sudipta Seal. «Cerium oxide nanoparticles: Applications and prospects in nanomedicine». In: *Nanomedicine* 8.9 (2013), pp. 1483–1508. ISSN: 17486963. DOI: 10.2217/nnm.13.133 (cit. on pp. 25–30).
- [32] Akram Ahangarpour, Ali Akbar Oroojan, Layasadat Khorsandi, Maryam Kouchak, and Mohammad Badavi. «Solid Lipid Nanoparticles of Myricitrin Have Antioxidant and Antidiabetic Effects on Streptozotocin-Nicotinamide-Induced Diabetic Model and Myotube Cell of Male Mouse». In: *Oxidative Medicine and Cellular Longevity* 2018 (2018). ISSN: 19420994. DOI: 10.1155/2018/7496936 (cit. on p. 25).
- [33] Mallappa Kumara Swamy, Mohd Sayeed Akhtar, Sudipta Kumar Mohanty, and Uma Rani Sinniah. «Synthesis and characterization of silver nanoparticles using fruit extract of Momordica cymbalaria and assessment of their in vitro antimicrobial, antioxidant and cytotoxicity activities». In: *Spectrochimica Acta - Part A: Molecular and Biomolecular Spectroscopy* 151 (2015), pp. 939–944. ISSN: 13861425. DOI: 10.1016/j.saa.2015.07.009 (cit. on p. 26).
- [34] Xingfu Bao, Jiahui Zhao, Jian Sun, Min Hu, and Xiurong Yang. «Poly-dopamine Nanoparticles as Efficient Scavengers for Reactive Oxygen Species in Periodontal Disease». In: *ACS Nano* 12.9 (2018), pp. 8882–8892. ISSN: 1936086X. DOI: 10.1021/acsnano.8b04022 (cit. on p. 26).

- [35] Antonella Rocca, Virgilio Mattoli, Barbara Mazzolai, and Gianni Ciofani. «Cerium oxide nanoparticles inhibit adipogenesis in rat mesenchymal stem cells: Potential therapeutic implications». In: *Pharmaceutical Research* 31.11 (2014), pp. 2952–2962. ISSN: 1573904X. DOI: 10.1007/s11095-014-1390-7 (cit. on pp. 26, 28, 30, 31).
- [36] Bryant C. Nelson, Monique E. Johnson, Marlon L. Walker, Kathryn R. Riley, and Christopher M. Sims. «Antioxidant cerium oxide nanoparticles in biology and medicine». In: *Antioxidants* 5.2 (2016), pp. 1–21. ISSN: 20763921. DOI: 10.3390/antiox5020015 (cit. on pp. 26–29, 36, 53, 54, 82).
- [37] Gianni Ciofani, Giada G. Genchi, Ioannis Liakos, Valentina Cappello, Mauro Gemmi, Athanassia Athanassiou, Barbara Mazzolai, and Virgilio Mattoli. «Effects of cerium oxide nanoparticles on PC12 neuronal-like cells: Proliferation, differentiation, and dopamine secretion». In: *Pharmaceutical Research* 30.8 (2013), pp. 2133–2145. ISSN: 07248741. DOI: 10.1007/s11095-013-1071-y (cit. on pp. 26, 30, 55).
- [38] Mpumelelo Nyoka, Yahya E. Choonara, Pradeep Kumar, Pierre P.D. Kondiah, and Viness Pillay. «Synthesis of cerium oxide nanoparticles using various methods: Implications for biomedical applications». In: *Nanomaterials* 10.2 (2020). ISSN: 20794991. DOI: 10.3390/nano10020242 (cit. on pp. 26, 28–30, 36).
- [39] Fanny Caputo, Marta Marni, Andrzej Sienkiewicz, Silvia Licocchia, Francesco Stellacci, Lina Ghibelli, and Enrico Traversa. «A novel synthetic approach of cerium oxide nanoparticles with improved biomedical activity». In: *Scientific Reports* 7.1 (2017), pp. 1–13. ISSN: 20452322. DOI: 10.1038/s41598-017-04098-6 (cit. on pp. 28, 29, 36, 62).
- [40] Z. Diaconeasa et al. «New insights regarding the selectivity and the uptake potential of nanocerium by human cells». In: *Colloids and Surfaces A: Physico-chemical and Engineering Aspects* 532.May 2017 (2017), pp. 132–139. ISSN: 18734359. DOI: 10.1016/j.colsurfa.2017.05.081 (cit. on pp. 31, 62, 71).
- [41] Matteo Battaglini et al. «Polydopamine Nanoparticles as an Organic and Biodegradable Multitasking Tool for Neuroprotection and Remote Neuronal Stimulation». In: *ACS Applied Materials and Interfaces* 12.32 (2020), pp. 35782–35798. ISSN: 19448252. DOI: 10.1021/acsami.0c05497 (cit. on p. 34).
- [42] Hye Rim Shin, Minjeong Kwak, Tae Geol Lee, and Ji Youn Lee. «Quantifying the level of nanoparticle uptake in mammalian cells using flow cytometry». In: *Nanoscale* 12.29 (2020), pp. 15743–15751. ISSN: 20403372. DOI: 10.1039/d0nr01627f (cit. on p. 69).
- [43] Joseph D Andrade. «(XPS)». In: (1985) (cit. on pp. 83, 84).

- [44] Ahram Kim, Wei Beng Ng, William Bernt, and Nam Joon Cho. «Validation of Size Estimation of Nanoparticle Tracking Analysis on Polydisperse Macromolecule Assembly». In: *Scientific Reports* 9.1 (2019), pp. 1–14. ISSN: 20452322. DOI: 10.1038/s41598-019-38915-x (cit. on pp. 84, 85).
- [45] Jörg Stetefeld, Sean A. McKenna, and Trushar R. Patel. «Dynamic light scattering: a practical guide and applications in biomedical sciences». In: *Biophysical Reviews* 8.4 (2016), pp. 409–427. ISSN: 18672469. DOI: 10.1007/s12551-016-0218-6 (cit. on p. 85).
- [46] Emil Joseph and Gautam Singhvi. «Chapter 4 Multifunctional nanocrystals for cancer therapy: a potential nanocarrier». In: *Nanomaterials for Drug Delivery and Therapy*. 2019, pp. 91–116. DOI: 10.1016/b978-0-12-816505-8.00007-2. URL: <https://app.dimensions.ai/details/publication/pub.1112766405> (cit. on p. 85).
- [47] Abeer Jabra Shnoudeh, Islam Hamad, Ruwaida W. Abdo, Lana Qadumii, Abdulmutallab Yousef Jaber, Hiba Salim Surchi, and Shahd Z. Alkelany. «Chapter 15 - Synthesis, Characterization, and Applications of Metal Nanoparticles». In: *Biomaterials and Bionanotechnology*. Ed. by Rakesh K. Tekade. Advances in Pharmaceutical Product Development and Research. Academic Press, 2019, pp. 527–612. ISBN: 978-0-12-814427-5. DOI: <https://doi.org/10.1016/B978-0-12-814427-5.00015-9>. URL: <https://www.sciencedirect.com/science/article/pii/B9780128144275000159> (cit. on p. 85).
- [48] Maria Kaliva and Maria Vamvakaki. «Chapter 17 - Nanomaterials characterization». In: *Polymer Science and Nanotechnology*. Ed. by Ravin Narain. Elsevier, 2020, pp. 401–433. ISBN: 978-0-12-816806-6. DOI: <https://doi.org/10.1016/B978-0-12-816806-6.00017-0>. URL: <https://www.sciencedirect.com/science/article/pii/B9780128168066000170> (cit. on pp. 85, 86).
- [49] J. Patel and P. H. Parsania. «Characterization, testing, and reinforcing materials of biodegradable composites». In: 2018 (cit. on p. 86).
- [50] «Chapter 3 - Methods for Assessing Surface Cleanliness». In: *Developments in Surface Contamination and Cleaning, Volume 12*. Ed. by Rajiv Kohli and K.L. Mittal. Elsevier, 2019, pp. 23–105. ISBN: 978-0-12-816081-7. DOI: <https://doi.org/10.1016/B978-0-12-816081-7.00003-6>. URL: <https://www.sciencedirect.com/science/article/pii/B9780128160817000036> (cit. on p. 86).
- [51] Alessandro Polini and F. Yang. «Physicochemical characterization of nanofiber composites». In: Dec. 2017, pp. 97–115. ISBN: 9780081001738. DOI: 10.1016/B978-0-08-100173-8.00005-3 (cit. on p. 86).

BIBLIOGRAPHY

- [52] Amina Sarfraz, Asif Raza, Mojtaba Mirzaeian, Qaisar Abbas, and Rizwan Raza. «Electrode Materials for Fuel Cells». In: Jan. 2020. ISBN: 9780128035818. DOI: 10.1016/B978-0-12-803581-8.11742-4 (cit. on p. 86).
- [53] Ming-ming Chen. «Thermal Analysis». In: Dec. 2016, pp. 249–272. ISBN: 9780128052563. DOI: 10.1016/B978-0-12-805256-3.00012-X (cit. on p. 87).